11

Streaming Interactions

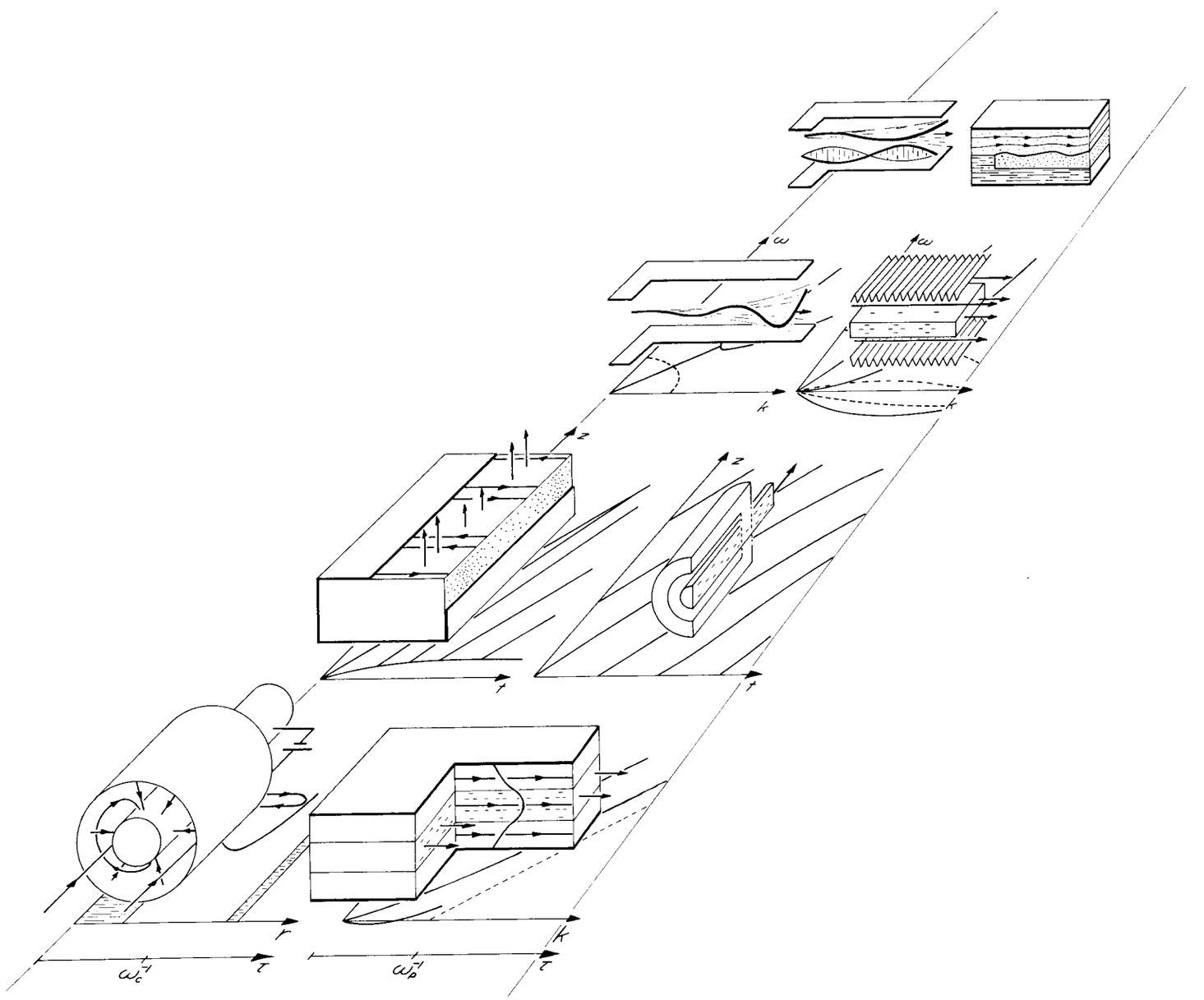

11.1 Introduction

Some of the most significant interactions between continua having large relative velocities involve charged particle beams accelerated under near-vacuum conditions. Thus, the first part of this chapter gives some background in electron beam dynamics. The charged particles of Chap. 5 become a continuum in their own right because their inertia is dominant. Section 11.2, on the laws and theorems for a charged particle gas, draws on the fluid mechanics of Chap. 7, and leads to the steady electron flows considered in Secs. 11.3 and 11.4. Flows illustrated in these latter sections are typical of those found in magnetrons and in electric and magnetic electron beam lenses. Pictured as they are in Lagrangian coordinates, the motions appear to be time varying. But, if viewed in Eulerian coordinates, the electron flows of these sections are steady and might be considered in Chap. 9. The remaining sections relate not only to electron beams, but to electromechanical continua introduced in previous chapters.

Sections 11.6-11.10 have as a common theme the use of the method of characteristics to understand dynamics in "real" space and time. The approach is restricted to two dimensions, here one space and the other time, but makes it possible to investigate such nonlinear phenomena as shock formation and nonlinear space-charge oscillations. Thus it is that these sections are concerned with quasi-one-dimensional models. As pointed out in Sec. 4.12, the small-amplitude limits of these models are identical with the long-wave limits of two- and three-dimensional models. Thus, the quasi-one-dimensional model represents what physical content there is to the dominant modes from the infinite number of spatial modes of a linear system. However, nonlinear phenomena can be incorporated into the quasi-one-dimensional model.

In addition to giving the opportunity to develop nonlinear phenomena, the method of characteristics gives the opportunity to explore the implications of causality for longitudinal boundary conditions and the general domain of dependence of a response pictured in the z-t plane. This gives an alternative to the complex-wave point of view, taken up in the remainder of the chapter, in appreciating the difference between absolute and convective instabilities and between evanescent and amplifying waves. The prototype configurations examined in Sec. 11.10 are analogous to traveling-wave electron beam or beam plasma systems taken up in later sections.

Sections 11.11-11.17 return to a theme of complex waves. Spatial transients in the sinusoidal steady state are considered in Sec. 5.17 with the tacit assumption that the response decays away from the excitation source. As illustrated in these sections, the response could just as well amplify from the region of excitation. How is an evanescent wave, which simply decays from the region of excitation, to be distinguished from one that amplifies? Temporal transients are first introduced in Sec. 5.15, and instability, defined as an unbounded response in time, illustrated in Sec. 8.9. In a system that is infinitely long in the longitudinal direction, a dispersion relation that gives "unstable" ω's for real k's can either imply that the response is unbounded in time at a given fixed location, or that there is unlimited growth for an observer moving with the response. In a given situation, how is an absolute instability to be distinguished from one that is convective? For special hyperbolic systems, these questions are answered in terms of the method of characteristics in Sec. 11.10. Sections 11.11 and 11.12 are devoted to the alternative of answering these questions in terms of complex waves. The remaining sections illustrate with classic examples.

BALLISTIC CONTINUA

11.2 Charged Particles in Vacuum; Electron Beams

Equations of Motion: In terms of the Eulerian coordinates of Sec. 2.4, Newton's law for a particle having mass m and charge q, subject to the Lorentz force (Eq. 3.2.1), is

$$m\left(\frac{\partial \vec{v}}{\partial t} + \vec{v}\cdot\nabla\vec{v}\right) = q(\vec{E} + \vec{v} \times \mu_o\vec{H}) \tag{1}$$

Multiplied by the particle number density, n, this expression is almost what would be written to describe a fluid. The pressure and viscous stress terms are absent from Eq. 1. To each point in space is ascribed the velocity, $\vec{v}$, of the particle that happens to be at that point at the given instant in time.

Because the pressure and viscous stresses are absent, much of the literature of electron beams pictures the motions in Lagrangian terms, as discussed in Sec. 2.4. Then, the initial coordinates of each particle are the independent variables as the partial derivative with respect to time is taken:

$$m\frac{\partial \vec{v}}{\partial t} = q(\vec{E} + \vec{v} \times \mu_o\vec{H}) \tag{2}$$

Thus, for example, in cylindrical coordinates the equations of motion for a particle having the instantaneous position (r,θ,z) are

$$\frac{d^2r}{dt^2} - r\left(\frac{d\theta}{dt}\right)^2 = \frac{q}{m} E_r + \frac{q}{m} \mu_o H_z r \frac{d\theta}{dt} \tag{3}$$

$$r \frac{d^2\theta}{dt^2} + 2 \frac{dr}{dt} \frac{d\theta}{dt} = \frac{1}{r} \frac{d}{dt} \left(r^2 \frac{d\theta}{dt}\right) = \frac{q}{m} \left(\mu_o H_r \frac{dz}{dt} - \mu_o H_z \frac{dr}{dt}\right) \tag{4}$$

$$\frac{d^2z}{dt^2} = \frac{q}{m} E_z - \frac{q}{m} \mu_o H_r r \frac{d\theta}{dt} \tag{5}$$

where the second terms on the left in Eqs. 3 and 4 are respectively the centripetal and Coriolis accelerations of rigid-body mechanics.

The dynamics of interest can be pictured as EQS with an imposed magnetic field. In Sec. 3.4 it is argued that in EQS systems, the magnetic force is negligible compared to the electric force. Now, the particles of interest include electrons or ions in vacuum. Their velocities can easily be large enough to make magnetic forces due to the imposed field important. The arguments of Sec. 3.4 show that the part of the force attributable to a magnetic field induced by the displacement current (or the current density associated with the accumulation of net charge) is still negligible provided that times of interest are long compared to the transit time of an electromagnetic wave.

The laws required to complete the description are usually written in Eulerian coordinates, much as in the description of charged migrating and diffusing particles in Sec. 5.2. With the charge density defined as nq, conservation of charge, Gauss' law and the condition that the electric field be irrotational are written as

$$\frac{\partial \rho}{\partial t} + \nabla \cdot \rho \vec{v} = 0 \tag{6}$$

$$\nabla \cdot \varepsilon_o \vec{E} = \rho \tag{7}$$

$$\vec{E} = -\nabla \Phi \tag{8}$$

Either Eq. 1 or 2 and these three expressions comprise two vector and two scalar equations in the dependent variables $\vec{v}$, $\vec{E}$ and ρ,Φ.

Energy Equation: The equivalent of Bernoulli's equation for charged ballistic particles is obtained following the same steps as in Sec. 7.8. With the use of a vector identity* and Eq. 8, Eq. 1 becomes

$$m\left(\frac{\partial \vec{v}}{\partial t} + \vec{\omega} \times \vec{v}\right) + \nabla\left(\frac{1}{2} m\vec{v} \cdot \vec{v} + q\Phi\right) = q\vec{v} \times \mu_o \vec{H} \tag{9}$$

where the vorticity, $\vec{\omega} \equiv \nabla \times \vec{v}$. Because both the vorticity and magnetic field terms in this expression are perpendicular to $\vec{v}$, it can be integrated along a stream line joining points a and b to obtain

$$\int_a^b m \frac{\partial \vec{v}}{\partial t} \cdot d\vec{\ell} + \left[\frac{1}{2} m\vec{v} \cdot \vec{v} + q\Phi\right]_a^b = 0 \tag{10}$$

In the steady state, the sum of the kinetic and electric potential energies of a particle are constant, regardless of the imposed magnetic field. Note that, in Eulerian coordinates, particle motions are steady provided Φ is constant.

Theorems of Kelvin and Busch: The curl of Eq. 9 describes the vorticity in Eulerian coordinates:

$$\frac{\partial \vec{\omega}}{\partial t} + \nabla \times (\vec{\omega} \times \vec{v}) = \frac{q}{m} \nabla \times (\vec{v} \times \mu_o \vec{H}) \tag{11}$$

This expression can be integrated over an open surface S enclosed by a contour C moving with the particles. The generalized Leibnitz rule, Eq. 2.6.4, then gives

---

*$\vec{v} \cdot \nabla \vec{v} = (\nabla \times \vec{v}) \times v + \frac{1}{2} \nabla (\vec{v} \cdot \vec{v})$

$$\frac{d}{dt}\int_S \vec{\omega}\cdot\vec{n}\,da = \frac{q}{m}\oint_C (\vec{v} \times \mu_o\vec{H})\cdot d\vec{\ell} \tag{12}$$

Provided there is no imposed magnetic field, the vorticity is conserved over a surface of fixed identity. The magnetic field generates vorticity.

Kelvin's theorem, represented in Eulerian terms by Eq. 12, is often exploited in Lagrangian terms in dealing with axisymmetric electron beams having no θ components of electric or magnetic field. Then, Eq. 4 describes the θ-directed particle motions. Because particle current contributions to $\vec{H}$ are ignored, $\vec{B}$ is solenoidal and can be represented in terms of a vector potential, $\vec{A} = [\Lambda(r,z)/r]\vec{1}_\theta$ (Eq. (g) of Table 2.18.1). Thus,

$$\frac{1}{r}\frac{d}{dt}\left(r^2\frac{d\theta}{dt}\right) = -\frac{q}{m}\left[\frac{1}{r}\frac{\partial\Lambda}{\partial z}\frac{dz}{dt} + \frac{1}{r}\frac{\partial\Lambda}{\partial r}\frac{dr}{dt}\right] \tag{13}$$

What is on the right in Eq. 13 is the rate of change of $\Lambda(r,z)$ for a given particle,

$$d\left(r^2\frac{d\theta}{dt}\right) = -\frac{q}{m}\,d\Lambda \tag{14}$$

From Sec. 2.18, $2\pi\Lambda$ is the total magnetic flux linking a circle of radius r. Thus, with $2\pi\Lambda_o$ defined as the flux linked by a surface on which the particles have no angular velocity, Eq. 14 can be integrated to obtain Busch's theorem:[1]

$$r^2\frac{d\theta}{dt} = -\frac{q}{m}(\Lambda - \Lambda_o) \tag{15}$$

This result is a useful integral of one of the equations of motion. It also lends immediate insight to the result of directing a beam of particles through a complex magnetic field, for if the beam enters from a field-free region with no angular velocity, so that $\Lambda_o = 0$, then it is clear that it leaves the magnetic field with no angular velocity.

11.3 Magnetron Electron Flow

Electron flow in a type of magnetron configuration illustrates the implications of the laws given in Sec. 11.2. A uniform magnetic field, B_z, is imposed collinear with the axis of a cylindrical cathode, surrounded by a coaxial anode, as shown in Fig. 11.3.1. The arrangement is essentially that of a cyclotron-frequency magnetron, an early type of device for converting d-c energy (supplied by the source constraining the anode to a potential V relative to the cathode) to microwave-frequency a-c.

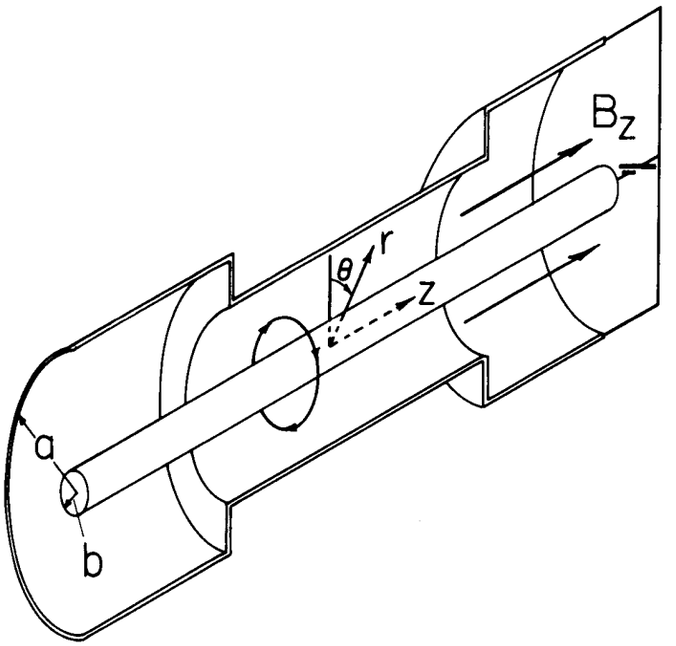

Fig. 11.3.1.

In configuration of cyclotron-frequency magnetron, electrons emitted from inner cathode execute cyclotron motions as they are accelerated toward anode across axial magnetic field.

1. J. R. Pierce, Theory and Design of Electron Beams, D. Van Nostrand Company, New York, 1949, p. 35.

Busch's theorem, Eq. 11.2.15, describes the tendency of the electrons to rotate about the magnetic field. Here, the flux density is uniform, so $2\pi\Lambda = \pi r^2 B_z$. Also, the electrons have no angular velocity at r = a, so $2\pi\Lambda_o = \pi b^2 B_z$. Thus, Eq. 11.2.15 becomes

$$\frac{d\theta}{dt} = \frac{1}{2}\omega_c\left(1 - \frac{b^2}{r^2}\right) \tag{1}$$

where q = -e, and the electron cyclotron frequency is defined as $\omega_c \equiv B_z e/m$.

An electron in the vicinity of the cathode is accelerated in the radial direction by the imposed electric field. As its radial position increases, Eq. 1 shows that it picks up an angular velocity, just as would be expected from the Lorentz force generated by the radial motion. The radial force equation is required to describe the trajectory. Because motions are in the steady state, the energy equation, Eq. 11.2.10, provides a convenient first integral of this equation. The potential and kinetic energies are both zero at the cathode, so that with the use of Eq. 1 for the angular velocity, it follows that

$$\left(\frac{dr}{dt}\right)^2 + \frac{r^2\omega_c^2}{4}\left(1 - \frac{b^2}{r^2}\right)^2 = \frac{2e}{m}\Phi \tag{2}$$

Thus, the electron executes radial motions in a potential well determined by the combination of the electric field tending to pull the electron outward and the magnetic field tending to divert it into an angular motion and eventually back toward the cathode. For the coaxial geometry, and in the absence of space-charge effects, the potential distribution is

$$\Phi = V \ln\left(\frac{r}{b}\right)/\ln\left(\frac{a}{b}\right) \tag{3}$$

and so, Eq. 2 becomes an expression for the velocity as a function of radial position,

$$\frac{d\underline{r}}{dt} = \frac{1}{2}\sqrt{V\frac{\ln r}{\ln a} - r^2\left(1 - \frac{1}{r^2}\right)^2} \tag{4}$$

where the normalization has been introduced,

$$\underline{r} = r/b, \quad \underline{a} = a/b, \quad \underline{t} = t\omega_c,$$

$$\underline{V} \equiv \frac{8\,eV}{\omega_c^2 m b^2} \qquad \omega_c \equiv \frac{B_z e}{m} \tag{5}$$

Typical potential wells are shown in Fig. 11.3.2. For $\underline{V} = 10$, the electron is returned to the cathode while for $\underline{V} = 16$ it collides with the anode. For a critical value, $\underline{V} = \underline{V}_c$, the electron just grazes the anode. This critical value is determined by setting Eq. 4 equal to zero with r = a,

$$V_c = \left(1 - \frac{1}{a^2}\right)a^2 \tag{6}$$

Integration of Eq. 4 gives

$$\underline{r}(t) = 2\int_o^r \frac{dr}{\sqrt{V\frac{\ln r}{\ln a} - r^2\left(1 - \frac{1}{r^2}\right)^2}} \tag{7}$$

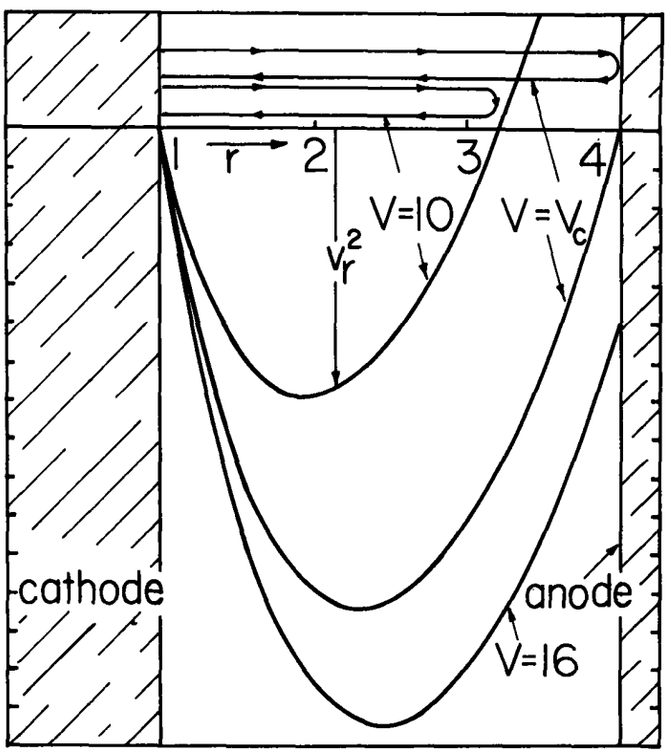

Fig. 11.3.2. Potential wells for cyclotron motions. All variables are normalized.

Numerical integration gives the radial dependence shown in Fig. 11.3.3. In turn, the angular position follows from Eq. 1:

$$\theta = \frac{1}{2}\int_o^t \left(1 - \frac{1}{r^2}\right)dt \tag{8}$$

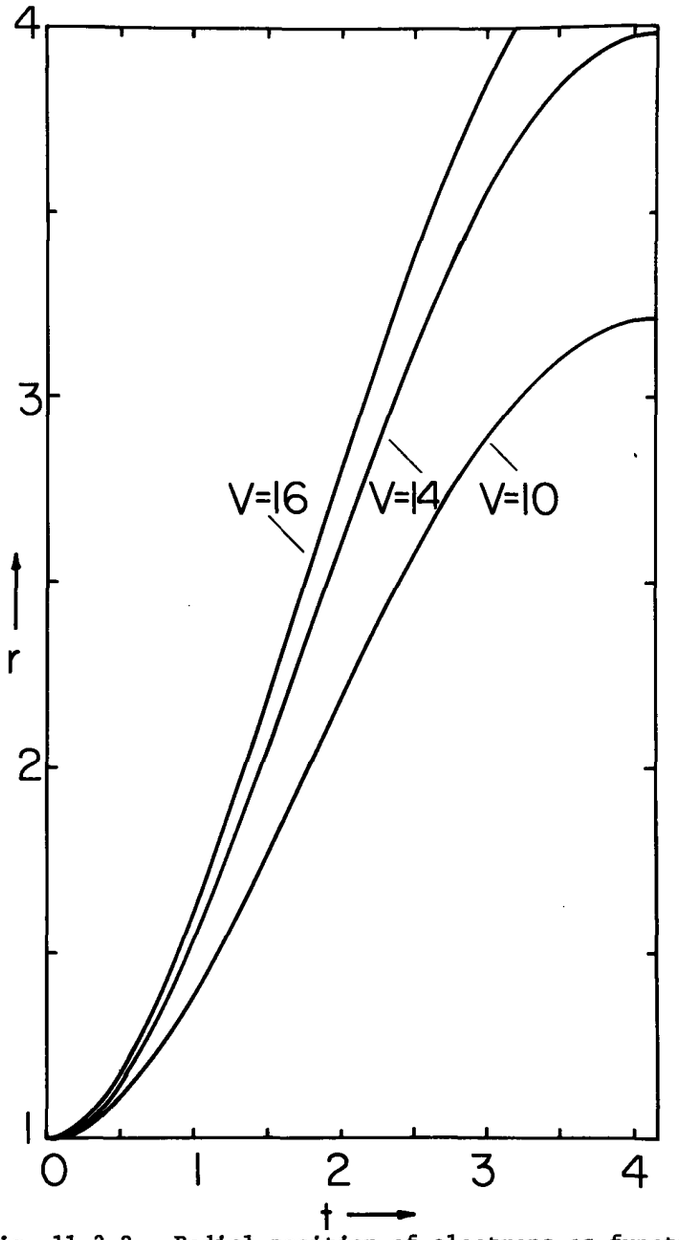

Fig. 11.3.3. Radial position of electrons as function of time. All variables are normalized.

The results from the radial integration can be used to numerically evaluate this expression and obtain the trajectories shown in Fig. 11.3.4.

For these trajectories, where the potential is held fixed, the electron kinetic plus potential energy is conserved. With the introduction of a potential component varying at a frequency on the order of ω_c, energy imparted to an electron by the d-c field can be removed in a-c form. With the d-c voltage adjusted to make $V = V_c$, the effect of a small increase in potential is dramatically different from that of a small decrease. Suppose that as a given electron departs from the cathode, the potential increases. The electron is accelerated by the potential and hence takes energy from the source. But, it also strikes the anode or cathode and is removed after only one orbit. By contrast, an electron that leaves the cathode as the potential is decreasing will be decelerated and hence give up energy to the a-c source. This electron does not strike the anode, and in fact tends to remain in the annulus for many cycles, contributing, along with electrons having a similar phase relation to the a-c field, to giving up energy to the a-c source.

If the a-c source is replaced by a low-loss resonator, the device can sustain self-oscillation. Hence, it can be used as a generator of energy having a frequency on the order of ω_c. For electrons with $B_z = 0.1$ tesla, $\omega_c/2\pi = 2.8$ GHz. Common magnetrons make use of resonators to provide for a traveling-wave interaction with the gyrating electrons.[1]

1. H. J. Reich, P. F. Ordnung, H. L. Krauss and J. G. Skalnik, Microwave Theory and Techniques, D. Van Nostrand Company, Princeton, N.J., pp. 708-735.

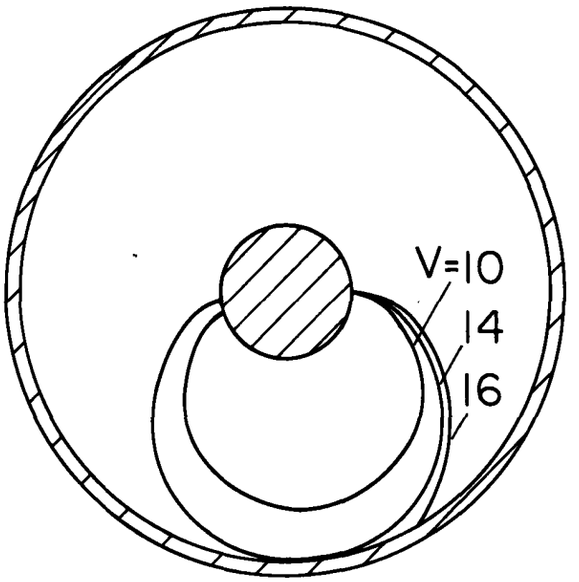

Fig. 11.3.4

Cyclotron motions in cylindrical magnetron with normalized voltage as a parameter.

11.4 Paraxial Ray Equation: Magnetic and Electric Lenses

Oscilloscopes and electron microscopes are devices exploiting electric and magnetic lenses. Simple lens configurations are shown in Fig. 11.4.1. In both the magnetic and electric configurations, the electron beam enters from a region where there is no magnetic field with an axial velocity which, according to the energy equation, Eq. 11.2.10, satisfies the relation

$$\frac{1}{2} m\left(\frac{dz}{dt}\right)^2 = e\Phi \tag{1}$$

The tendency of the axisymmetric magnetic field to focus the beam can be seen by considering the Lorentz force on an electron entering the field somewhat off axis. The longitudinal velocity crosses with the radial component of $\vec{B}$ to produce an angular velocity. Busch's theorem, Eq. 11.2.15, exploits the solenoidal character of $\vec{B}$ to represent this effect of the rotational field in terms of the axial field alone. Thus, even if the magnetic flux density near the axis is approximated as independent of r, for an electron entering from a field-free region, $\Lambda_o = 0$, and the angular velocity can be simply taken as

$$\frac{d\theta}{dt} = \frac{eB_z}{2m} \tag{2}$$

This component in turn crosses with the axial component of $\vec{B}$ to deflect the electron toward the axis. Thus, while in the magnetic field, the electron is deflected toward the z axis; but, in accordance with Eq. 2, once through the field it continues toward the axis without an angular velocity.

In the electric lens, the electron tends to be focused toward the axis as it enters the fringing field, but to be diverted toward the electrode as it leaves the field. The net focusing effect derives from the fringing field having a greater intensity as the electron enters than as it leaves.

Paraxial Ray Equation: An equation for the radial position, r, of an electron as a function of its longitudinal position, z, is the basis for designing both magnetic and electric lenses. It pertains to electrons traversing the fields near the axis where the magnetic flux density is essentially independent of radius, i.e., of the form $B_z(z)$. The radial component of $\vec{B}$ implied by the z dependence is already built into Eq. 2. The radial component of $\vec{E}$ near the axis has an r dependence that can be represented in terms of a given dependence of the potential $\Phi = \Phi(z)$ at $r \approx 0$ by exploiting Gauss' law (Prob. 4.12.1):

$$E_r \simeq -\frac{r}{2}\frac{d^2\Phi}{dz^2} \tag{3}$$

Given $B_z(z)$ and $\Phi(z)$, what is r(z)? With the use of Eqs. 2 and 3, the radial component of the force equation, Eq. 11.2.3, becomes

$$\frac{d^2r}{dt^2} + \frac{1}{4}\left(\frac{eB_z}{m}\right)^2 r = -\frac{e}{m}\frac{r}{2}\frac{d^2\Phi}{dz^2} \tag{4}$$

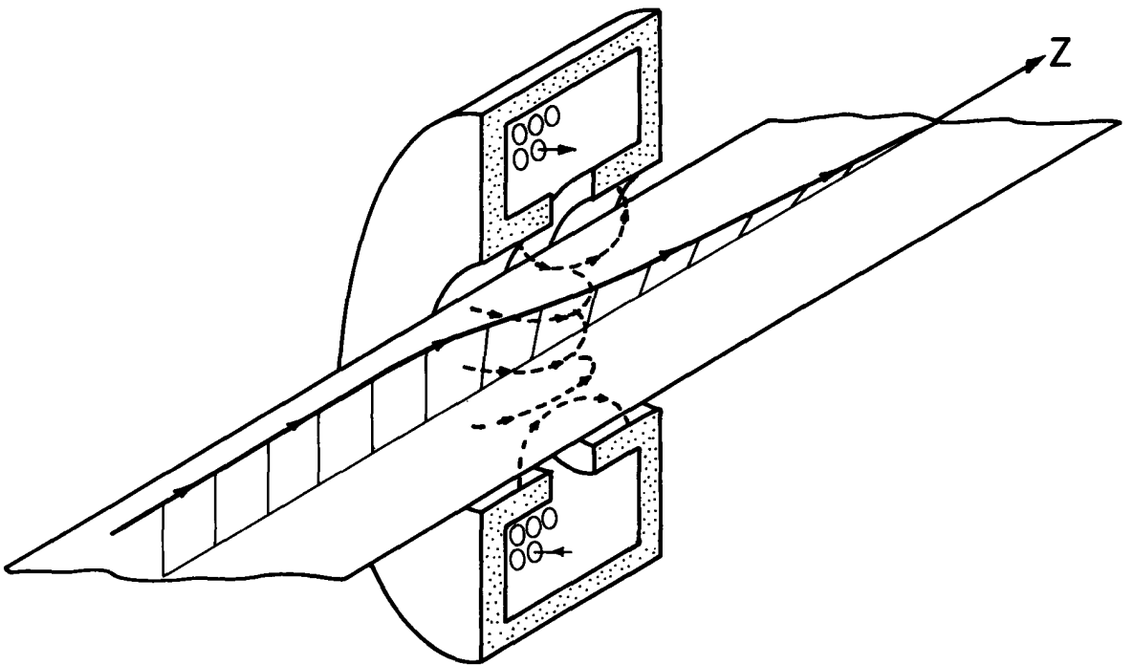

Fig. 11.4.1. (a) Magnetic electron beam lens approximated by fields and focal length of Fig. 11.4.2.

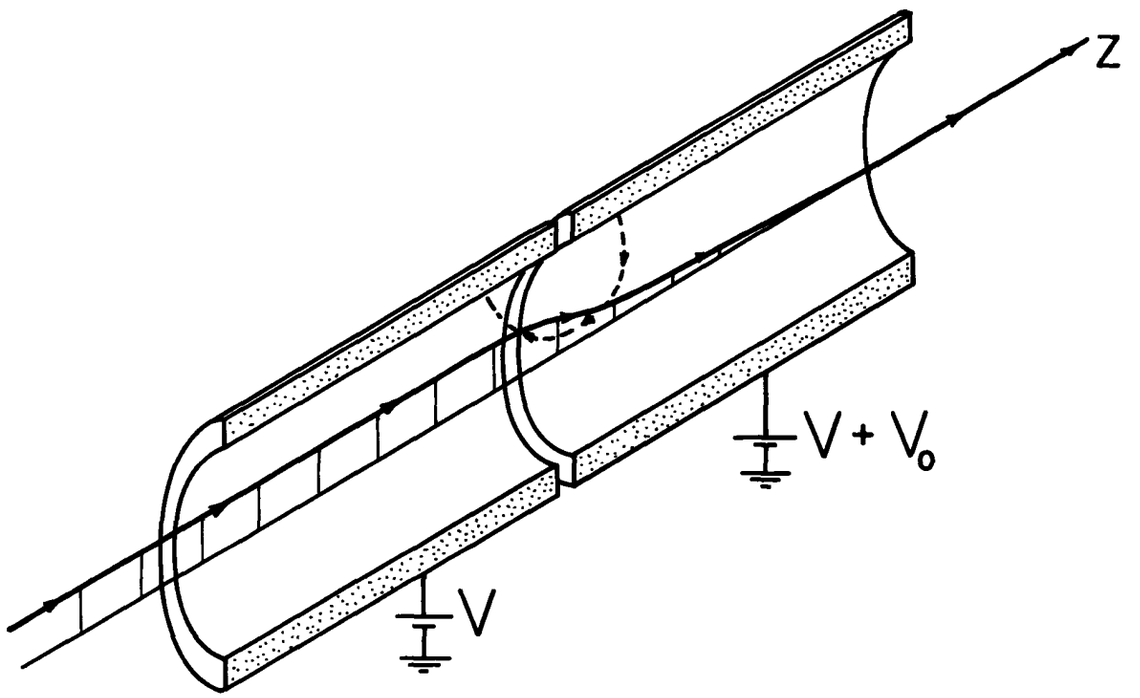

Fig. 11.4.1. (b) Electric electron beam lens with trajectory exemplified by Fig. 11.4.3.

Here, the electron position is pictured with time as the independent parameter. With Φ and B_z independent of time, the electron flow is steady so that time can be eliminated as a parameter and $r = r(z)$. With the objective of writing Eq. 4 with z as the independent variable, observe that

$$\frac{dr}{dt} = \frac{dr}{dz}\frac{dz}{dt} \tag{5}$$

and from the time derivative of Eq. 1 that

$$\frac{d^2z}{dt^2} \simeq \frac{e}{m}\frac{d\Phi}{dz} \tag{6}$$

In the lens region, Eq. 1 is approximate. With Eq. 6, it is therefore assumed that the longitudinal kinetic energy is much greater than that due to the radial and angular velocities. With the use of Eqs. 5 and 6 it follows that

$$\frac{d^2r}{dt^2} = \frac{d^2r}{dz^2}\left(\frac{dz}{dt}\right)^2 + \frac{dr}{dz}\left(\frac{d^2z}{dt^2}\right) = \frac{2e}{m}\Phi\frac{d^2r}{dz^2} + \frac{e}{m}\frac{d\Phi}{dz}\frac{dr}{dz} \tag{7}$$

Thus, the radial component of the force equation, Eq. 4, becomes the paraxial ray equation,[1]

$$\frac{d^2r}{dz^2} + A\frac{dr}{dz} + Cr = 0 \tag{8}$$

where

$$A = \frac{1}{2\Phi}\frac{d\Phi}{dz}; \quad C = \frac{1}{\Phi}\left[\frac{1}{8}\frac{e}{m}B_z^2 + \frac{1}{4}\frac{d^2\Phi}{dz^2}\right]$$

Magnetic Lens: The limiting form of Eq. 8 for a purely magnetic lens is misleading in its simplicity (Prob. 11.4.1):

$$\frac{d^2r}{dz^2} + \kappa^2 r = 0; \quad \kappa \equiv \sqrt{\frac{e}{m8\Phi}}\,B_z \tag{9}$$

Through Eq. 1, Φ represents the incident axial velocity. A reasonable approximation to the on-axis axial field for a solenoidal coil that is long compared to its radius is the distribution shown in Fig. 11.4.2. Thus, in Eq. 9, $B_z = 0$ for $z < 0$ and $z > \ell$, and $B_z = B_o$ over the length ℓ of the lens. An electron entering at the radius r_o, with $dr/dz = 0$, therefore has the trajectory

$$r = r_o \cos \kappa z \tag{10}$$

inside the lens and leaves on a straight-line trajectory with the slope

$$\frac{dr}{dz}(z = \ell) = -r_o\kappa \sin \kappa\ell \tag{11}$$

With the focal length, f, defined as shown in Fig. 11.4.2, it follows that

$$\frac{f}{\ell} = (\kappa\ell \sin \kappa\ell)^{-1} \tag{12}$$

Thus, the focal length decreases with B_z (represented by $\kappa\ell$) as shown in Fig. 11.4.2.

Electric Lens: For numerical integration, Eq. 8 is written in terms of a pair of first-order equations

$$\frac{d}{dz}\begin{bmatrix} r \\ u \end{bmatrix} = \begin{bmatrix} u \\ -Au - Cr \end{bmatrix} \tag{13}$$

where $\underline{z} = z/a$, $\underline{r} = r/a$, $\underline{u} = u$, $\underline{A} = aA$, and $\underline{C} = a^2C$.

As an example, consider the electric lens of Fig. 11.4.1. The potential distribution inside the abutting cylindrical electrodes with radius a that comprise the lens is found in Prob. 5.17.3 to be an infinite series with radial dependences represented by Bessel functions. The z dependences of the dominant terms have an exponential decay away from the plane $z = 0$, $\exp \beta\underline{z}$, where $\beta = 2.4$ is the first root of the Besssel function $J_0(\beta)$. For the present purposes, this longitudinal distribution of

---

1. J. R. Pierce, Theory and Design of Electron Beams, D. Van Nostrand Company, New York, 1949, pp. 72-91.

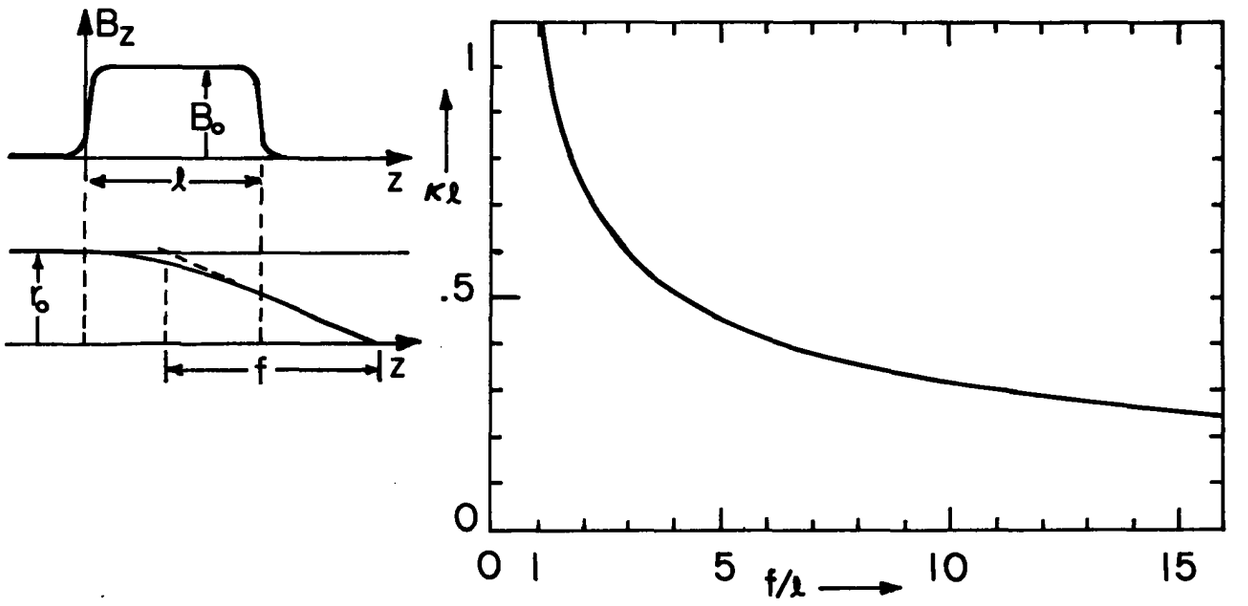

Fig. 11.4.2. For magnetic lens of Fig. 11.4.1a, having essentially uniform axial field B_o over length ℓ, focal length f normalized to ℓ is given as a function of κℓ, defined with Eq. 10.

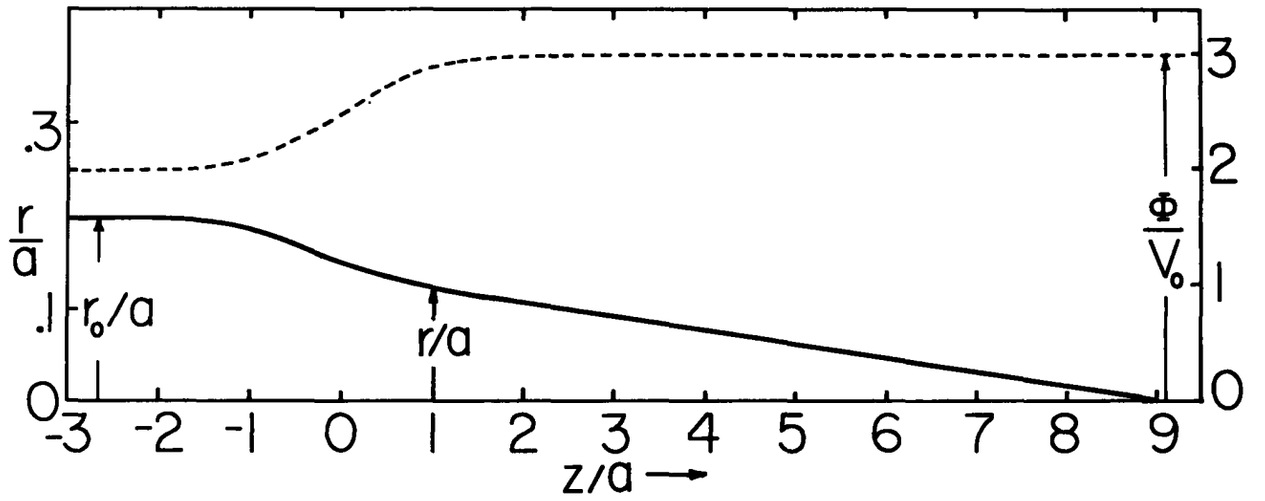

Fig. 11.4.3. For the electric lens of Fig. 11.4.1b, the axial potential distribution is represented by the broken curve. The solid curve is the electron trajectory predicted by Eqs. 13 and 14 with $V_o/V = 0.5$ and $\beta = 2$.

potential is approximated by

$$\Phi = V + \frac{V_o}{2}\left(1 + \tanh\frac{\beta z}{2}\right) \qquad (14)$$

This distribution of potential is shown in Fig. 11.4.3.

Using Eq. 14, A and C (given with Eq. 8) are given functions of z. Note that, although it has space-varying coefficients, the paraxial ray equation, Eq. 8, is linear. Thus, general properties of the electron flow can be deduced using superposition. Numerical integration, using Eqs. 13, is straightforward and results in electron trajectories typified in Fig. 11.4.3. Note that the electron velocity, deduced at any given point from Eq. 1, is increased in the conservative transition through the lens.

11.5 Plasma Electrons and Electron Beams

A model often used to represent electronic motions in a "cold" plasma, and even electron beams in "vacuum," gives the electrons a background of ions that neutralize the space charge. Because the ions are much more massive than the electrons, on time scales of interest for the electron motions, the ions remain essentially motionless.

A uniform axial magnetic field is imposed. In equilibrium, the electrons stream with a uniform velocity U along the magnetic field lines. Electron motions across the magnetic field result in cyclotron orbits that tend to confine the motions to the axial direction.

Because the electron motions are axial, the transverse components of the force equation only give an after-the-fact approximation to the transverse components of the velocity. The axial component of the force equation is, to linear terms in the velocity $\vec{v} = (v_z + U)\vec{i}_z$,

$$m\left(\frac{\partial v_z}{\partial t} + U\frac{\partial v_z}{\partial z}\right) = \frac{e}{m}\frac{\partial \Phi}{\partial z} \tag{1}$$

The current density for electrons having a number density $n_o+n(x,y,z,t)$ and this velocity is

$$\vec{J} = -en_oU\vec{i}_z - e(nU + n_ov_z)\vec{i}_z \tag{2}$$

so that to linear terms, conservation of charge requires that

$$-\frac{\partial}{\partial z}(enU + en_ov_z) - \frac{\partial(ne)}{\partial t} = 0 \tag{3}$$

Finally, because the equilibrium electronic space-charge density, $-n_oe$, is cancelled by that due to positive ions, Gauss' law requires that

$$\nabla^2\Phi = \frac{ne}{\varepsilon_o} \tag{4}$$

Perturbations v_z, n and Φ are described by Eqs. 1, 3 and 4.

Transfer Relations: Consider now a planar layer of plasma or beam having thickness Δ in the x direction. Solutions to Eqs. 1 and 3 take the form $\hat{v}_z = \mathrm{Re}\hat{v}_z(x)\exp j(\omega t - k_y y - k_z z)$, so substitution into Eq. 1 gives

$$\hat{v}_z = -\frac{e}{m}\frac{k_z\hat{\Phi}}{(\omega - k_zU)} \tag{5}$$

In turn, Eq. 3 and this result give

$$\hat{n} = \frac{k_zn_o\hat{v}_z}{(\omega - kU)} = -\frac{k_z^2n_oe}{(\omega - k_zU)^2m}\hat{\Phi} \tag{6}$$

Finally, this relation combines with Eq. 4 to show that the potential distribution must satisfy

$$\frac{d^2\hat{\Phi}}{dx^2} - \gamma^2\hat{\Phi} = 0; \quad \gamma^2 = k_y^2 + k_z^2\left[1 - \frac{\omega_p^2}{(\omega - k_zU)^2}\right] \tag{7}$$

where the plasma frequency is defined as $\omega_p = \sqrt{n_oe^2/\varepsilon_om}$. This relation is of the same form as for representing Laplace's equation in Sec. 2.16. Thus, the transfer relations are the same as in Table 2.16.1, provided that γ is defined as in Eq. 7. Note that a similar derivation leads to transfer relations in cylindrical geometry so that the transfer relations for an annular beam are as given by the relations of Table 2.16.2 with coefficients suitably defined. For example, $f_m(x,y) \to f_m(x,y,k \to \gamma)$, where γ may differ from one annular region to another.

Space-Charge Dynamics: The sheet beam shown in Fig. 11.5.1 exemplifies the dynamics of beams in uniform structures. The surrounding region is free space, with walls to either side constrained by a traveling wave of potential. The wall potential can be regarded as a given drive, although more generally it can be made consistent with external electromagnetic structures. The velocity is purely axial, so the boundaries do not deform and boundary conditions are simply

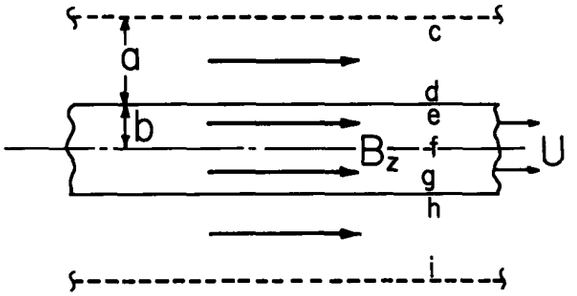

Fig. 11.5.1

Planar electron beam in uniform axial magnetic field.

$$\hat{\Phi}^c = \hat{V}_o, \quad \hat{\Phi}^d = \hat{\Phi}^e, \quad \hat{D}_x^d = \hat{D}_x^e, \quad \hat{D}_x^f = 0 \tag{8}$$

Here, interest is restricted to motions that are even in the potential, so with the last boundary condition it is presumed that $\hat{\Phi}^c = \hat{\Phi}^i$.

Transfer relations for the free-space region and for the beam follow from Eq. 7 and Table 2.16.1:

$$\begin{bmatrix} \hat{D}_x^c \\ \hat{D}_x^d \end{bmatrix} = \varepsilon k \begin{bmatrix} -\coth ka & \frac{1}{\sinh ka} \\ -\frac{1}{\sinh ka} & \coth ka \end{bmatrix} \begin{bmatrix} \hat{\Phi}^c \\ \hat{\Phi}^d \end{bmatrix} \tag{9}$$

$$\begin{bmatrix} \hat{D}_x^e \\ 0 \end{bmatrix} = \varepsilon\gamma \begin{bmatrix} -\coth \gamma b & \frac{1}{\sinh \gamma b} \\ -\frac{1}{\sinh \gamma b} & \coth \gamma b \end{bmatrix} \begin{bmatrix} \hat{\Phi}^d \\ \hat{\Phi}^f \end{bmatrix} \tag{10}$$

The last equation gives $\hat{\Phi}^f$ in terms of $\hat{\Phi}^d$. This is inserted into Eqs. 9b and 10a, set equal to each other. The resulting expression can be solved for $\hat{\Phi}^d$. Substituted into Eq. 9a, that gives

$$\hat{D}_x^c = -\varepsilon k \frac{(k + \gamma \coth ka \tanh \gamma b)}{D(\omega,k)} \hat{\Phi}^c; \quad D \equiv k \coth ka + \gamma \tanh \gamma b \tag{11}$$

This result gives the driven response, but also embodies the temporal modes and spatial modes, as discussed in Secs. 5.15 and 5.17. These are described by the dispersion equation, $D(\omega,k) = 0$.

Temporal Modes: It is clear that there are no roots of this expression having γ purely real. Purely imaginary roots abound, as is evident by substituting $\gamma \to j\alpha$:

$$(\alpha b)\tan(\alpha b) = (kb)\coth[(kb)\frac{a}{b}] \tag{12}$$

Graphical solution of this expression, for a given a/b, results in roots, α_n. The frequencies of associated temporal modes follow from the definition of $\gamma^2 = -\alpha^2$ given with Eq. 7:

$$\frac{\omega}{\omega_p} = bk\left(\frac{U}{\omega_p b}\right) \pm \left[1 + \frac{(b\alpha_n)^2}{(bk)^2}\right]^{-1/2} \tag{13}$$

Here it has been assumed that $k_y = 0$. This dispersion equation is represented graphically by Fig. 11.5.2.

For each real wavenumber, k, there are two eigenfrequencies representing space-charge waves. In the absence of convection these have phase velocities, ω/k, in the positive and negative directions. With convection, these waves are respectively the fast and slow space-charge waves that are central to a variety of electron-beam devices and interactions. The transverse dependence of a temporal mode having a real wavenumber $k_z = k$ is sinusoidal within the beam and exponential in the surrounding regions of free space, as depicted by the inserts to Fig. 11.5.2.

Without the equilibrium streaming, the temporal modes are similar to those of the internal electrohydrodynamic space-charge waves of Sec. 8.18. There are an infinite number of modes, $n > p$, within the region of the ω-k plot bounded by the fast and slow wave branches for any given mode $n = p$. In the

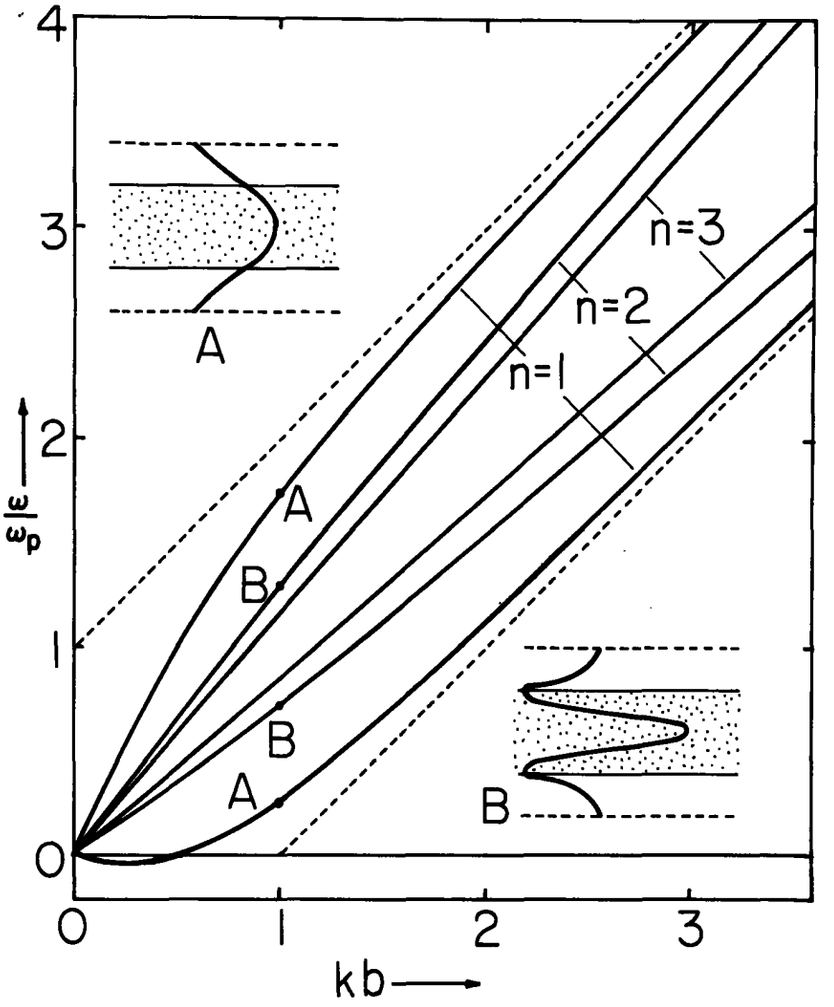

Fig. 11.5.2. Normalized angular frequency as a function of normalized wavenumber for space-charge waves on planar electron beam of Fig. 11.5.1. Inserts show transverse distribution of potential for two lowest eigenmodes at longitudinal wavenumber kb = 1.

frame of reference moving with the beam velocity U, the frequencies, $\omega - kU$, of these modes approach zero as the mode number, and hence the number of oscillations over the transverse dimension of the beam, approaches infinity.

Spatial Modes: Typically, in electron beam devices, it is the response to a given driving frequency that is of interest. The homogeneous part of the response is made up of spatial modes having wavenumbers that are solutions to $D(\omega,k) = 0$, with ω the specified driving frequency. In general, these are complex roots of a complex equation. However, those modes having real wavenumbers for the real driving frequency can be identified from Fig. 11.5.2.

11.6 Method of Characteristics

In representing the evolution of a continuum of particles, it is natural to express the partial differential equations of motion as ordinary equations with time as the independent variable. As illustrated in Secs. 5.3, 5.6 and 5.10, what can result is a complete picture of the temporal evolution, but one viewed along a characteristic line in $(\vec{r},t)$ space. The price paid for the characteristic formulation is an implicit dependence on space. That the characteristic lines do not have to be identified with particles is illustrated in this and the next five sections. Physically, the characteristics now represent waves rather than particles. However, the objective is again to reduce partial differential equations to ordinary ones.

If the equations, written as a system of first-order expressions, have coefficients that are not functions of the independent variables, they are said to be quasi-linear. An example comes from the one-dimensional longitudinal motions of a highly compressible gas.

For now, there is no external force density and viscous effects are ignored. Thus, with the assumption that $\vec{v} = v(z,t)\vec{i}_z$, $p = p(z,t)$ and $\rho = \rho(z,t)$, the force equation, Eq. 7.16.6, becomes

$$\rho\left(\frac{\partial v}{\partial t} + v\frac{\partial v}{\partial z}\right) + \frac{\partial p}{\partial z} = 0 \tag{1}$$

The flow is not only assumed adiabatic, but initiated in such a way that every fluid particle can be traced backward in time along a particle line to a point in space and time when it had the same state $(p,\rho) = (p_o,\rho_o)$. The flow is initiated from a uniform state. Thus, Eq. 7.23.13 holds throughout the region of interest, and it follows that

$$\frac{\partial p}{\partial z} = a^2\frac{\partial \rho}{\partial z}; \quad a \equiv \sqrt{\gamma\frac{p_o}{\rho_o}}\left(\frac{\rho}{\rho_o}\right)^{(\gamma-1)/2} \tag{2}$$

It follows that Eq. 1 can be written as

$$(0)\frac{\partial \rho}{\partial t} + (a^2)\frac{\partial \rho}{\partial z} + (\rho)\frac{\partial v}{\partial t} + (\rho v)\frac{\partial v}{\partial z} = 0 \tag{3}$$

Conservation of mass, Eq. 7.2.3, provides the second equation in (v,ρ):

$$(1)\frac{\partial \rho}{\partial t} + (v)\frac{\partial \rho}{\partial z} + (0)\frac{\partial v}{\partial t} + (\rho)\frac{\partial v}{\partial z} = 0 \tag{4}$$

These last two expressions typify systems of first-order partial differential equations with two independent variables (z,t). They are not linear, but do have coefficients depending only on the dependent variables (v,ρ). The characteristic equations are now deduced following the reasoning of Courant and Friedrichs.[1]

First Characteristic Equations: Arbitrary incremental changes in the time and position result in changes in (ρ,v) given by

$$d\rho = \frac{\partial \rho}{\partial t}dt + \frac{\partial \rho}{\partial z}dz \tag{5}$$

$$dv = \frac{\partial v}{\partial t}dt + \frac{\partial v}{\partial z}dz \tag{6}$$

The objective now is to find a linear combination of Eqs. 3 and 4 that takes the form

$$f(\rho)d\rho + g(v)dv = 0 \tag{7}$$

because this equation can be integrated. To this end, note that a line in the z-t plane along which $d\rho$ and dv are to be evaluated has not yet been specified. It can be selected to guarantee the desired form of the equations of motion.

---

1. R. Courant and K. O. Friedrichs, Supersonic Flow and Shock Waves, Interscience Publishers, New York, 1948, pp. 40-45.

A linear combination of Eqs. 3 and 4 is written by multiplying Eq. 3 by the parameter λ_1 and Eq. 4 by λ_2 and taking the sum:

$$\frac{\partial \rho}{\partial t}(\lambda_1) + \frac{\partial \rho}{\partial z}(\lambda_1 v + \lambda_2 a^2) + \frac{\partial v}{\partial t}(\rho\lambda_2) + \frac{\partial v}{\partial z}(\lambda_1 \rho + \lambda_2 v\rho) = 0 \tag{8}$$

If this expression is to have the same form as Eq. 7, where $d\rho$ and dv are given by Eqs. 5 and 6, then

$$\frac{dz}{dt} = \frac{\lambda_1 v + \lambda_2 a^2}{\lambda_1}; \quad \frac{dz}{dt} = \frac{\lambda_1 \rho + \lambda_2 v\rho}{\rho\lambda_2} \tag{9}$$

These expressions are linear and homogeneous in the coefficients (ρ, v):

$$\begin{bmatrix} \frac{dz}{dt} - v & -a^2 \\ -\rho & \frac{dz}{dt} - v \end{bmatrix} \begin{bmatrix} \lambda_1 \\ \lambda_2 \end{bmatrix} = \begin{bmatrix} 0 \\ 0 \end{bmatrix} \tag{10}$$

It follows that if the coefficients are to be finite, the determinant of the coefficients must vanish. Thus,

$$\frac{dz}{dt} = v \pm a; \quad C^{\pm} \tag{11}$$

If v, ρ and hence $a(\rho)$ were known functions of (z,t), these expressions could be solved to give families of curves along which Eq. 8 would take the form of Eq. 7. Apparently two such families have been found. They are called the Ist characteristic equations and respectively designated by C^+ and C^-.

Differential equations, such as Eqs. 3 and 4, for which the Ist characteristic equations are real, are said to be hyperbolic. Elliptic equations, for which the Ist characteristics are not real, must be solved by some other method than now described.

Second Characteristic Lines: The goal of writing Eq. 8 in the form of Eq. 7 is achieved by factoring λ_1 from the first two terms and λ_2 from the third and fourth terms, and then substituting for the coefficients of the second and fourth terms, respectively, using Eqs. 5 and 6:

$$\lambda_1\left(\frac{\partial \rho}{\partial t} + \frac{\partial \rho}{\partial z}\frac{dz}{dt}\right) + \rho\lambda_2\left(\frac{\partial v}{\partial t} + \frac{\partial v}{\partial z}\frac{dz}{dt}\right) = 0 \tag{12}$$

If this expression is multiplied by dt and divided by λ_1, the desired form follows:

$$d\rho + \rho\frac{\lambda_2}{\lambda_1} dv = 0 \tag{13}$$

To establish the ratio λ_2/λ_1, either of Eqs. 10 can be used. For example, substituting λ_2/λ_1 as found from Eq. 10a gives

$$d\rho + \frac{\rho}{a^2}\left(\frac{dz}{dt} - v\right)dv = 0 \tag{14}$$

This expression is further simplified by using the Ist characteristic equations, Eqs. 11, to write

$$dv \pm \frac{a}{\rho} d\rho = 0 \quad \text{on } C^{\pm} \tag{15}$$

where the choice of signs is determined by which sign is being used in Eqs. 11.

With $a(\rho)$ specified by Eq. 2, the IInd characteristic equations can be integrated:

$$v \pm \frac{2a(\rho)}{\gamma - 1} = c_{\pm} \text{ on } C^{\pm} \tag{16}$$

Here, c_+ and c_- are respectively invariants along the C^+ and C^- characteristic lines.

Systems of First-Order Equations: The method used to determine the first and second characteristic equations makes their deduction a logical response to the objective. As long as the number of independent variables (z,t) remains only two, the same technique can be used with more complex problems.

But, it is convenient in dealing with several first order equations to use a more formal approach to finding the characteristics. Although the formalism now considered appears to be different, in fact the characteristic equations are the same.

Equations 3 and 4 are particular cases of the first two expressions in the set of four,

$$\begin{bmatrix} C \\ D \\ d\rho \\ dv \end{bmatrix} = \begin{bmatrix} A_1 & A_2 & A_3 & A_4 \\ B_1 & B_2 & B_3 & B_4 \\ dt & dz & 0 & 0 \\ 0 & 0 & dt & dz \end{bmatrix} \begin{bmatrix} \frac{\partial \rho}{\partial t} \\ \frac{\partial \rho}{\partial z} \\ \frac{\partial v}{\partial t} \\ \frac{\partial v}{\partial z} \end{bmatrix} \tag{17}$$

Here, the coefficients A_i and B_i are in general functions of (ρ,v,z,t). Also, for generality, $C = C(\rho,v,z,t)$ and $D = D(\rho,v,z,t)$ represent the possibility that the differential equations are inhomogeneous in the sense that they have terms which do not involve partial derivatives. The last two expressions will be recognized as the differential relations for $d\rho$ and dv, Eqs. 5 and 6.

Following the formalism leading to Eqs. 11 and 15, Eqs. 17a and 17b are multiplied respectively by λ_1 and λ_2, and added. Then the ratio of coefficients for the respective $\partial/\partial t$'s and $\partial/\partial z$'s are required to be dz/dt, and the result is two homogeneous equations in the λ's:

$$\begin{bmatrix} (A_2 - A_1 \frac{dz}{dt}) & (B_2 - B_1 \frac{dz}{dt}) \\ (A_4 - A_3 \frac{dz}{dt}) & (B_4 - B_3 \frac{dz}{dt}) \end{bmatrix} \begin{bmatrix} \lambda_1 \\ \lambda_2 \end{bmatrix} = 0 \tag{18}$$

The first characteristic equations are found by requiring that the determinant of the coefficients in Eq. 18 vanish.

This same condition is obtained by requiring that the determinant of the coefficients in Eq. 17 vanish. To see this, rows three and four are multiplied by $(dt)^{-1}$. Then rows three and four are multiplied respectively by $-A_1$ and $-A_3$ and added to row one. Similarly, rows three and four can be multiplied respectively by $-B_1$ and $-B_3$ and added to row two. The result is the determinant

$$\begin{bmatrix} 0 & A_2 - A_1 \frac{dz}{dt} & 0 & A_4 - A_3 \frac{dz}{dt} \\ 0 & B_2 - B_1 \frac{dz}{dt} & 0 & B_4 - B_3 \frac{dz}{dt} \\ dt & dz & 0 & 0 \\ 0 & 0 & dt & dz \end{bmatrix} = 0 \tag{19}$$

Now, by expanding about the dt's that appear in columns with all other entries zero, the same requirement as given by Eq. 18 is obtained. The first characteristic equations are obtained by writing the differential equations in the form of Eq. 17 and simply requiring that the determinant of the coefficients vanish. The same approach can be used with an arbitrary number of dependent variables.

To solve Eqs. 17 for any one of the four partial differentials would require substituting the column on the left for the column of the square matrix corresponding to the desired partial derivative, and to divide the determinant of the resulting matrix by the coefficient determinant. However, the coefficient determinant has already been required to vanish, since that is just the condition for obtaining the Ist characteristic equations. Thus, if the partial derivatives are not infinite, the numerator determinants must also vanish. Four equations result which are reducible to the IInd characteristic equations.

As an example, consider once again Eqs. 3 and 4. The coefficient determinant is

$$\begin{bmatrix} 1 & v & 0 & \rho \\ 0 & a^2 & \rho & \rho v \\ dt & dz & 0 & 0 \\ 0 & 0 & dt & dz \end{bmatrix} = 0 \tag{20}$$

and can be expanded, taking advantage of the zeros, to give Eqs. 11. Then the numerator determinant for finding $\partial\rho/\partial t$ is the coefficient matrix with the column matrix on the left in Eq. 17 substituted for the first column on the right, or

$$\begin{bmatrix} 0 & v & 0 & \rho \\ 0 & a^2 & \rho & \rho v \\ d\rho & dz & 0 & 0 \\ dv & 0 & dt & dz \end{bmatrix} = 0 \qquad (21)$$

With the use of the first characteristic equations, Eq. 21 reduces to the second characteristic equations given by Eqs. 15. A check of the other three equations obtained by substituting the column matrix in the second, third and fourth columns gives the same result.

11.7 Nonlinear Acoustic Dynamics: Shock Formation

The longitudinal motions of a gas under adiabatic conditions both serve as a vehicle for seeing how the characteristic equations are used, and provide insight into the nonlinear phenomena that are responsible for wave steepening and shock formation.[1] (See Reference 10, Appendix C.)

Initial Value Problem: The characteristic equations are given by Eqs. 11.6.11 and 11.6.16. Although there is no necessity for linearizing, it is helpful to realize how perturbations from a uniform flow with velocity U, density ρ_o and acoustic velocity a_o are represented by the characteristics. (The linearized versions of Eqs. 11.6.3 and 11.6.4 are the one-dimensional forms of Eqs. 7.11.1-7.11.3.) In that limit, the first characteristic equations have $U \pm a_o$ on the right, and are therefore integrable to give straight lines with slopes equal to the wave velocities $U \pm a_o$ in the $\pm z$ directions. These families of lines are illustrated in Fig. 11.7.1a.

In general, v and a can vary and the characteristic lines sketched in Fig. 11.7.1b in the z-t plane are not known. However, the functions v and $a(\rho)$ are known at an intersection of the C^+ and C^- characteristics, wherever that may be. That is, suppose the initial values of v and a at points A and B shown in Fig. 11.7.2 are given (at t = 0 but at different points along the z axis). Then, from Eq. 11.6.16a, c_+ is

$$c_+^a = [v]_A + \left[\frac{2a(\rho)}{\gamma - 1}\right]_A \qquad (1)$$

Similarly, from the initial conditions at B,

$$c_-^b = [v]_B - \left[\frac{2a(\rho)}{\gamma - 1}\right]_B \qquad (2)$$

Now, c_+^a is invariant along the C^+ characteristic, and c_-^b is invariant along the C^- characteristic. At point C, certainly at a later time and generally at a different point in space than either A or B, Eqs. 11.6.16 both hold, with $c_+ = c_+^a$ and $c_- = c_-^b$. Hence, they can be solved simultaneously for either v or $a(\rho)$. For the former, addition yields

$$[v]_C = \frac{c_+^a + c_-^b}{2} \qquad (3)$$

Given conditions at A and B, the solution at C is established. The solution is known, but where and when does it apply? The Ist characteristic equations must be integrated to determine the location of C in the z-t plane.

The characteristic lines have the physical interpretation of being wave fronts. Conditions at A and B propagate along the respective lines and combine at C to give the response. It is remarkable that what happens at C depends only on the conditions at A and B. But the "location" of C is determined by initial conditions everywhere between A and B, as can be seen by considering how a computer can be used to "march" from left to right in the z-t plane and determine the solution in a stepwise fashion.

---

1. R. Courant and K. O. Friedrichs, Supersonic Flow and Shock Waves, Interscience Publishers, New York, 1948, pp. 40-45.

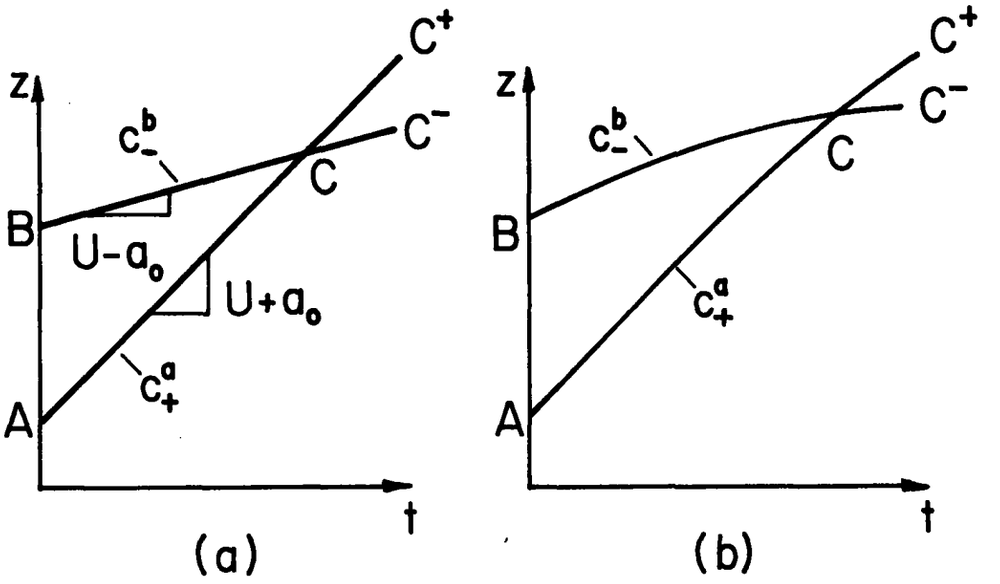

Fig. 11.7.1. (a) Linear case where v and a are known constants and the characteristics are straight lines. (b) c_+^a and c_-^b are established from the initial conditions at A and B. Because they are invariant along the C^+ and C^- characteristics respectively, the solution is established where the characteristics intersect at C.

The Response to Initial Conditions: In the linearized case, the characteristics are straight lines as shown in Fig. 11.7.1a. The point of intersection, C, is then determined because the z coordinates of A and B, as well as the characteristic slopes, are known. The effect of the nonlinearity is to bend the characteristic lines in the z-t plane. This is not surprising, because it would be expected that the velocity of propagation of wavefronts (the slope of dz/dt of a characteristic line) depends on the local speed of sound superimposed on the local velocity of the fluid.

In Fig. 11.7.2, a discrete representation of the characteristics is made. Initial values are given at the positions $z = z_i$. The C^+ line emanating from z_j and the C^- line from z_k cross at some point (j,k). To find the solution throughout the z-t plane,

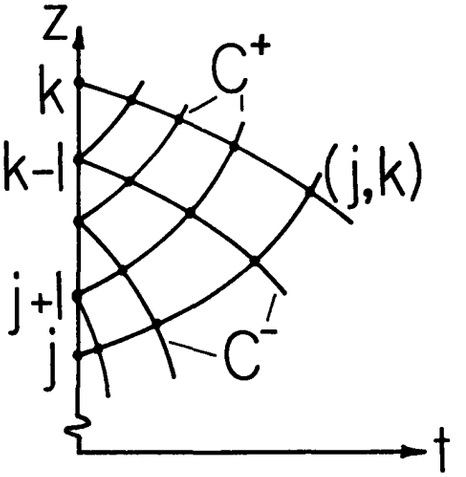

Fig. 11.7.2. The (z-t) intersection of jth C^+ characteristic and kth C^- characteristic is denoted by (j,k).

a) Evaluate the invariants using the initial values in Eqs. 1 and 2:

$$c_{\pm}^i = [v] \pm [\frac{2a}{\gamma-1}] \tag{4}$$

b) Tabulate solutions at all intersections (j,k) by solving simultaneously Eqs. 4:

$$[v]_{(j,k)} = \frac{1}{2}(c_+^j + c_-^k)$$

$$[a]_{(j,k)} = \frac{1}{2}(c_+^j - c_-^k)(\frac{\gamma-1}{2}) \tag{5}$$

c)Use the results of (b) to tabulate all characteristic slopes at the intersections (j,k):

$$[\frac{dz}{dt}]_{(j,k)}^{\pm} = [v]_{(j,k)} \pm [a]_{(j,k)} \tag{6}$$

d) Start when t = 0 and build up grid by approximating characteristic lines as being straight between points of intersection. Coordinates and slopes at neighboring points $(z_{j,k-1})$ and $(z_{j+1,k})$ determine z-t coordinates of point $(z_{j,k})$. Thus both the solution and the z-t coordinate at which it applies are determined.

Simple Waves: Initial and boundary conditions are illustrated in Fig. 11.7.3 in which the fluid is initially static [v = 0, a(ρ) = a] and is driven by a piston at one end. The piston, with position shown as a function of time in the figure, is initially at rest at z = 0 and is pushed into the gas until it reaches the final position $z = z_o$. The slope of the piston trajectory has the physical significance of being the piston velocity; hence the velocity of the fluid along the piston trajectory is the slope of the trajectory, $(dz/dt)_p$.

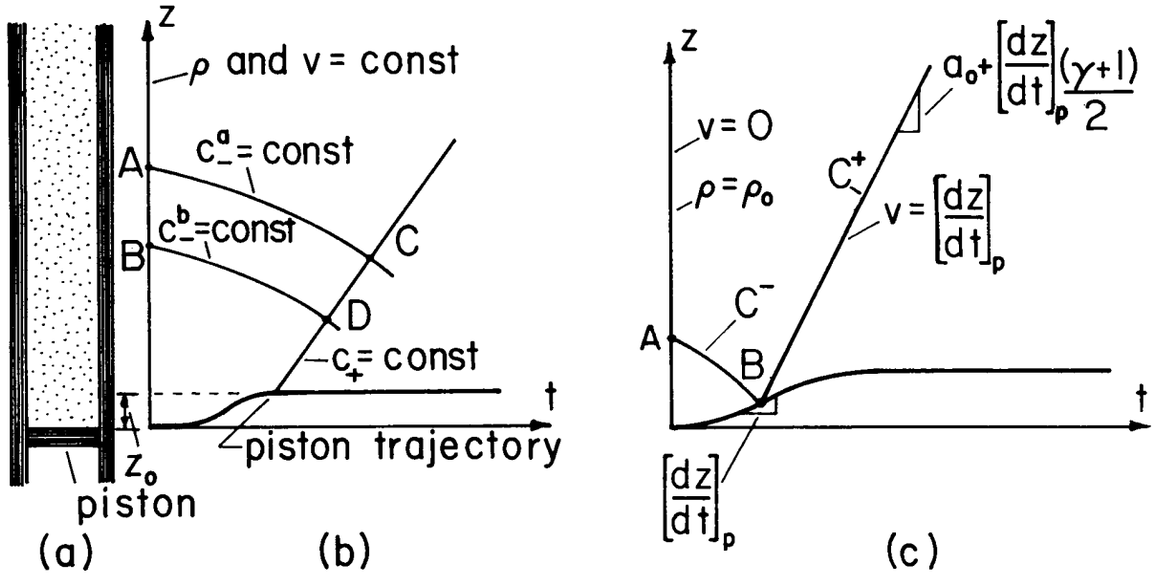

Fig. 11.7.3. (a) Gas filled tube driven by piston. (b) Boundary and initial value problem where the initial state of the fluid is uniform (when t = 0) and an excitation is applied by means of a piston which is initially at z = 0. (c) a and v are constant along C^+ characteristics, which are straight lines.

By definition, the initial boundary value problem described leads to simple-wave motions. This name designates the response to a boundary condition with the region of interest having a uniform initial state.

Consider the two C^- characteristics sketched in Fig. 11.7.3b. They intersect the z-axis at points A and B, where the initial conditions require that the fluid is stationary (v = 0), and that the velocity of sound is a_o. From this, it follows that the invariants c_-, established at point A and at point B using Eq. 11.6.16, are the same,

$$c_-^a = c_-^b = \frac{-2a_o}{\gamma-1} \tag{7}$$

Points C and D are intersections with the same C^+ characteristic. Hence, the invariant c_+ is the same at points C and D. Given c_+ and c_- along the characteristics which intersect at C, the velocity and density at that point are found by simultaneously solving Eqs. 11.6.16,

$$v(C) = \frac{c_+ + c_-^a}{2} \tag{8}$$

Similarly,

$$v(D) = \frac{c_+ + c_-^b}{2} \tag{9}$$

However, because of the special nature of the initial conditions, Eq. 7 requires that $c_-^a = c_-^b$, and it follows that v, and by similar arguments, a(ρ) or ρ, are constant along any given C^+ characteristic. Even more, because v and a are constant, it then follows from Eqs. 11.6.11 that the C^+ characteristics have constant slope.

The C^+ characteristics appear as shown in Fig. 11.7.3c. Along the characteristics shown, the velocity, v, remains equal to that of the fluid at the piston (point B), where

$$v = \left(\frac{dz}{dt}\right)_p \tag{10}$$

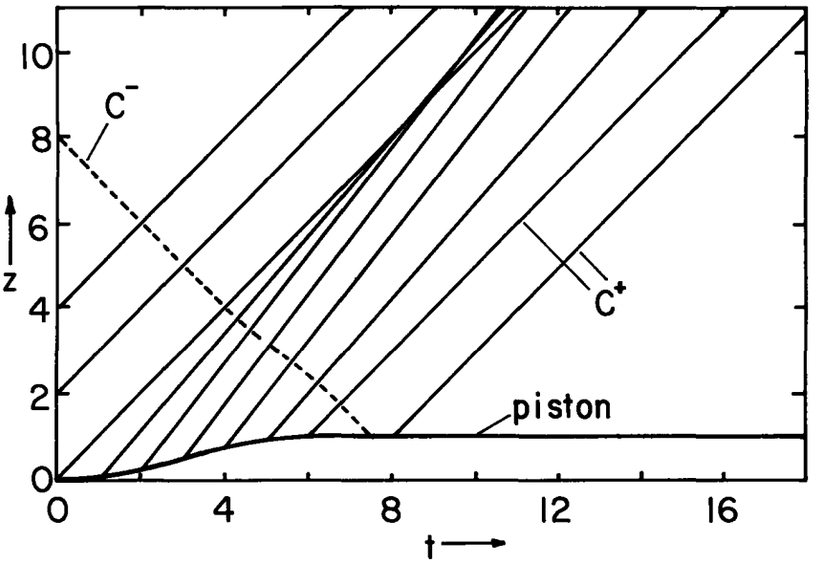

Fig. 11.7.4. Simple-wave characteristic lines initiated by piston.

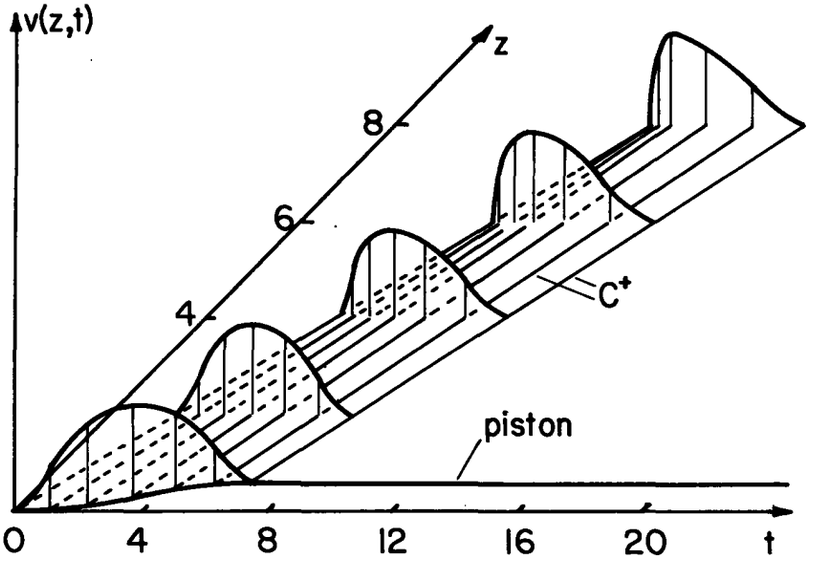

Fig. 11.7.5. Velocity of fluid as a function of z and t.

With Eq. 7, c_- is established along the C^- characteristic, and it follows from Eq. 11.6.16 that the sound velocity $a(\rho)$ at the point B on the piston surface, where v is $(dz/dt)_p$, is

$$a = a_o + \frac{(\gamma-1)}{2}\left(\frac{dz}{dt}\right)_p \tag{11}$$

This velocity of sound, a, along with the implied density ρ and velocity v from Eq. 10, remain constant along the C^+ characteristic. The picture of the dynamics is now complete, because the C^+ characteristic emerging from B has a constant slope given by the Ist characteristic equation, Eq. 11.6.11:

$$\frac{dz}{dt} = a_o + \left(\frac{dz}{dt}\right)_p \frac{(\gamma+1)}{2} \tag{12}$$

Suppose that the piston position depends on time, as shown in Figs. 11.7.4 and 11.7.5. With no instantaneous change in velocity when t = 0, the piston reaches a maximum velocity when t = 3, and then decelerates to zero velocity by the time t = 6. The C^+ characteristics originating on the piston can be plotted directly using Eq. 12. Here, it is assumed for convenience in making the drawing that γ and

a_o are unity. Note that as the piston velocity increases, the characteristic lines increase in slope, while characteristics originating from the piston when it decelerates decrease in slope. Remember that the fluid velocity v at the surface of the piston is just the slope of the piston trajectory. This velocity remains constant along any given C^+ characteristic. Hence, a plot of the fluid velocity as a function of (z,t) appears as shown in Fig. 11.7.5. In regions where the characteristics tend to cross, the waveform tends to steepen, until at points in the z-t plane where the characteristics cross, the velocity becomes discontinuous. This discontinuity in the wavefront is referred to as a shock wave. With the steepening, variables change more and more rapidly in space. This shortening of characteristic lengths brings into play phenomena not included in the adiabatic model.

Note that a shock wave tends to form from a compression of the gas. By contrast, the deceleration of the piston tends to produce a waveform which smoothes out. Fluid near the leading edge of the pulse is moving in the positive z direction, and this adds to the velocity of a perturbation, a, in that region. Hence, variables within the pulse tend to propagate more rapidly than those nearer the leading edge, and the wave steepens at the leading edge. Similar arguments can be used to explain the smoothing out of the pulse at the trailing edge. In any actual situation, γ will exceed unity, and the increase in density, and hence acoustic velocity, makes a further contribution toward the nonlinear effect of shock formation. In actuality, effects of viscosity and heat conduction prevent the formation of a perfectly abrupt discontinuity in ρ, a, and v.

Limitation of the Linearized Model: To be quantitative in giving conditions under which nonlinearities are important, suppose that the piston is set into motion when t = 0 and reaches the velocity $(dz/dt)_p$ by the time t = T. Then the characteristics are essentially as shown in Fig. 11.7.6, where the displacement of the piston is ignored compared to other lengths of interest. From Eq. 12, the characteristic originating at t = 0, z = 0, is

$$z = a_o t \tag{13}$$

while that originating at t = T, z = 0 is

$$z = [a_o + (\frac{dz}{dt})_p(\frac{\gamma+1}{2})](t - T) \tag{14}$$

Nonlinear effects will be important at z = ℓ, where these characteristics cross. Solving Eqs. 13 and 14 simultaneously for z = ℓ by eliminating t gives

$$\ell = a_o T\left[\frac{a_o}{(\frac{dz}{dt})_p(\frac{\gamma+1}{2})} + 1\right] \tag{15}$$

Hence, for a given characteristic time T, say the period in a sinusoidally excited system, there is a length (some fraction of ℓ) over which a linear model gives an adequate prediction. This distance becomes large as $(dz/dt)_p$ becomes small compared to the velocity of sound, a_o. It is clear, also, that making the period small (the frequency high) can also lead to nonlinearities. This fact is not as limiting as it seems, since the peak piston velocity in any real system is likely also to decrease as the frequency is increased.

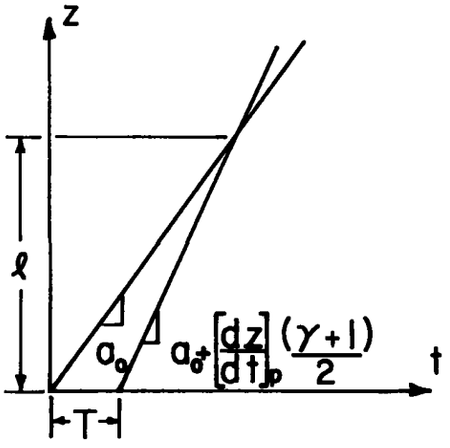

Fig. 11.7.6

An excitation at z = 0 raises the fluid velocity from 0 to $(dz/dt)_p$ in the characteristic time, T. Then nonlinear effects become important in the distance ℓ required for the resulting characteristics to cross.

11.8 Nonlinear Magneto-Acoustic Dynamics

The longitudinal motions of a perfectly conducting gas stressed by a transverse magnetic field, discussed in Sec. 8.8 for small perturbations of a slightly compressible fluid, provide an example of nonlinear electromechanical waves. The methods of Secs. 11.6. and 11.7 are put to work in many investigations of magnetohydrodynamic waves and shocks, especially in the limit of perfect conductivity considered here.[1] Motions, considered here perpendicular to the imposed magnetic field, have been considered for arbitrary orientations of the field.[2]

Equations of Motion: At the outset it is assumed that the motions are one-dimensional:

$$\vec{v} = v(z,t)\vec{i}_z; \quad \vec{H} = H(z,t)\vec{i}_y \tag{1}$$

The physical laws governing the dynamics are those of compressible fluid flow and magnetoquasistatics. Reduced to one-dimensional form, conservation of mass, Eq. 7.2.3, requires that

$$\frac{\partial \rho}{\partial t} + v\frac{\partial \rho}{\partial z} + \rho\frac{\partial v}{\partial z} = 0 \tag{2}$$

In writing the force equation, Eq. 7.16.6, viscous forces are ignored. The magnetic force density is conveniently written by using the stress tensor, Eq. 3.8.14 of Table 3.10.1:

$$\rho\left(\frac{\partial v}{\partial t} + v\frac{\partial v}{\partial z}\right) + \frac{\partial p}{\partial z} = -\mu_o H\frac{\partial H}{\partial z} \tag{3}$$

In the perfectly conducting fluid, there is by definition no electrical dissipation. If in addition effects of dissipation and heat conduction are negligible, the energy equation, Eq. 7.23.3, reduces to an expression representing an isentropic process, Eq. 7.23.7:

$$\frac{D}{Dt}(p\rho^{-\gamma}) = \left(\frac{\partial}{\partial t} + v\frac{\partial}{\partial z}\right)(p\rho^{-\gamma}) \tag{4}$$

In view of the one-dimensional approximation and Eq. 1, the field automatically has zero divergence. The combination of the laws of Ohm, Faraday and Ampère are represented by Eq. 6.2.3. The x component of that equation, in the limit where $\sigma \to \infty$, becomes

$$\frac{\partial}{\partial z}(vH) + \frac{\partial H}{\partial t} = 0 \tag{5}$$

The other components of Eqs. 3 and 5 are automatically satisfied.

Characteristic Equations: Following the technique outlined in Sec. 11.7, Eqs. 2-5, together with the relations between changes in the dependent variables along the characteristic lines and the partial derivatives, are arranged in a matrix. For convenience, $\partial\rho/\partial t \equiv \rho_{,t}$, $\partial\rho/\partial z = \rho_{,z}$, etc.:

$$\begin{bmatrix} 0 \\ 0 \\ 0 \\ 0 \\ d\rho \\ dv \\ dp \\ dH \end{bmatrix} = \begin{bmatrix} 1 & v & 0 & \rho & 0 & 0 & 0 & 0 \\ 0 & 0 & \rho & \rho v & 0 & 1 & 0 & \mu_o H \\ -\gamma p & -\gamma p v & 0 & 0 & \rho & \rho v & 0 & 0 \\ 0 & 0 & 0 & H & 0 & 0 & 1 & v \\ dt & dz & 0 & 0 & 0 & 0 & 0 & 0 \\ 0 & 0 & dt & dz & 0 & 0 & 0 & 0 \\ 0 & 0 & 0 & 0 & dt & dz & 0 & 0 \\ 0 & 0 & 0 & 0 & 0 & 0 & dt & dz \end{bmatrix} \begin{bmatrix} \rho_{,t} \\ \rho_{,z} \\ v_{,t} \\ v_{,z} \\ p_{,t} \\ p_{,z} \\ H_{,t} \\ H_{,z} \end{bmatrix} \tag{6}$$

---

1. G. W. Sutton and A. Sherman, Engineering Magnetohydrodynamics, McGraw-Hill Book Company, New York, 1965, pp. 309-339.

2. W. F. Hughes and F. J. Young, The Electromagnetodynamics of Fluids, John Wiley & Sons, New York, 1966, pp. 312-318.

To obtain the Ist characteristic equations, the determinant of the coefficients is required to vanish. The determinant is reduced by following steps similar to those that lead from Eq. 11.6.17 to 11.6.19, and then expanding by minors:

$$\frac{dz}{dt} = v \text{ on } C^P$$

$$\frac{dz}{dt} = v \pm a_b \text{ on } C^{\pm}; \quad a_b \equiv \left[\frac{\mu_o H^2}{\rho} + \frac{\gamma p}{\rho}\right]^{1/2} \tag{7}$$

The C^P characteristics are the particle lines, and actually represent two degenerate sets of characteristics. The $C^{\pm}$ characteristics represent magneto-acoustic waves, discussed for small amplitudes in Sec. 8.8.

The second characteristic equations are obtained from Eq. 6 by solving the determinant arrived at by substituting the column on the left into the first column of the square matrix. Straightforward expansion gives

$$(\frac{dz}{dt} - v)\{dv\left[-\rho(\frac{dz}{dt} - v)\frac{dz}{dt}\right] + d\rho\left[-v(\frac{dz}{dt} - v)^2 + \frac{\gamma p v}{\rho} + \frac{\mu_o H^2 v}{\rho}\right]$$

$$-dp\,\frac{dz}{dt} - [\mu_o H\,\frac{dz}{dt}]dH\} = 0 \tag{8}$$

The second characteristic equations along the particle lines are found from Eq. 8 using Eq. 7a. That the determinantal equations are degenerate is again reflected by the first factor in Eq. 8; remember that (dz/dt - v) appeared as a quadratic factor in the denominator. The second term in brackets is zero if dz/dt = v, so that

$$[\frac{\gamma p}{\rho}\,d\rho - dp] + \mu_o H^2[\frac{d\rho}{\rho} - \frac{dH}{H}] = 0 \text{ on } C^P \tag{9}$$

This equation is actually the sum of two independent expressions, as can be seen by considering Eq. 4, which on the particle characteristic can be written as

$$\frac{\gamma p}{\rho}\,d\rho - dp = 0 \text{ or } d(p\rho^{-\gamma}) = 0 \text{ on } C^P \tag{10}$$

On the same particle characteristics, Eqs. 2 and 5 combine to give

$$\frac{d\rho}{\rho} - \frac{dH}{H} = 0 \text{ or } d(\frac{H}{\rho}) = 0 \text{ on } C^P \tag{11}$$

These last two equations insure that 9 is satisfied, and account for the degeneracy of the two characteristic equations.

Using Eqs. 7b in 8 gives the two additional characteristic equations

$$\mp\rho a_b dv - dp - \mu_o H dH = 0 \text{ on } C^{\pm} \tag{12}$$

Thus, the Ist characteristic equations are summarized by 7 and the IInd characteristic equations given by Eqs. 10-12.

Initial Value Response: To any given point in the (z,t) plane can be ascribed four intersecting characteristic lines, two of which are simply the particle line. These are illustrated in Fig. 11.8.1. In general, the solution at the given point is obtained by simultaneously solving Eqs. 10-12, which are four equations in four unknowns. The first two of these expressions can simply be integrated to give invariants along C^P:

$$p\rho^{-\gamma} = p_c\rho_c^{-\gamma} \text{ on } C^P \tag{13}$$

$$H/\rho = H_c/\rho_c \text{ on } C^P \tag{14}$$

The second of these states that a fluid circuit of fixed identity must conserve magnetic flux. Hence, an increase in density caused by the compression of a fluid element is accompanied by a local increase in H. The model of Fig. 8.8.1a remains a useful way of viewing the interaction.

Suppose that, at some time in the evolution of the system, the pressure, density and field are uniform and are (p_o,ρ_o,H_o). The invariants on the right in Eqs. 13 and 14 are independent of position thereafter:

$$p\rho^{-\gamma} = p_o\rho_o^{-\gamma} \tag{15}$$

$$\frac{H}{\rho} = \frac{H_o}{\rho_o} \tag{16}$$

It follows that the remaining IInd characteristic equations, Eqs. 12, become

$$\frac{a_b}{\rho}\, d\rho \pm dv = 0; \quad a_b = [p_o\rho_o^{-\gamma}(\gamma\rho^{\gamma-1}) + \rho\mu_o(\frac{H_o}{\rho_o})^2]^{\frac{1}{2}} \tag{17}$$

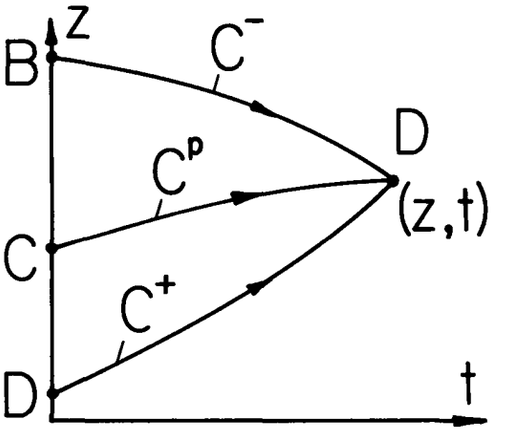

Fig. 11.8.1. The solution at (z,t) results from invariants carried along the four characteristic lines shown, with C^P representing two families of characteristics.

In effect, the dynamics now involve only the characteristics $C^{\pm}$ and two of the four original variables. Given (ρ,v) from solving Eqs. 7b and 17, p and H are found from 15 and 16. The dynamics are similar to those for the gas alone, except that $a \to a_b(\rho)$. Note that the dependence of the magneto-acoustic velocity on ρ is in part determined by H_o.

11.9 Nonlinear Electron Beam Dynamics

The nonlinear motions of streaming electrons are usually described in terms of Lagrangian coordinates. Nevertheless, an Eulerian description affords considerable insight if it is couched in terms of characteristics. By contrast with the equations of Secs. 11.7 and 11.8, those now considered are inhomogeneous.

The laws describing an electron beam neutralized by a background of ions are of the same nature as used in Sec. 11.5. Here, they are written without linearization but with the assumption that motions and fields are one-dimensional and that fields, like the motion, are z-directed. Hence, particle conservation requires that

$$(n_o + n)\frac{\partial v_z}{\partial z} + \frac{\partial n}{\partial t} + v_z\frac{\partial n}{\partial z} = 0 \tag{1}$$

where n_o is the equilibrium number density and $n(z,t)$ is the departure from that equilibrium. The longitudinal force equation is

$$\frac{\partial v_z}{\partial t} + v_z\frac{\partial v_z}{\partial z} = -\frac{e}{m}E_z \tag{2}$$

and in one dimension, Gauss' law is

$$\frac{\partial E_z}{\partial z} = -\frac{en}{\varepsilon_o} \tag{3}$$

Variables are normalized at the outset so that time is measured in terms of the plasma frequency $\omega_p \equiv \sqrt{e^2n_o/m\varepsilon_o}$,

$$\underline{t} = t\omega_p; \quad \underline{z} = z/\ell; \quad \underline{n} = n/n_o; \quad \underline{\dot{e}} = \dot{e}/\omega_p; \quad \underline{v} = v_z/(\ell\omega_p);$$
$$\underline{E} = E_z/(n_o\, e\ell/\varepsilon_o) \tag{4}$$

By definition,

$$\underline{\dot{e}} = \frac{\partial v}{\partial z} \tag{5}$$

and Eq. 3 becomes

$$n = \frac{\partial E}{\partial z} \tag{6}$$

Then, Eq. 1 and $\partial(\ )/\partial z$ of Eq. 2, combined with Eq. 3, are the first two of the four equations,

$$\begin{bmatrix} 1 & v & 0 & 0 \\ 0 & 0 & 1 & v \\ dt & dz & 0 & 0 \\ 0 & 0 & dt & dz \end{bmatrix} \begin{bmatrix} \frac{\partial n}{\partial t} \\ \frac{\partial n}{\partial z} \\ \frac{\partial \overset{o}{e}}{\partial t} \\ \frac{\partial \overset{o}{e}}{\partial z} \end{bmatrix} = \begin{bmatrix} -(1+n)\overset{o}{e} \\ n - \overset{o}{e}^2 \\ dn \\ d\overset{o}{e} \end{bmatrix} \tag{7}$$

The third and fourth are expressions for dn and de, introduced following the procedure described in Sec. 11.6.

That the determinant of the coefficients vanish gives the Ist characteristic equations. There are two families of lines, but these are degenerate:

$$\frac{dz}{dt} = v \text{ on } C^{\pm} \tag{8}$$

The second characteristic equations could be obtained by substituting the column on the right for any pair of columns on the left and setting the respective determinants equal to zero:

$$\frac{dn}{dt} = -(1+n)\overset{o}{e} \text{ on } C^{+} \tag{9}$$

$$\frac{d\overset{o}{e}}{dt} = n - \overset{o}{e}^2 \text{ on } C^{-} \tag{10}$$

These expressions are simple enough that they could have been obtained directly from Eqs. 7a and 7b by inspection.

A configuration typical of klystron beam-cavity interactions is shown in Fig. 11.9.1. The electron beam passes through screen electrodes at $z = 0$ and $z = \ell$. These are constrained to the potential difference, $V(t) = \underline{V}(t)(n_o e \ell^2/\varepsilon_o)$, which will be taken here as a given drive. In reality, V(t) might be associated with a resonator that is used to either excite the beam or extract energy.

The region of interest in the z-t plane is between the electrodes, $0 < z < \ell$ and for $0 < t$. Characteristic lines that enter this region along the z-axis (when $t = 0$) are denoted by $K = N\cdots M$, while those that enter along the t-axis (where $z = 0$) are represented by $K = 1\cdots N$. To integrate Eqs. 9 and 10, it is appropriate to have two initial conditions for the latter and two entrance boundary conditions for the former.

When $t = 0$, the velocity and electric field distributions between the screens are taken as known. As an example, if the beam is initially unmodulated, the electron velocity is constant and there is no space charge between the screens:

$$v = U, \quad E = V(0) \tag{11}$$

For the boundary conditions, it is assumed that the beam enters with a constant velocity, U. In passing through the screen, an electron is subjected to a step in electric field, but not to an impulse. Hence, this velocity is continuous through the screen, this means that along the t-axis, where the electrons enter the region of interest, $\partial v/\partial t$ is also continuous. It follows from the force equation for an electron, Eq. 2, that $\overset{o}{e}$ is not continuous through the screen. Rather, if $\overset{o}{e} = 0$ just upstream of the screen at $z = 0$, according to Eq. 2, $\overset{o}{e}$ assumes the value

$$\overset{o}{e}(0,t) = -\frac{E(0,t)}{U} \tag{12}$$

just downstream. The number density is continuous through the screen, so that if the beam is unmodulated upstream, then just downstream

$$n(0,t) = 0 \tag{13}$$

Although not relevant as a boundary condition, it can be seen from Eq. 1 that the step in $\overset{o}{e}$ across the screen is accompanied by a step in $\partial n/\partial z$.

To make Eq. 12 a useful boundary condition, E(0,t) must be related to V(t). To this end, two integrations of Eq. 6, with the condition that the second intergration give V(t), result in

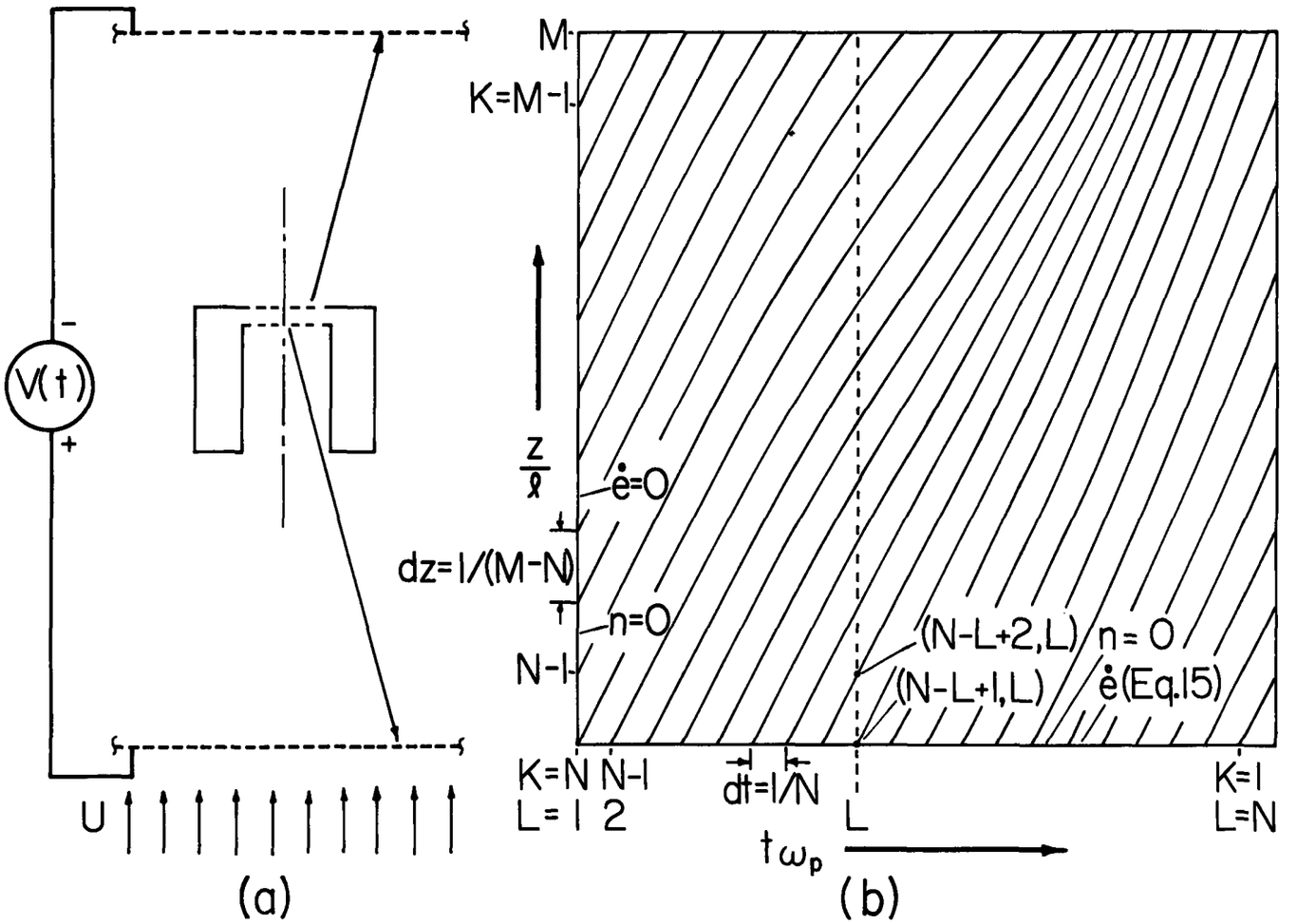

Fig. 11.9.1. (a) Beam enters region between screen electrodes with velocity U. At microwave frequencies, the screens typically provide coupling to cavity resonators, as shown by the inset. (b) Characteristic lines in the z-t plane. Coordinate (x,t) is denoted by characteristic line (K) and time (L).

$$E = V - \int_0^1\int_0^z n(z',t)dz'dz + \int_0^z n(z',t)dz' \qquad (14)$$

so that the electric field at z = 0 can be evaluated and used to express Eq. 12 as

$$\overset{o}{e}(0,t) = -\frac{V}{U} + \frac{1}{U}\int_0^1\int_0^z n(z',t)dz'dz \qquad (15)$$

Equations 13 and 15 comprise the boundary conditions at z = 0.

The integration of the second characteristic equations, Eqs. 9 and 10, can be carried out by treating them as simultaneous ordinary differential equations. This is possible only because the characteristic lines to which they apply are the same. Depending on whether the characteristic line of interest enters through the t = 0 axis or the z = 0 axis, the initial conditions or boundary conditions serve as "initial" conditions for this integration. However, the integration is not quite this straightforward, because superimposed on the propagational dynamics is Poisson's equation, which makes the entrance field instantaneously reflect both the net effect of the charge in the region of interest and the voltage V(t). This is why the boundary condition on $\overset{o}{e}$, Eq. 15, depends not only on the voltage but also on the charge throughout.

Consider the numerical steps that portray the space-time dynamics while marching forward in time. The initial conditions when t = 0 (L = 1) can be used with Eqs. 9 and 10 to establish n(z,dt) ≡ n(K,2) and $\overset{o}{e}$(z,dt) ≡ $\overset{o}{e}$(K,2) at the points where the characteristics (K = N···M) intersect the t = dt axis (L=2). Also, Eqs. 8 can be used to determine where these solutions apply, i.e., where

$$v(z,dt) = U + \int_0^z \overset{o}{e}(z,0)dz \qquad (16)$$

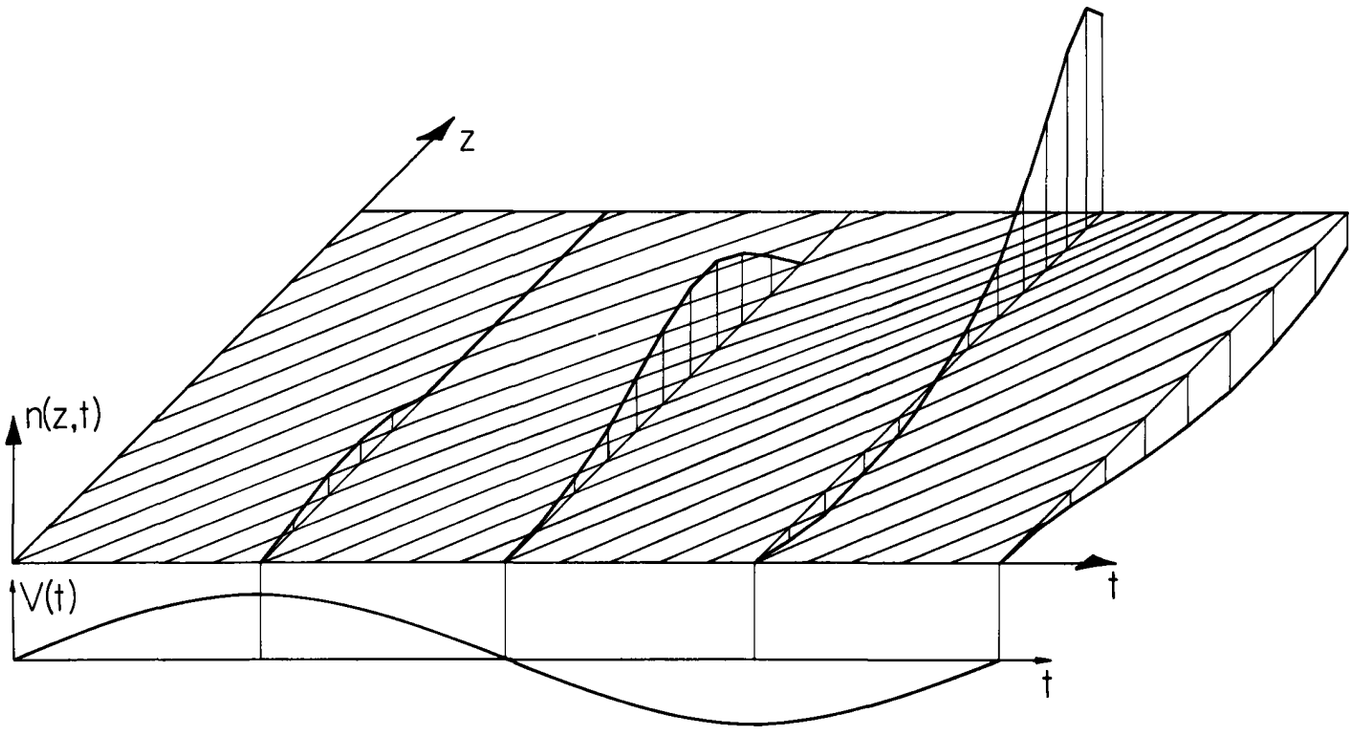

Fig. 11.9.2. Turn-on transient in configuration of Fig. 11.9.1 with sinusoidal voltage applied to screens. Normalized U = 2, V = 2 and angular frequency $\omega = (2\pi\omega_p)$.

The characteristic line K = N-1 entering at z = 0 when t = dt does so with conditions set by the boundary conditions of Eqs. 13 and 15. Note that because n(0,dt) ≡ n(N-1,2) is known and n(z,dt) has already been determined at the location K = N···,L = 2, integration called for in Eq. 15 can be carried out. Hence, $\overset{o}{e}(0,dt)$ is determined. Thus, the dynamical picture is completely established when t = dt. This process can now be repeated to determine the response when t = 2dt, and so on. The turn-on transient resulting from the application of a voltage V(t) = V sin ωt, is shown in Fig. 11.9.2.

Note that even though the transient has a well defined wave front, determined by the characteristic line passing through the origin, the characteristic lines are distorted even ahead of this wave front. This is because the applied voltage and the space charge between the screens have an instantaneous effect on the velocity of electrons throughout. Where the characteristic lines converge, abrupt changes in density occur. By increasing the driving voltage, characteristic lines can be made to cross. Electrons entering at one time are overtaken by those entering at a later time. It is to handle this situation that Lagrangian coordinates are often used.[1]

Once an electron has entered the interaction region, so that its initial conditions are established, its evolution in the state space $(\overset{o}{e},n)$ is determined. This can be seen by combining Eqs. 9 and 10 so as to eliminate time as the parameter:

$$\frac{d\overset{o}{e}}{dn} = \frac{\overset{o}{e}^2 - n}{(1 + n)\overset{o}{e}} \qquad (17)$$

Given an initial position in the state space $(\overset{o}{e},n)$, numerical integration of Eq. 17 results in one of the trajectories of Fig. 11.9.3. It follows from Eqs. 9 and 10 that as time progresses, the trajectories are traced out in the direction indicated by the arrows. Thus, the number density in the neighborhood of a given electron (moving along a characteristic line) is oscillatory in nature, with a frequency typified by the plasma frequency, ω_p. For the particular initial conditions of Eqs. 13 and 15, which pertain along characteristics emanating from the t axis, the trajectories all start from the $\overset{o}{e}$ axis, but with an amplitude determined by Eq. 15. The picture is now one of particles acting as nonlinear oscillators translating in the z direction with the velocity v.

The perturbation dynamics are governed by the linearized forms of Eqs. 9 and 10, which combine to show that

---

1. H. M. Schneider, "Oscillations of an Inhomogeneous Plasma Slab," Ph.D. Thesis, Department of Electrical Engineering, Massachusetts Institute of Technology, Cambridge, Mass., 1969.

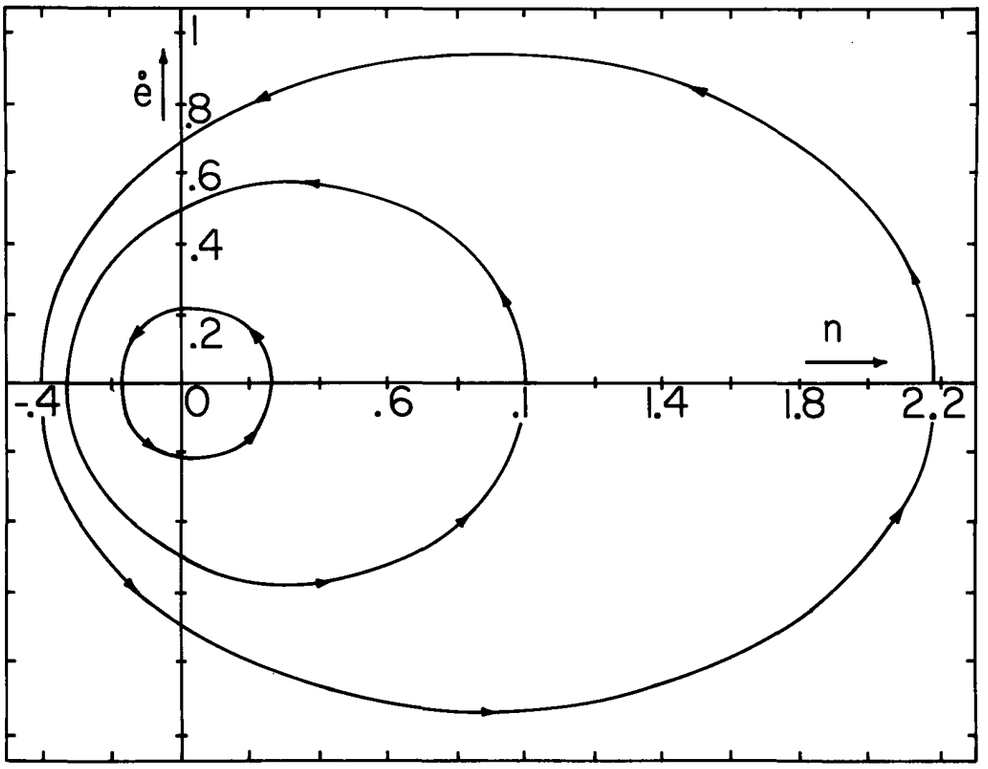

Fig. 11.9.3. Phase-plane ($\dot{e}$-n) trajectories of oscillations of electron beam.

$$\frac{d^2n}{dt^2} + n = 0 \tag{18}$$

Thus, on a characteristic crossing the t axis when $t = t_o$ (where $n = 0$), (19)

$$n = A(t_o) \sin (t - t_o)$$

Linearized, Eq. 8 can be integrated to express the characteristic line along which Eq. 19 applies:

$$z = U(t - t_o) \tag{20}$$

Found from Eq. 20, t_o can be substituted into Eq. 19 to obtain

$$n = A(t - \frac{z}{U}) \sin (\frac{\omega_p z}{U}) \tag{21}$$

where dimensional variables have been reintroduced.

The response is the product of a stationary emvelope having a wavelength $\lambda = 2\pi U/\omega_p$ and a part traveling in the z direction with the electron velocity, U. The envelope is stationary in space because every electron oscillator passes the $z = 0$ plane with $n = 0$. The amplitude of its oscillation is determined by the initial condition on $\dot{e}$ when it passed the screen at $z = 0$. Note that in this small-amplitude limit, the phase-plane trajectories of Fig. 11.9.3 are circles with radii much less than one. It follows that to achieve linear dynamics, $\dot{e} << \omega_p$.

11.10 Causality and Boundary Conditions: Streaming Hyperbolic Systems

Objectives in this section are: (a) to develop readily visualized prototype models for streaming interactions; (b) to picture in z-t space the evolution of absolute and convective instabilities and of systems which if driven in the sinusoidal steady state would display evanescent and amplifying waves; (c) to use the method of characteristics to illustrate the crucial role of causality in the choice of boundary conditions. In terms of complex waves (and eigenmodes) a small-amplitude version of the dynamics will be considered again in Sec. 11.12. There, causal boundary conditions, as discussed here, will be essential to understanding the stability of systems of finite extent in the longitudinal direction.

Emphasized in this section is the dependence on the longitudinal (streaming) direction. Transverse dependences, at least in linear systems, are represented by higher order transverse modes. Linearized, the quasi-one-dimensional models now used represent the long-wave "dominant modes" from a complete small-amplitude model. This interrelationship of models, represented by Fig. 4.12.2, is illustrated in the problems.

Quasi-One-Dimensional Single Stream Models: Planar fluid jets are shown in Fig. 11.10.1. In the electric version, the sheet jet is perfectly conducting in the sense that charges can relax on the interface in times short enough to render the interfaces equipontials. (Perhaps a jet of water in air.) The jet has a thickness $\Delta << a$ and each of the interfaces has a surface tension γ. Electrodes to either side of the jet have a potential $V_o \equiv aE_o$ relative to the jet.

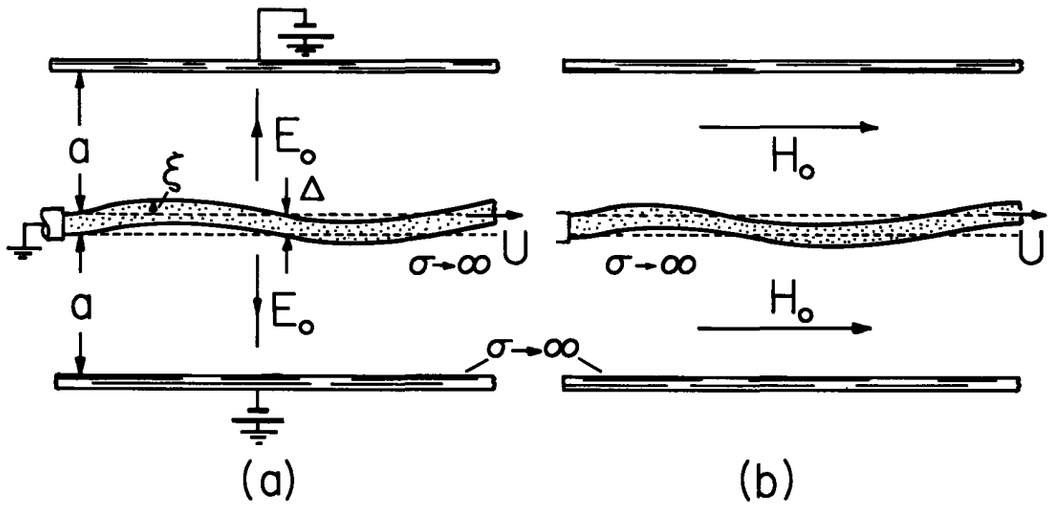

Fig. 11.10.1. Prototype single-stream systems consisting of perfectly conducting sheets convecting to the right with velocity U. (a) Potential constrained EQS configuration; (b) flux constrained MQS configuration.

For long-wave motions, the transverse electric surface force density, T(z,t), can be approximated by picturing the jet as having a deflection $\xi(z,t)$ from the center line, with essentially negligible slope. Thus, perhaps by using the stress tensor on a control volume enclosing a section of the jet, it follows that

$$T = \frac{1}{2}\varepsilon_o\left[\frac{(aE_o^2)}{(a-\xi)^2} - \frac{(aE_o)^2}{(a+\xi)^2}\right] \tag{1}$$

In the magnetic version, the jet is also perfectly conducting, but now so much so that the magnetic diffusion time $\mu\sigma\Delta a >> 1$. The system is then the antidual (Sec. 8.5) of the electric one, and T obtained from Eq. 1 by replacing $\varepsilon_o E_o^2 \to -\mu_o H_o^2$. In either system, the inertial and surface tension forces acting on the sheet are now also written with the assumption that deflections are slowly varying with respect to z. With U defined as the streaming velocity, and approximated here as constant, and ρ the jet mass density, it follows that Newton's law for motions in the transverse direction is

$$\Delta\rho\left(\frac{\partial}{\partial t} + U\frac{\partial}{\partial z}\right)^2\xi = 2\gamma\frac{\partial^2\xi}{\partial^2 z} + T \tag{2}$$

The same expression would be written to describe a membrane having surface mass density $\Delta\rho$ and tension 2γ. The velocity of waves on a fixed membrane would then be $V \equiv \sqrt{2\gamma/\Delta\rho}$.

For motions having a typical time scale τ, it is convenient to write Eq. 2 in terms of the normalized variables

$$\underline{\xi} = \xi/a, \quad \underline{t} = t/\tau, \quad \underline{z} = z/\tau V \tag{3}$$

New variables are introduced:

$$v = \frac{\partial \xi}{\partial t}; \quad e = \frac{\partial \xi}{\partial z} \tag{4}$$

so that Eqs. 1 and 2 can be written as two first-order expressions:

$$\left(\frac{\partial v}{\partial t} + M\frac{\partial v}{\partial z}\right) + M\left(\frac{\partial e}{\partial t} + M\frac{\partial e}{\partial z}\right) = \frac{\partial e}{\partial z} + \frac{P}{4}\left[\frac{1}{(1-\xi)^2} - \frac{1}{(1+\xi)^2}\right] \tag{5}$$

$$\frac{\partial v}{\partial z} - \frac{\partial e}{\partial t} = 0 \tag{6}$$

where

$$P = \frac{2\varepsilon E_o^2}{\rho \Delta a}\tau^2 = (\tau/\tau_{EI})^2 \text{ or } -\frac{2\mu_o H_o^2}{\rho \Delta a}\tau^2 = (\tau/\tau_{MI})^2 \text{ and } M \equiv U/V$$

The last expression follows from taking cross-derivatives of Eqs. 4. Note that P is the square of the ratio of the characteristic time to an electro or magneto inertial time, while M is a Mach number. The magnetic and electric systems are respectively described with P positive and negative. With P>0, the transverse force acts in the same direction as the displacement, and hence promotes instability. With P<0, the force acts as a nonlinear spring to recenter the sheet.

Single Stream Characteristics: The characteristic representation of Eqs. 5 and 6 follows from writing Eqs. 5 and 6 in the form of Eq. 11.6.7 and using the procedures outlined in Sec. 11.6:

$$dv + de(M \mp 1) = \frac{P}{4}\left[\frac{1}{(1-\xi)^2} - \frac{1}{(1+\xi)^2}\right]dt \tag{7}$$

on

$$\frac{dz}{dt} = M \pm 1; \quad (C^{\pm}) \tag{8}$$

It follows from the definition of e, Eq. 4, that

$$\xi = \int^z e\, dz \tag{9}$$

where the lower limit of integration is selected as one where ξ is either known or can be related to other variables through a boundary condition.

Because the nonlinearity is confined to the second characteristic equations, Eqs. 8 can be integrated:

$$z^{\pm} = (M \pm 1)t + Z^{\pm} \tag{10}$$

Thus, the characteristics are straight lines in the z-t plane, as illustrated in Fig. 11.10.2. By contrast with the situation in Sec. 11.7, where the second characteristics could be integrated, but the first not, here the z-t lines along which Eqs. 7 apply are known. It is the second characteristic equations that cause the trouble.

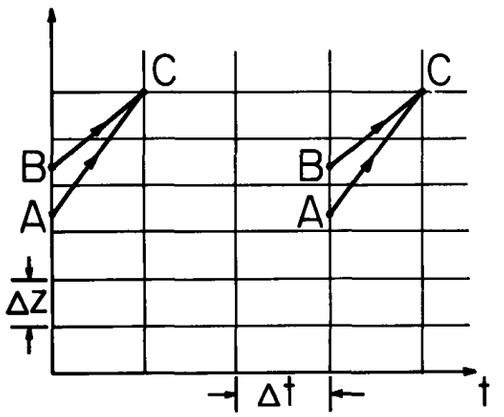

Fig. 11.10.2

Characteristic lines in z-t plane used to determine response at C given initial conditions at A and B.

There are two rewards for following the discussion now undertaken of how the characteristics can be used to give a numerical picture of the dynamics. The finite difference algorithm can be used to compute the response to initial and boundary conditions in a straightforward fashion. Perhaps more important, the implications of causality for boundary conditions becomes evident in the process.

Consider the determination of the response at C in Fig. 11.10.2, given that at B and A an instant, Δt, earlier. With the understanding that $\Delta v_A^{\pm}$ and $\Delta v_B^{\pm}$ are incremental quantities computed respectively at the points A and B:

$$v_C = \begin{cases} v_A + \Delta v_A^+ \\ v_B + \Delta v_B^- \end{cases} \tag{11}$$

These two expressions must result in the same response at C. Hence, they can be simultaneously solved. The result is the first of the following four relations between the incremental variables evaluated at one or the other of the previous points on the incident characteristics;

$$\begin{bmatrix} 1 & -1 & 0 & 0 \\ 0 & 0 & 1 & -1 \\ 1 & 0 & M-1 & 0 \\ 0 & 1 & 0 & M+1 \end{bmatrix} \begin{bmatrix} \Delta v_A^+ \\ \Delta v_B^- \\ \Delta e_A^+ \\ \Delta e_B^- \end{bmatrix} = \begin{bmatrix} v_B - v_A \\ e_B - e_A \\ Pf_A \Delta t \\ Pf_B \Delta t \end{bmatrix} \tag{12}$$

where

$$f \equiv \frac{1}{4}\left[\frac{1}{(1-\xi)^2} - \frac{1}{(1+\xi)^2}\right]$$

The second of these equations is analogous to the first with v replaced by e. The third and fourth represent the second characteristics, Eqs. 7. Solution of Eqs. 12 results in expressions for the incremental quantities in terms of the variables evaluated at the previous time step:

$$\Delta v_A^+ = \frac{1}{2}\{[v_A - v_B](M-1) + [e_A - e_B](M^2-1) + P[f_A(M\ 1) - f_B(M-1)]\Delta t\} \tag{13}$$

$$\Delta e_A^+ = -\frac{1}{2}\{[v_A - v_B] + (M+1)[e_A - e_B] + P[f_A - f_B)\Delta t\} \tag{14}$$

As indicated by the superscripts, these are the incremental changes in v and e along the C^+ characteristics.

Single Stream Initial Value Problem: Suppose that when $t = 0$, $\xi(z,0)$ [and hence $e(z,0)$] and $v(z,0)$ are given at equally spaced points along the z axis. Further, suppose it is decided that for convenience the response is to be found when $t = \Delta t$ at points C similarly selected to fall at intervals Δz. The values of e, ξ and v at A and B can be determined from the initial conditions by interpolating between the initial values.

Then the values of e_C and v_C, e and v when $t = \Delta t$, follow from Eqs. 13 and 14 used with expressions of the form of Eq. 11. Numerical integration, as called for by Eq. 9, then gives the distribution of ξ at this time. The situation when $t = \Delta t$ is now the same as was the initial one, so the process can be repeated to find the response when $t = 2\Delta t$. Thus, the dynamics are unraveled by "marching" forward in time along the characteristic lines. Of course some error will be introduced by the interpolation required to evaluate v and e at A and B and by the numerical integration of Eq. 9.

Typical responses are shown in Fig. 11.10.3. In the absence of a field (P=0) the initial pulse divides into components propagating upstream and downstream relative to the convecting sheet. These pulses propagate without distortion, leaving a null response between. Because they can be represented analytically, this case gives a check on the numerical scheme (Prob. 11.10.1).

Regardless of the sign of P, one effect of the inhomogeneity is to fill the region between these pulses with a response. With $P < 0$, physically the sheet is subject to a spring-like magnetic restoring force. In the extreme of no tension ($V = 0$), the situation would be one of convecting nonlinear oscillators, similar to that considered in Sec. 11.9. The tension adds wave propagation effects already familiar from part (a) of Fig. 11.10.3. The combined result, illustrated in part (b) of the figure, once again shows waves propagating along the characteristic lines, but now attenuating and

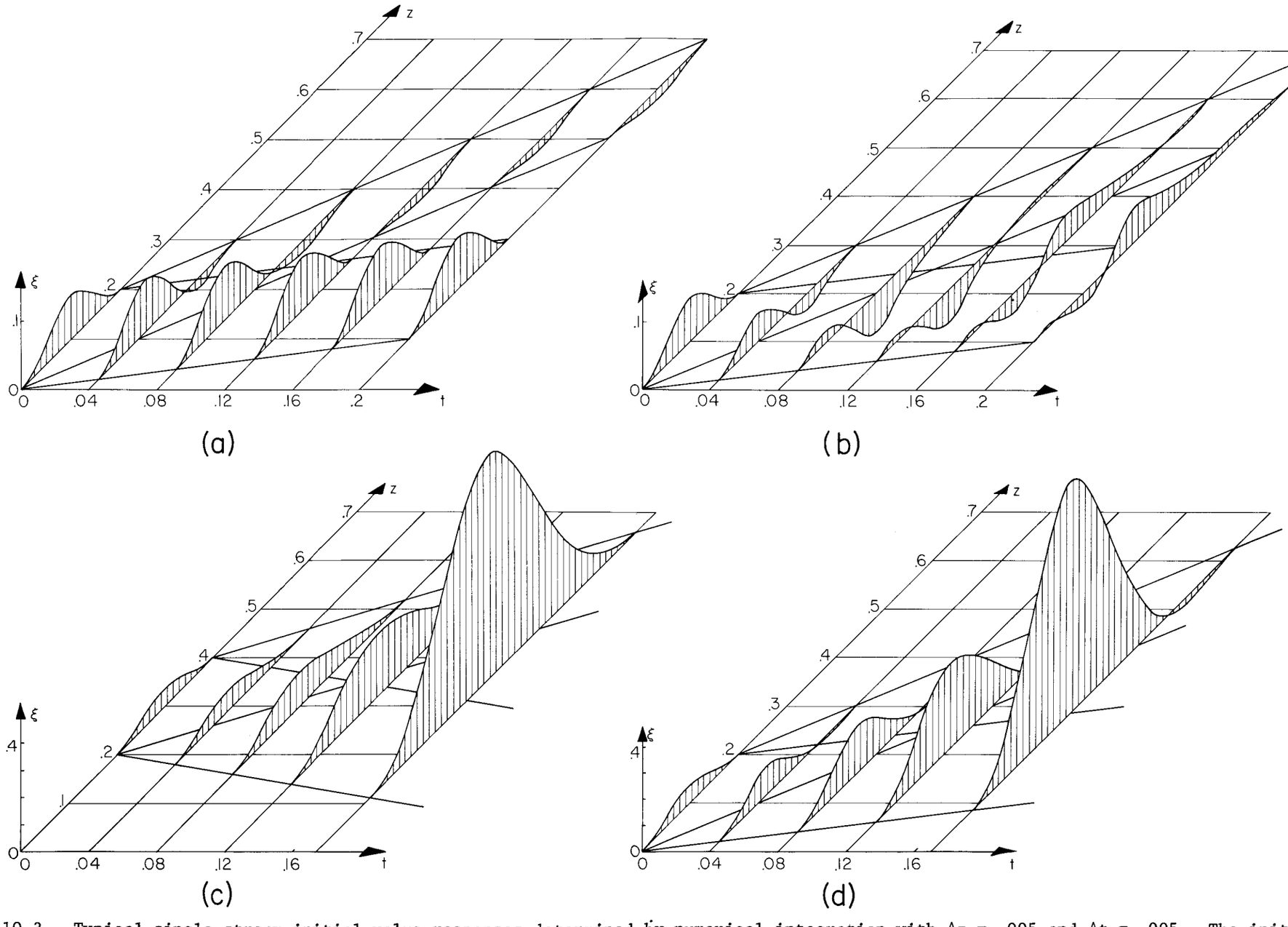

Fig. 11.10.3. Typical single-stream initial value responses determined by numerical integration with $\Delta z = .005$ and $\Delta t = .005$. The initial velocity is zero and displacement is as shown. (a) With no field, and hence no inhomogeneity, the initial pulse divides into fast and slow pulses that propagate without distortion. (b) With $P < 0$ (magnetic field), wave evanescence results. For the case shown, $M > 1$, so the response is swept downstream. (c) For $P > 0$ (electric field) and $M > 1$ ("sub"), an absolute (nonconvective) instability results. (d) For $P > 0$ but $M > 1$ ("super"), the instability is convective and the response at a given position remains bounded.

leaving behind an oscillating remnant. This oscillating part tends to be carried by the convection and have an angular frequency $\sqrt{-P}$.

As would be expected for $P > 0$, which represents a transverse electric force acting much as a nonlinear "negative" spring force, the response in parts (c) and (d) of Fig. 11.10.3 grows with time. Two types of instability are illustrated. For $M < 1$, where the flow is "sub" relative to the wave velocity V, the response becomes unbounded for an observer having a fixed location along the z axis. This is termed an absolute instability or, to distinguish it from the type of response shown for $M > 1$, a nonconvective instability.

For the convective instability of part (d), $M > 1$ and the response at a given location remains bounded. But, for an observer moving downstream it grows. Such an instability can be excited by a temporarily periodic signal at some location along the z axis and a sinusoidal steady-state established downstream in which the response takes the form of a spatially amplifying wave. At least for linear systems, such waves are best considered in the frequency domain, as illustrated in Secs. 11.11-11.13.

The nonlinear field coupling has its most pronounced effect in the electric field case. As $\xi \to a$ (its maximum possible value), the electric force becomes infinite. Thus, the peaks of the deflection tend to sharpen. In the $P > 0$ examples shown by Fig. 11.10.3, the initial deflection, consisting of a cosinusoid plus a constant in the intervals shown, tends to become a triangular pulse.

Quasi-One-Dimensional Two-Stream Models: Consider now the two-stream configurations of Fig. 11.10.4. The sheets have the respective convective velocities U_1 and U_2 and the same wave velocities V. They are now not only subject to the "self-field" effects resulting from the electric and magnetic fields, much as for the single streams, but they are also coupled to each other by this field. Thus, a given sheet is subject to "self" and "mutual" forces, represented on the right in the transverse force equations:

$$\Delta\rho\left(\frac{\partial}{\partial t} + U_1 \frac{\partial}{\partial z}\right)^2 \xi_1 - 2\gamma \frac{\partial^2 \xi}{\partial z^2} = \frac{1}{2} \varepsilon_o E_o^2 f_1 \tag{15}$$

$$\Delta\rho\left(\frac{\partial}{\partial t} + U_2 \frac{\partial}{\partial z}\right)^2 \xi_2 - 2\gamma \frac{\partial^2 \xi_2}{\partial z^2} = \frac{1}{2} \varepsilon_o E_o^2 f_2 \tag{16}$$

where, with the displacements normalized to a,

$$f_1(\xi_1, \xi_2) = \frac{1}{4}\left[\frac{1}{(1 - \xi_1)^2} - \frac{1}{(1 + \xi_1 - \xi_2)^2}\right] \tag{17}$$

$$f_2(\xi_1, \xi_2) = \frac{1}{4}\left[\frac{1}{(1 + \xi_1 - \xi_2)^2} - \frac{1}{(1 + \xi_2)^2}\right] \tag{18}$$

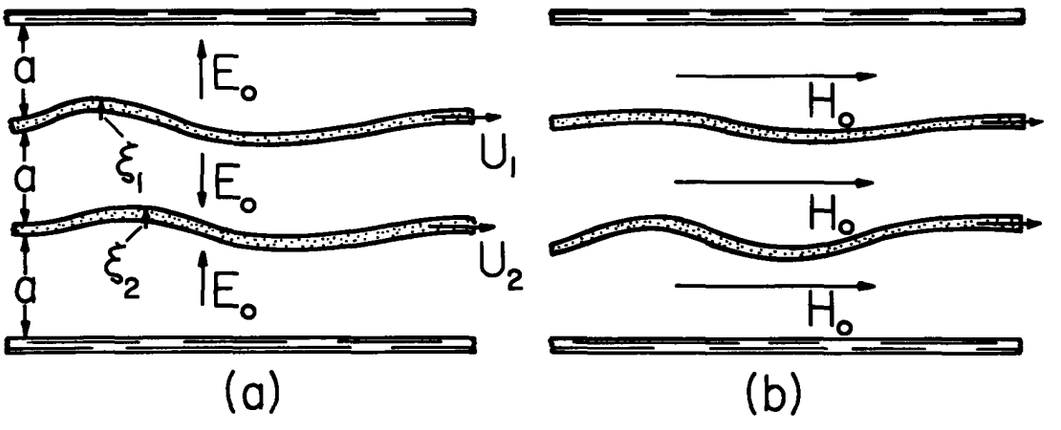

Fig. 11.10.4. Prototype two-stream configurations. (a) Potential constrained EQS configuration. (b) Flux constrained MQS configuration.

With variables defined as in Eq. 4 and normalized as suggested by the single-stream model, these equations are written as four first-order expressions:

$$(\frac{\partial}{\partial t} + M_1 \frac{\partial}{\partial z})v_1 + M_1(\frac{\partial}{\partial t} + M_1 \frac{\partial}{\partial z})e_1 - \frac{\partial e_1}{\partial z} = Pf_1(\xi_1,\xi_2) \quad (19)$$

$$(\frac{\partial}{\partial t} + M_2 \frac{\partial}{\partial z})v_2 + M_2(\frac{\partial}{\partial t} + M_2 \frac{\partial}{\partial z})e_2 - \frac{\partial e_2}{\partial z} = Pf_2(\xi_1,\xi_2) \quad (20)$$

$$\frac{\partial v_1}{\partial z} - \frac{\partial e_1}{\partial t} = 0 \quad (21)$$

$$\frac{\partial v_2}{\partial z} - \frac{\partial e_2}{\partial t} = 0 \quad (22)$$

Again, for the EQS system, $P > 0$ while for the MQS system, $P < 0$.

Two-Stream Characteristics: The same determinant approach used to find the single-stream characteristics can be applied to Eqs. 19-22. However, it is more convenient to recognize that the only coupling between streams is through the inhomogeneous terms. Thus, in view of Eqs. 7 and 8 found for a single stream, the characteristics are just what they would be for the individual streams with the inhomogeneous terms appropriately altered. Thus

$$dv_1 + de_1(M_1 \mp 1) = Pf_1(\xi_1,\xi_2)dt \quad (23)$$

on

$$\frac{dz}{dt} = M_1 \pm 1; \quad (C_1^{\pm}) \quad (24)$$

and

$$dv_2 + de_2(M_2 \mp 1) = Pf_2(\xi_1,\xi_2)dt \quad (25)$$

on

$$\frac{dz}{dt} = M_2 \pm 1; \quad (C_2^{\pm}) \quad (26)$$

The solution at some position, E, when $t = t + \Delta t$ is now determined by the response at positions A,B,C and D on the respective characteristics when $t = 1$, as illustrated in Fig. 11.10.5.:

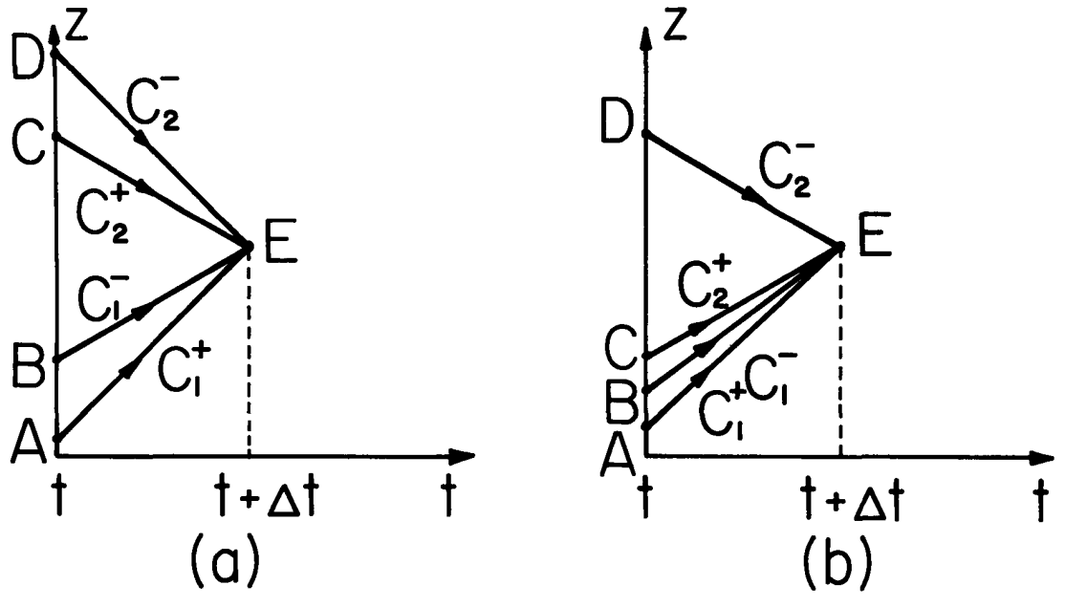

Fig. 11.10.5. Characteristics in the z-t plane illustrating (a) "super" counter-streaming and (b) "super" stream-structure interactions.

Just as Eqs. 13 and 14 follow from Eqs. 7, Eqs. 23 imply that the changes in v_1 and e_1 along the C_1^+ characteristic from A to E are given by

$$\Delta v_{1A}^+ = \frac{1}{2}\{(v_{1A}-v_{1B})(M_1-1)+(e_{1A}-e_{1B})(M_1^2-1)+P[f_{1A}(M_1+1)- {}_{1B}(M_1-1)]\Delta t\} \quad (27)$$

$$\Delta e_{1A}^+ = -\frac{1}{2}\{(v_{1A}-v_{1B})+(e_{1A}-e_{1B})(M_1+1)+P(f_{1A}-f_{1B})\Delta t\} \quad (28)$$

Similarly, from Eqs. 25, changes in v_2 and e_2 along C_2^+ from C to E are as given by these equations with $1 \to 2$, $A \to C$ and $B \to D$. As before, numerical integration of e_1 and e_2 gives the distributions of ξ_1 and ξ_2. The lower limits of integration in Eq. 9 should be made consistent with the entrance conditions on the respective streams.

Two-Stream Initial Value Problem: Given the initial distributions of ξ_1, v_1, ξ_2 and v_2, the evolution of these variables with time can be determined numerically, much as for the single streams. Given that P can be positive or negative (the two configurations of Fig. 11.10.4) and that M_1 and M_2 can be greater or less than unity (each stream can be "super" or "sub") and can be negative or positive (streaming in either direction), it is clear that there are now many physical interactions that might be considered. The super counter-streaming and super stream-structure interactions illustrated in Fig. 11.10.5 perhaps add the most physical insight.

The characteristics alone make it clear that with counter-streaming "super" streams it is possible to have an absolute instability. With $P > 0$, this instability has much the same character as for the single "sub" stream. But what might be surprising is the instability that results even with $P < 0$. In this case of magnetic field coupling, the effect of the field on the single stream is to produce decaying oscillations. With two counter-streams, oscillations are fed from one stream to the other and then back to the point of origin with a phase shift. Thus, certain oscillations build up, as the numerically computed response of Fig. 11.10.6 illustrates. Note that the instability is unbounded at a fixed position along the z axis. It takes the form of an absolute instability, in that the displacement at a given z tends to grow with time.

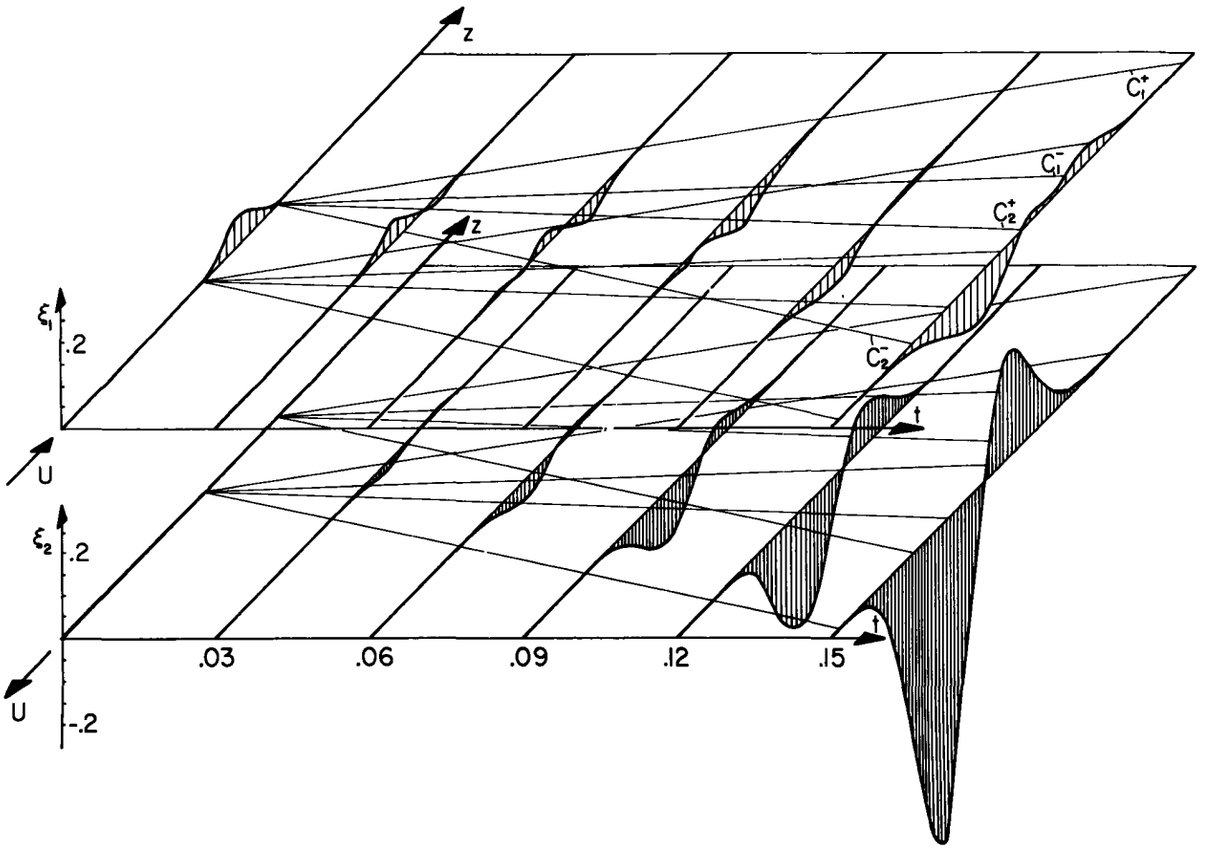

Fig. 11.10.6. Counter-streaming interactions between "super" streams coupled by magnetic field ($P = -1000$, $M_1 = 1.5$, $M_2 = -1.5$). Two-stream instability is in this case absolute.

Causality and Boundary Conditions: Any real system is of course bounded in the axial direction. One merit of the characteristic viewpoint is that causality is implicit to a specification of the conditions imposed to account for these boundaries. The dynamics unfold along the characteristic lines, always proceeding forward in time. Boundary conditions must be consistent with this requirement.

Consider first the boundary conditions for the single-stream configurations. The differential equation of motion is second-order in the longitudinal coordinate, so two conditions are required. Mathematically, these could be both imposed at $z = 0$, both at a downstream position $z = \ell$, or one at each position. But which of these is consistent with having a causal relation between the response and the initial conditions depends on whether the stream is "super" or "sub."

If the stream is supercritical, both families of characteristics are directed downstream, as illustrated in Fig. 11.10.7a. As time goes on, the response at C that depends on the initial conditions between A and B becomes one at C' that depends on both initial conditions and conditions at the upstream boundary. Finally, at points such as C", the response is fully determined by the boundary conditions at the entrance. Periodic entrance conditions clearly result in a temporally periodic reponse. The supercritical boundary conditions are equivalent to initial conditions and the response is found following the same line of reasoning as illustrated for the initial value problems. Two boundary conditions must be imposed at the upstream boundary, but none are imposed on the region $0 < z < \ell$ by the downstream boundary.

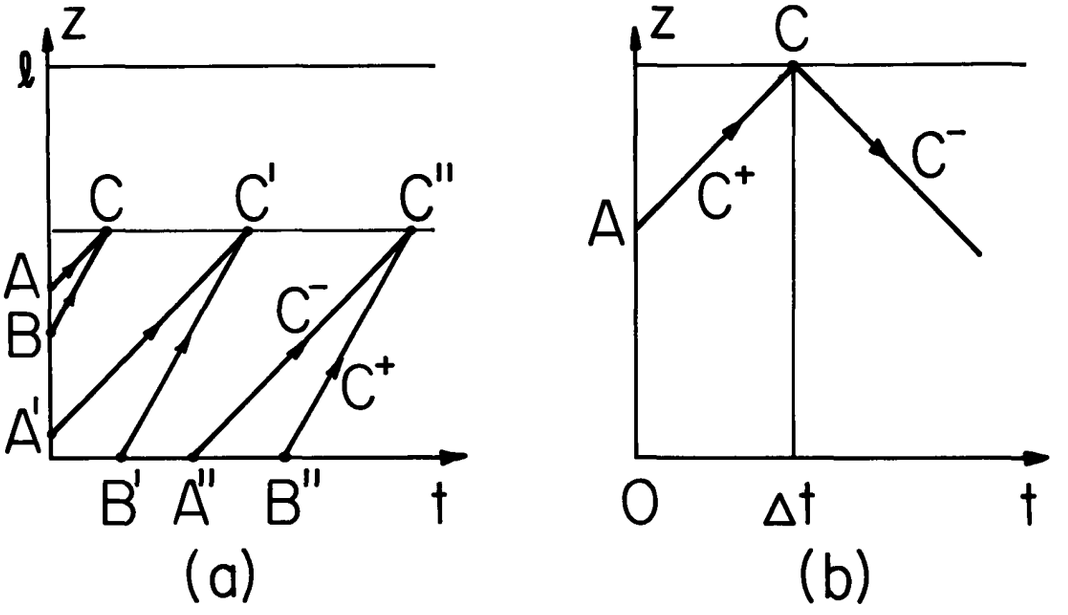

Fig. 11.10.7. Boundary conditions consistent with causality. (a) Supercritical characteristics implying two upstream conditions and none downstream, (b) Subcritical flow with one condition at each extreme.

By contrast, if the flow is subcritical, as illustrated by Fig. 11.10.7b, two conditions at either boundary leave the representation over-specified, and one condition must be imposed at each boundary. To see this, consider how the solution in the neighborhood of the downstream boundary would be found using the characteristics. To find the solution when $t = \Delta t$, the procedure is as already outlined except for the end points, like C of Fig. 11.10.7b. At this boundary point, $v = v_C$ is stipulated (say). Thus, because v_A is also known from the initial conditions, the change in v along the C^+ characteristic incident on the boundary, Δv_A^+, follows from Eq. 11a. From the second characteristic equation along C^+, Eq. 12c, the value of Δe_A^+ is then determined and hence e at the boundary, e_C, is found. Thus, e cannot be independently specified as a boundary condition. With the variables determined at the boundaries in this fashion, the stage is set for repeating the process to determine the solution when $t = 2\Delta t$.

Of course, two boundary conditions can be arbitrarily imposed, say two upstream conditions in a subcritical flow. But it is clear that the resulting solution answers the question, what initial conditions are required to make the solution satisfy the desired subsequent conditions at the boundaries? Boundary conditions are usually intended as statements made in advance to predict future events. If not causal, they place requirements on what must have taken place before to have certain conditions at the boundaries now.

Consider now causal boundary conditions for the two-stream configurations. The system is now fourth-order in z and therefore four boundary conditions are required. With the understanding that characteristics have a direction determined by increasing time, one condition must be imposed where each family of lines enters the region of interest.

As an example, consider again the supercritical counter-streaming configuration. The characteristics C_1^- enter at z = 0 while the $C_2^\pm$ characteristics enter at z = ℓ. To see that the imposition of these conditions is consistent with marching forward in time, consider how the solution is determined when t = t + Δt, given the solution when t = t. Provided that Δz and Δt are selected so that the characteristics passing through every interior point on the grid when t = t + Δt pass through the line t = t in the interval 0 < z < ℓ, the solution at each of the interior points is found by the same procedure as for the initial value problem. The solution at an end point, such as E in Fig. 11.10.8a, is then found by using Eqs. 27 and 28 to find v_1 and e_1 at E. The boundary conditions provide the values of v_2 and e_2 at E. In this way, the response is determined over the entire interval, including the end points, and the stage is set for the next time step. The example of Fig. 11.10.6 is in fact computed taking into account boundary conditions $\xi_1(0,t)$, $v_1(0,t)$, $\xi_2(\ell,t)$, $v_2(\ell,t)$ all zero. However, time has not progressed far enough to make these conditions significant.

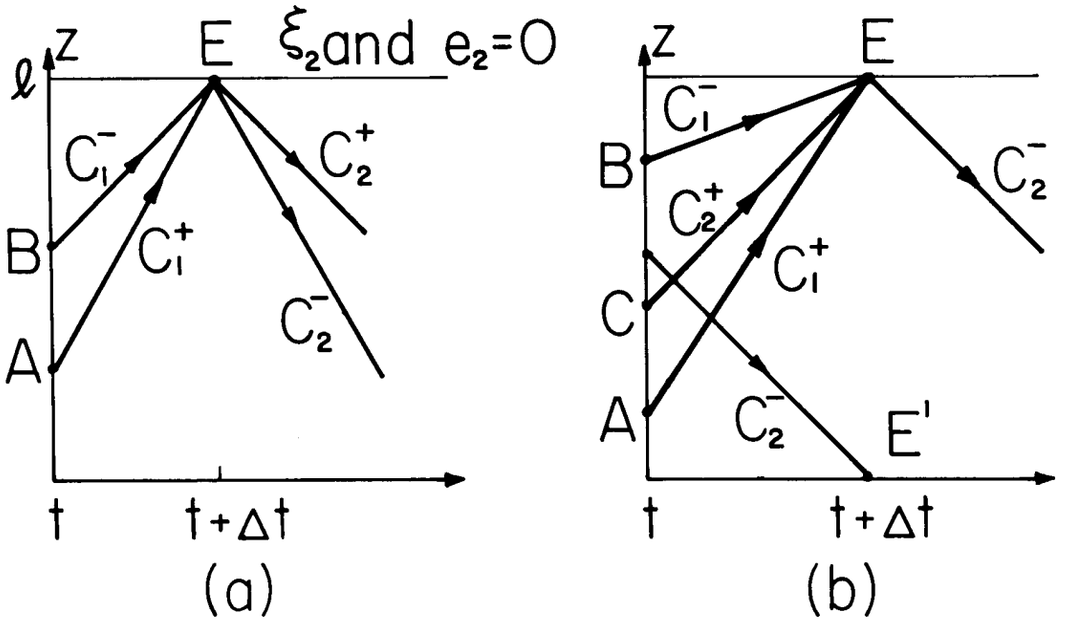

Fig. 11.10.8. (a) Downstream boundary of counter-streaming configuration at which two conditions, on ξ_2 (and hence v_2) and e_2, are imposed.

It is because coupling between characteristics for the two streams occurs only through the inhomogeneous terms that this simple procedure takes into account boundary conditions on the counter-steaming supercritical streams.

In Fig. 11.10.8b, the stream-structure interaction makes more evident what is in general required. Stream (1) is supercritical while (2) is not only subcritical but is not streaming at all. To find the response at a downstream boundary, like point E of Fig. 11.10.8b, Eqs. 27 and 28 again provide (v_1, e_1) at E. One boundary condition is imposed, say v_2 is given. Because v_2 at C is also known, Δv^+_{2C} follows. In turn, Eq. 25a (the second characteristic equation on C_2^+) can be used to solve for Δe^+_{2C}. Thus, e_{2E} is determined and all conditions at E are known.

At the upstream boundary, v_1 and e_1 are imposed as is a third condition, say that v_2 is known. From this last condition the second characteristic equation along C_2^+ can be used to determine e_2 at E'. Again, all conditions at the end points of the grid when t = t + Δt are established and the stage is set for the next iteration.

In the absence of longitudinal boundary effects, the "super-sub" streaming interaction with P > 0 is convectively unstable. That is, the response to initial conditions at a fixed position is bounded in time. In this case, boundary conditions have a profound effect. Those just described turn the convective instability into an absolute one that builds up in an oscillatory fashion.

11.11 Second Order Complex Waves

The remaining sections in this chapter continue a subject begun in Sec. 5.17. There, Fourier transforms are used to represent spatial transients in terms of the sinusoidal steady-state spatial modes. The example considered there, of charge relaxation on a moving sheet, is typical of a wide class of linear systems that are uniform in the longitudinal direction, z, and excited from transverse boundaries, perhaps over an interval $0 < z < \ell$. In Sec. 5.17, the resulting temporal sinusoidal steady state consists of responses, shown in Fig. 5.17.8, that spatially decay upstream and downstream from this range. These are a superposition of the appropriate spatial modes. Within the excitation range, the response is also a superposition of spatial modes. But in addition, in this range there is the driven response having not only the same temporal frequency as the drive, but the same wavenumber as well. The Fourier transform provides a formalism for "splicing" the modes and driven response together in the planes $z = 0$ and $z = \ell$.

As pointed out in Sec. 5.17, there are two questions left unanswered in the process of finding the spatial transient. First, it is assumed there that the sinusoidal steady-state complex waves decay away from the excitation region. Thus, those spatial modes having positive imaginary k are excluded from the downstream range $\ell < z$, while those with negative imaginary parts are left out in the region $z < 0$. The examples introduced in this section include the possibility that the downstream response in fact grows with increasing z. In Sec. 11.12, the objective is to have a means of distinguishing such amplifying waves from those that are evanescent, or decay away from the drive.

Any discussion of a sinusoidal steady state is predicated on having an answer to the second question. Is the system absolutely stable, in the sense that the response is bounded with increasing time at a fixed location in space? Only then will the temporal sinusoidal steady state have a chance to establish itself. The difficulty here is that a system is not necessarily absolutely unstable even if it displays temporal modes with negative imaginary frequencies. Temporal modes, having frequencies given by the dispersion equation evaluated using real values of the wavenumber, are the response to initial conditions that are spatially periodic. These extend from $z = -\infty$ to $z = +\infty$. Thus, in an infinite system, temporal modes do not suggest whether the instability grows with time at a fixed location, z (absolute instability), or rather grows only for an observer that moves with some velocity in the z direction (convective).

The identification of an absolute instability is taken up in Sec. 11.13.

Second Order Long-Wave Models: It is the purpose of this section to set the stage for the next two sections. Although the ω-k picture of the evolution of a system in space and time is widely applicable, it is helpful to have in mind simple situations that make it possible to establish a physical rapport for what the mathematics represents. In Fig. 11.11.1, sheets of liquid stream in the z direction between plane-parallel plates or electrodes. (These same configurations are considered from another point of view in Sec. 11.10.) With the stream in steady equilibrium there is no transverse deflection, ξ, and there are uniform fields between the plane-parallel perfectly conducting walls and the sheets, as shown. Over the range $0 < z < \ell$, the transverse boundaries are driven either by electric or magnetic potentials superimposed on the uniform bias potentials which give rise to the equilibrium fields.

The models now developed highlight the dominant modes of systems actually having an infinite number of spatial modes. The higher order modes that are left out of the models come into play if "wavelengths" of interest are as short as the spacing, a, or the sheet thickness, Δ. The magnetic configuration is the antidual of the electric one, as defined in Sec. 8.5. Thus, the equation of motion follows directly from the electric case now derived, with $\varepsilon_o \rightarrow \mu_o$, $E_o \rightarrow H_o$, $\Phi \rightarrow A/\mu_o$.

With the stream modeled as a membrane having a tension twice that due to the surface tension, the equation of motion is Eq. 11.10.2. Taking into account the excitation potentials, the transverse surface force density in the long-wave limit is simply the difference between the electric stresses acting on the top and the bottom of the sheet:

$$T = \frac{1}{2}\varepsilon_o\left[\frac{(-E_o a + \Phi_d)^2}{(a - \xi)^2} - \frac{(-E_o a - \Phi_d)^2}{(a + \xi)^2}\right] \tag{1}$$

For small amplitudes of the drive and response,

$$T \simeq -\left(\frac{2\varepsilon_o E_o}{a}\right)\Phi_d + \left(\frac{2\varepsilon_o E_o^2}{a}\right)\xi \tag{2}$$

This expression is now used to complete the transverse force equation, Eq. 11.10.2, which takes the

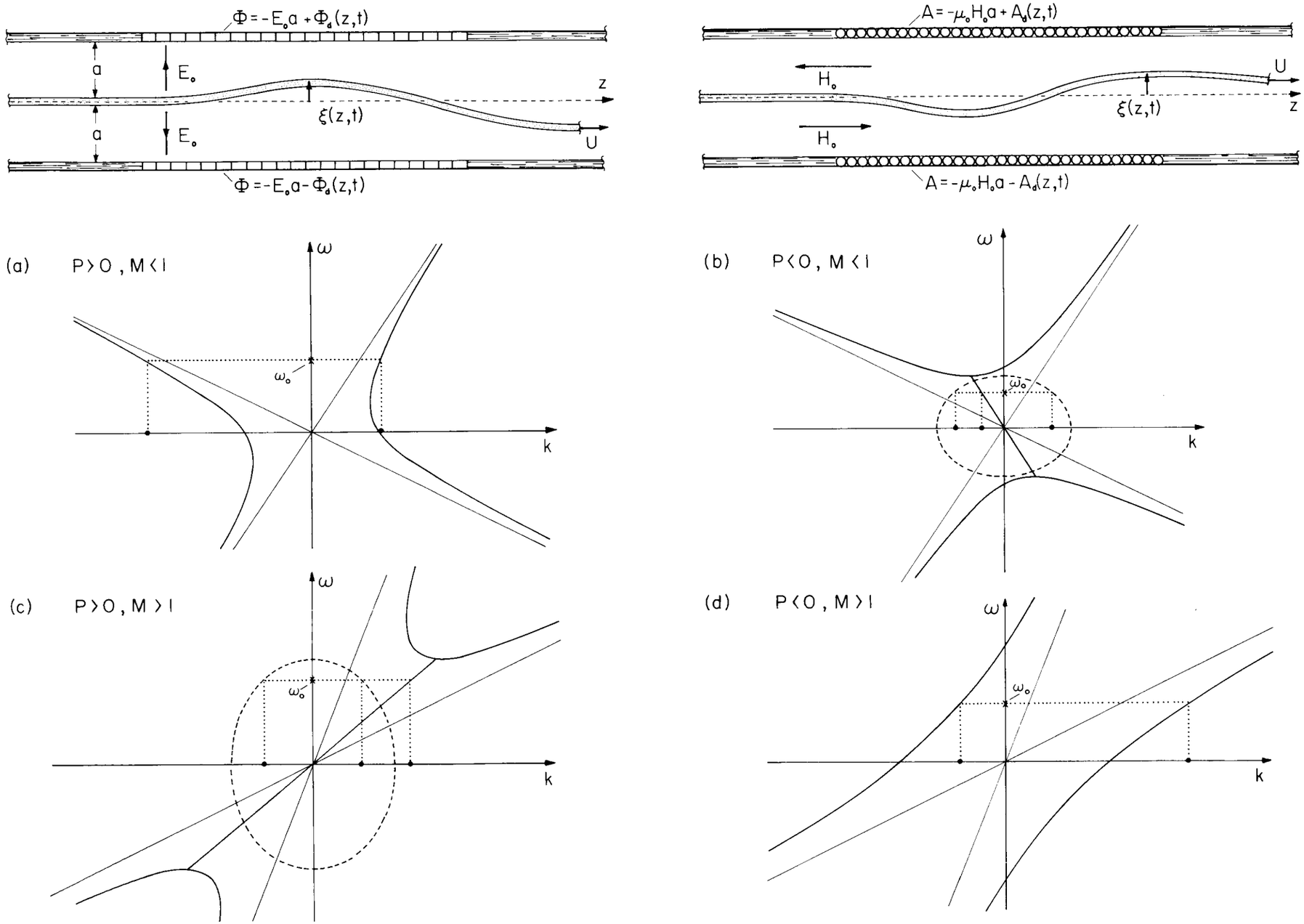

Fig. 11.11.1. Electric and magnetic long-wave models that are described by Eq. 3 together with dispersion relations. Complex values of k are shown for real values of ω: k_r ——, k_i ----. (a) Subcritical electric, (b) subcritical magnetic, (c) supercritical electric, and (d) supercritical magnetic.

normalized form ($\xi = \underline{\xi}a$, $t = \underline{t}\tau$, and $z = \underline{z}\tau V$):

$$(\frac{\partial}{\partial t} + M\frac{\partial}{\partial z})^2\xi = \frac{\partial^2\xi}{\partial z^2} + P\xi - Pf(z,t) \qquad (3)$$

The membrane wave velocity and Mach number are defined as

$$V = \sqrt{\frac{2\gamma}{\Delta\rho}};\quad M = \frac{U}{V}$$

and "pressure" parameters and forcing functions making the equation applicable to the electric and magnetic configuration, respectively, are

$$P = \frac{2\varepsilon_o E_o^2 \tau^2}{\Delta\rho a} \qquad \left| \qquad P = -\frac{2\mu_o H_o^2 \tau^2}{\Delta\rho a} \right. \qquad (4)$$

$$\underline{f} = \frac{\Phi_d}{aE_o} \qquad \left| \qquad \underline{f} = \frac{A_d}{\mu_o a H_o} \right. \qquad (5)$$

Thus, with $P > 0$ the configuration is electric, and the self-field part of the transverse force is destabilizing. That is, a deflection results in a field intensification and hence a transverse force on the stream tending to further increase the deflection. In the magnetic field configuration, $P < 0$, and it is as though there were a continuum of magnetic springs between the stream and the walls. A deflection leads to a force tending to return the stream to its equilibrium.

Whether the underlying method of characteristics from Sec. 11.10 has been followed or not, it is useful at this point to review the response to initial conditions, shown in Fig. 11.10.3, for these streaming configurations. It is the Mach number, M, that determines if the initial pulse can propagate upstream. For $M < 1$, wave fronts propagate in both directions, whereas if $M > 1$, the entire response is washed downstream.

If P is positive, the amplitude becomes unbounded. But, whether the growth is at a fixed location or for an observer moving with some velocity depends on M. Thus, in this electric case, the infinite system is *absolutely unstable* if $M < 1$ and *convectively unstable* if $M > 1$.

If P is negative, the response consists of forward and backward waves. The magnetic field results in their leaving an oscillation in the region between. If $M < 1$, this oscillation decays with time at a fixed location, while if $M > 1$, the response falls abruptly to zero as the wave front that is trying to propagate upstream is swept downstream.

With these predispositions as to what should be expected, consider now the representation of the dynamics in terms of complex waves.

Spatial Modes: Consider first the response to excitations that are in the sinusoidal steady state, having a frequency $\omega = \omega_o$. Because they involve the same manipulations, but contrasting issues, two types of problems are now considered. In the first, the system is bounded by the planes $z = 0$ and $z = \ell$. The transverse boundaries are not driven. Rather, the drive is through one of the longitudinal boundary conditions which varies at the angular frequency ω_o.

The second type of problem is one extending from $z = -\infty$ to $z = +\infty$ with the excitation from the transverse boundaries over the range $0 < z < \ell$. These bounded and unbounded situations, pictured in Fig. 11.11.2, are similar enough that they are now considered at the same time.

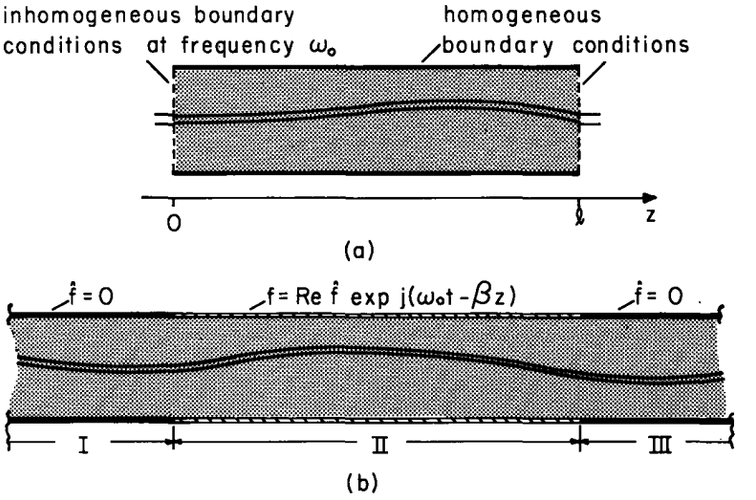

Fig. 11.11.2. Typical systems that are uniform in the z direction; (a) bounded longitudinally by planes where boundary conditions are imposed; (b) unbounded in the z direction with drive from a transverse boundary over the interval $0 < z < \ell$.

To be consistent with normalization of Eq. 3, deflections are taken to be of the form

$$\xi = \mathrm{Re}\,\hat{\xi}e^{j(\omega t - kz)} \qquad (6)$$

where frequencies and wavenumbers are normalized such that $\omega\tau = \underline{\omega}$, $k\tau V = \underline{k}$. The inhomogeneous solution to Eq. 3, caused by the drive on the transverse boundaries and applying over the range $0 < z < \ell$, follows by substituting this form of solution into Eq. 3 with $\omega = \omega_o$ and $k = \beta$. Solving for $\hat{\xi}$ gives

$$\hat{\xi} = \frac{\hat{Pf}}{D(\omega_o,\beta)} \tag{7}$$

where the dispersion function is

$$D(\omega_o,\beta) = (\omega_o - M\beta)^2 - \beta^2 + P \tag{8}$$

For solutions of the form of Eq. 6 to satisfy the homogeneous form of Eq. 3, k must satisfy the dispersion equation $D(\omega,k) = 0$. Thus, with amplitudes $\hat{A}$ and $\hat{B}$ at this point arbitrary, the solution over any range of z is

$$\xi = Re\left[\frac{\hat{Pf}e^{-j\beta z}}{D(\omega_o,\beta)} + \hat{A}e^{-jk_1 z} + \hat{B}e^{-jk_2 z}\right]e^{j\omega_o t} \tag{9}$$

where

$$D(\omega,k) = (\omega - Mk)^2 - k^2 + P \tag{10}$$

Thus, the wavenumbers k_1 and k_2 in Eq. 9 are given by solving the quadratic expression $D(\omega_o,k) = 0$:

$$\underline{k}_{\underline{1}} = \eta \pm \gamma \tag{11}$$

where

$$\eta \equiv \frac{\omega_o M}{M^2 - 1}, \quad \gamma \equiv \frac{\sqrt{\omega_o^2 + P(1 - M^2)}}{M^2 - 1}$$

As a graphical representation of the spatial modes, these roots are displayed in Fig. 11.11.1. For a particular driving frequency ω_o, the roots of $D(\omega_o,k)$ are represented by the intersections with the horizontal line. The solid curves indicate the real part, k_r, while the broken lines are the imaginary part, k_i. Where one k is shown, it is in common to both roots.

Four possibilities are distinguished in Fig. 11.11.1. The configuration can be electric or magnetic ($P > 0$ or $P < 0$) and it can be subcritical or supercritical ($|M| < 1$ or $|M| > 1$). As can be seen from Eq. 1, two of the four have ranges of frequency over which the wavenumbers are complex:

$$\omega_o^2 < P(M^2 - 1) \tag{12}$$

One is the subcritical magnetic case, where $P < 0$ and $|M| < 1$. The other is the supercritical electric case, where $P > 0$ but $|M| > 1$. In each of these, one spatial mode apparently "grows" with increasing z while the other "decays." Of course, in the magnetic subcritical case the spatial mode that appears to grow in the z direction is really an evanescent mode decaying upstream from a downstream drive. The supercritical electric case actually does involve a wave that is amplifying in the z direction as it moves away from an upstream source.

Section 11.12 shows how the distinction can be made between evanescent and amplifying waves by considering how the waves are established in the sinusoidal steady state subsequent to turning on the excitation.

The remainder of this section is intended to develop a physical understanding of evanescent and amplifying waves and of absolute and convective instabilities.

Driven Response of Bounded System: If $|M| < 1$, boundary conditions can be imposed at $z = 0$ and $z = \ell$. That these conditions are consistent with causality can be established by the method of characteristics (Sec. 11.10), or by using the arguments of the next section to determine that one spatial mode propagates in the +z direction (and hence can be used to satisfy a boundary condition at $z = 0$), while the other propagates in the -z direction (and can be used to satisfy the condition at $z = \ell$). As an example, suppose that the sheet is given a sinusoidally varying excitation at $z = 0$ and fixed at $z = \ell$. Also, make the transverse boundary excitation zero, so $f = 0$. Then, the coefficients $\hat{A}$ and $\hat{B}$ in Eq. 9 are determined and the solution becomes: (Note that in the normalized expression, $\underline{\ell} = \ell/\tau V$.)

$$\xi = -Re\ \hat{\xi}_d \frac{\sin \gamma(z - \ell)}{\sin \gamma\ell} e^{j(\omega_o t - \eta z)} \tag{13}$$

If the frequency is below the cutoff frequency, Eq. 12, γ is imaginary and the evanescent nature of the response is made more evident by writing Eq. 13 as

$$\xi = -\mathrm{Re}\ \hat{\xi}_d \frac{\sinh |\gamma|(z - \ell)}{\sinh |\gamma|\ell} e^{j(\omega_o t - \eta z)} \qquad (14)$$

Some features of this steady-state response are illustrated by the experiment shown in Fig. 11.11.3. Here, the sheet is replaced by a wire under tension. In the absence of a magnetic force, it too has a deflection described by the wave equation. There is no longitudinal motion, so $M = 0$ and hence $\eta = 0$ in Eqs. 13 and 14. By passing a current through the wire and imposing a magnetic field that is all gradient along its zero-deflection axis, a magnetic force is produced that is proportional to ξ. This force tends to restore the undeflected wire to its original position. The configuration is described in Prob. 11.11.2, where it is shown that the equation of motion is again Eq. 3 with $P < 0$ and $M = 0$.

In the first picture of the sequence, the current is zero and what is seen is the standing wave resulting from the interference of two oppositely propagating ordinary waves. (In these pictures, the z direction is to the left, so the excitation is to the right.) The frequency is such that the wire is very nearly in the lowest resonance condition that prevails if $\gamma\ell = n\pi$. As the current is raised, the magnetic force tends to counteract the inertial force (that makes the wire bow outward). The current is reached where these forces just balance, and the deflections decay away from the excitation. The rate of decay is largest at zero frequency (a static deflection).

Consider next the dramatic effect of having the continuum not only stream, but be supercritical, so that $|M| > 1$. Then, two boundary conditions must be imposed at the inlet, where $z = 0$, and none that influence matters in the range of interest are imposed at the exit. For example, the deflection is again the sinusoidal one assumed before, but the spatial derivative is constrained to be zero. Then, the coefficients $\hat{A}$ and $\hat{B}$ are determined and the solution is

$$\xi = \mathrm{Re}\ \hat{\xi}_d \frac{(k_1 e^{j\gamma z} - k_1 e^{-j\gamma z})}{2\gamma} e^{j(\omega_o t - \eta z)} \qquad (15)$$

The case of most interest has the electric configuration of Fig. 11.11.1 as a prototype and hence $P > 0$. If P is raised high enough that $\omega_o^2 < P(M^2 - 1)$, γ is imaginary, and the space-time picture of the deflections given by Eq. 15 is more apparent if it is written in the form

$$\xi = -\mathrm{Re}\ \hat{\xi}_d \frac{(k_1 e^{|\gamma| z} - k_1 e^{-|\gamma| z})}{2\gamma} e^{j(\omega_o t - \eta z)} \qquad (16)$$

In the case of this supercritical stream, a demonstration is made by letting the continuum be a jet of water, with capillarity providing the (surface) tension (see Prob. 11.11.3). The drive is provided by spherical electrodes positioned just upstream of ($z = 0$) on each side of the stream and biased by a constant potential relative to the stream with a superimposed sinusoidally varying voltage having the angular frequency ω_o.

With $P = 0$, so that γ is real, the response is illustrated in Fig. 11.11.4. (Again, streaming is from right to left with the excitation at the right.) The fast and slow waves carried downstream by the convection interfere to form "beats." That is, the envelope of the deflection is a standing wave having wavelength $2\pi/\gamma$. In Fig. 11.11.4b, the frequency has been raised to the point where about one half-wavelength of the envelope appears within view. In a slow motion picture (Complex Waves II, Reference 11, Appendix C), the phases propagate through this envelope with velocity ω_o/η.

With a field applied to the jet, the kinking motions of the jet are very similar to those of the planar sheet. Thus, raising the voltage is equivalent to raising P, and has the effect on the dispersion equation and jet that is illustrated in Fig. 11.11.5. Over most of its length, the response described by Eq. 16, is dominated by the growing exponential. Again phases have the velocity ω_o/η with the exponentially growing envelope.

Instability of Bounded Systems: The importance of imposing boundary conditions that are consistent with causality is made dramatically evident by considering implications for stability of correct and incorrect conditions. For a bounded system, it is not meaningful to envision a convective instability. Once boundary conditions have been imposed, there remains only the possibility of an absolute instability in the response to initial conditions. This transient response is represented by a superposition of modes satisfying homogeneous transverse and longitudinal boundary conditions ($\hat{f}$ and $\hat{\xi}_d \to 0$).

For the subcritical system, it can be seen from Eq. 13 that the eigenvalues for these modes are

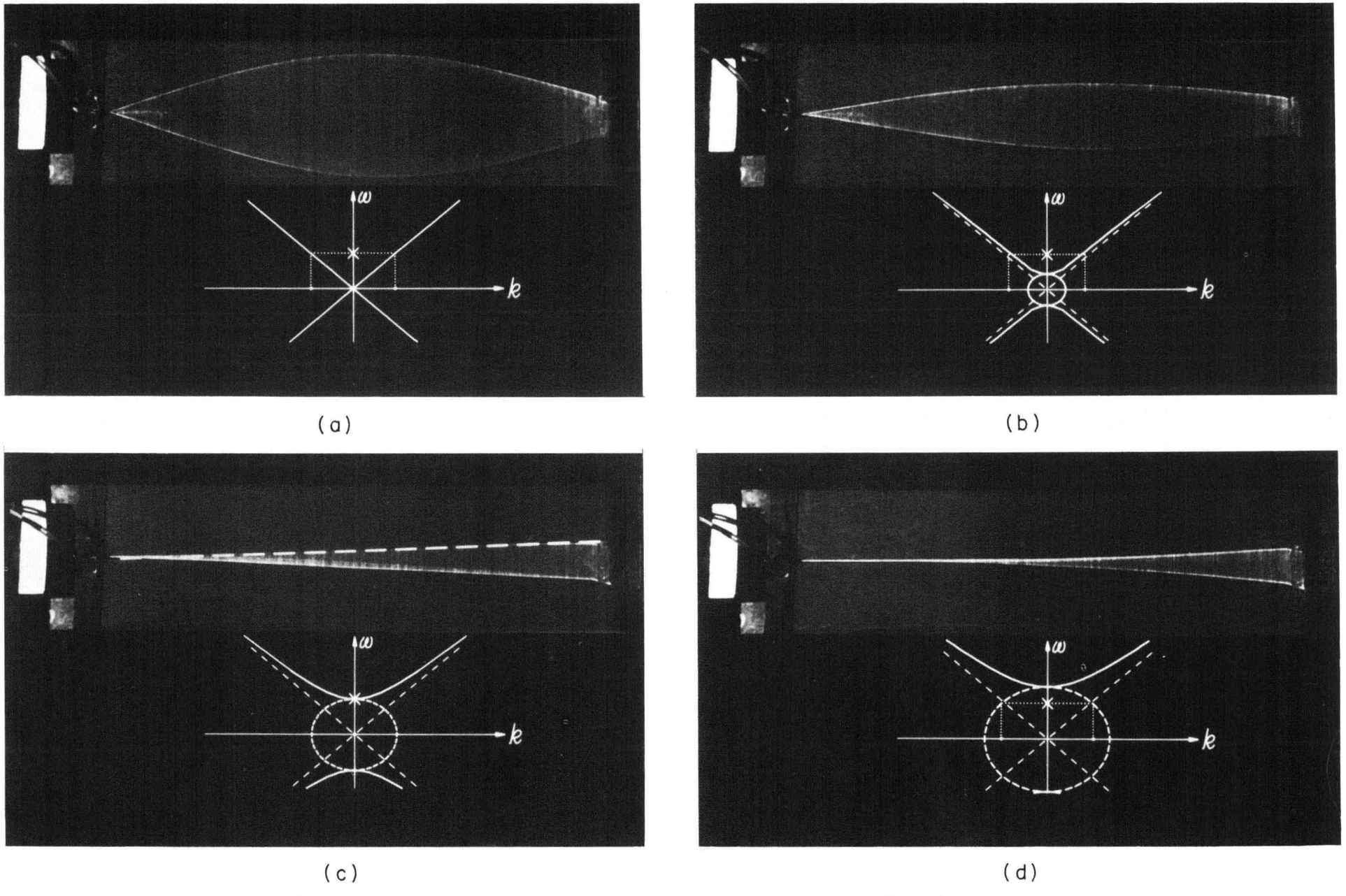

Fig. 11.11.3. Time exposure of sinusoidal steady state for a "string" represented by Eq. 3 with M = 0, P < 0 and the excitation at the right. (a) Magnetic field is off (P = 0) and frequency is such that response is near the first resonance. (b) Magnetic field raised somewhat, but frequency still above cutoff. (c) Field raised to cutoff condition. (d) Evanescent response resulting as field is raised to a point where frequency is less than cutoff. (From Complex Waves I, Reference 11, Appendix C.)

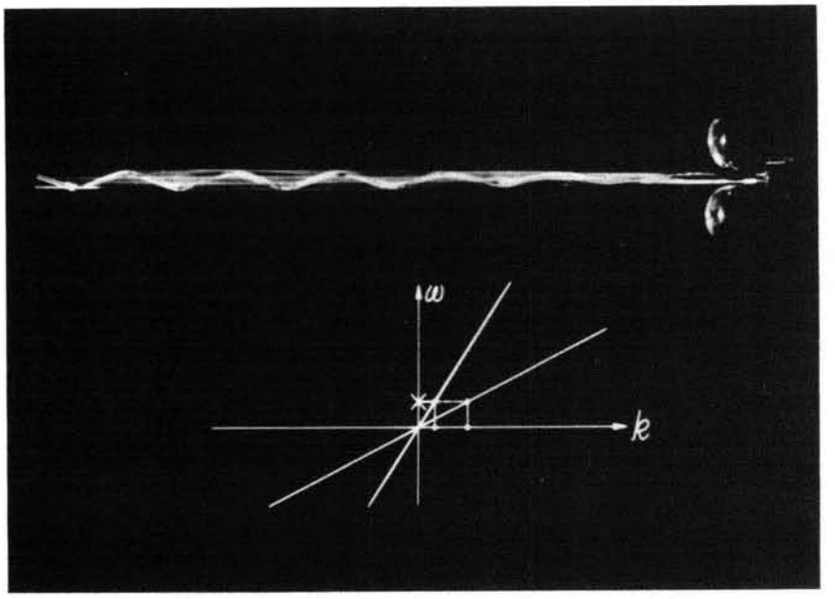

(a)

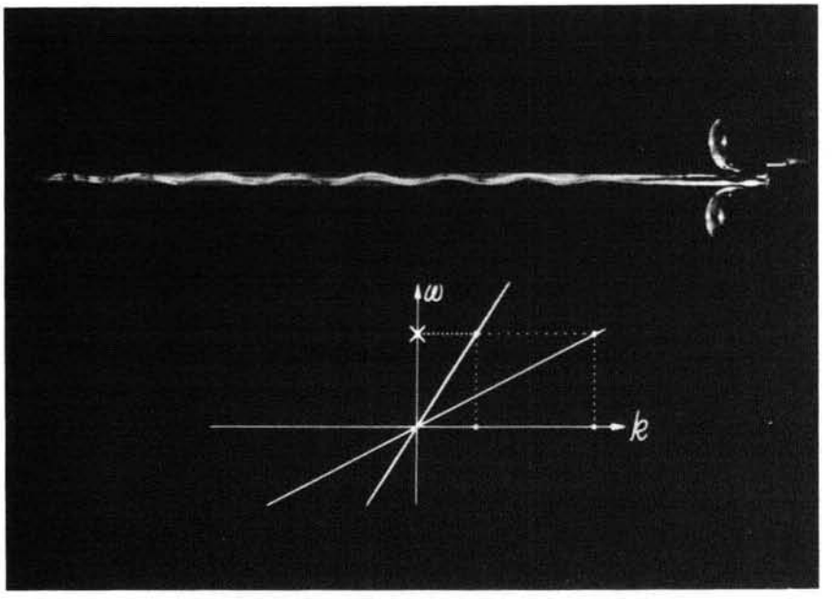

(b)

Courtesy of Education Development Center, Inc. Used with permission.

Fig. 11.11.4

Supercritical stream (M > 1) with no field (P = 0) and excitation to the right. Raising the frequency just brings one half-wavelength of "beat" into view. (From Complex Waves II, Reference 11, Appendix C.)

given simply by

$$\sin \gamma \ell = 0 \Rightarrow \gamma = n\pi/\ell, \; n = 1,2,3\cdots \qquad (17)$$

In evaluating this expression, using the definition of γ given by Eq. 11, the frequency is now the eigenfrequency, conveniently represented here as $j\omega \to s_n$. Thus,

$$s_n^2 = -(\frac{n\pi}{\ell})^2(M^2 - 1)^2 + P(1 - M^2) \qquad (18)$$

Because $|M| < 1$, it follows that P must be positive if there is to be instability. As P is raised, the n = 1 mode is the first to become unstable and that occurs if

$$P = (\frac{\pi}{\ell})^2(M^2 - 1) \qquad (19)$$

At this threshold, the deflection has a shape given by Eq. 13, with an envelope having the shape of a half-wave of a sinusoid. This instability is illustrated in the limit $M \to 0$ in Complex Waves II (Reference 11, Appendix C).

Consider the consequence of an unjustified use of Eq. 18. Suppose that it is valid for the supercritical case, $|M| > 1$. It would then be concluded that the system is unstable with P made sufficiently negative (the magnetic case in Fig. 11.11.1). Of course, with $|M| > 1$, one boundary condition underlying the identification of these eigenmodes is not consistent with causality. From

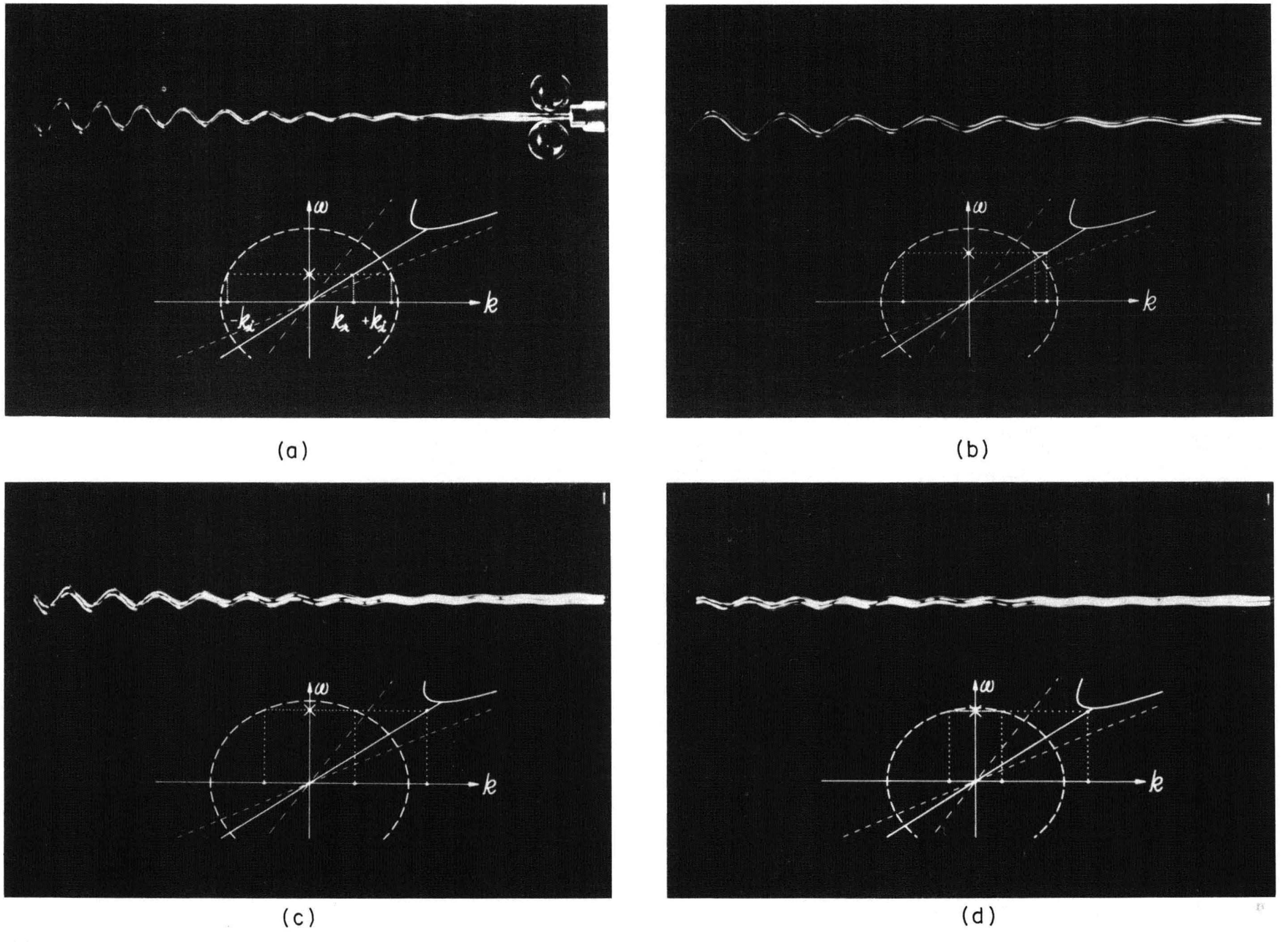

Fig. 11.11.5. Liquid jet in electric field is excited in the sinusoidal steady state by the spheres to the right. Amplifying waves, modeled by Eq. 3 with P > 0 and M > 1. Parts (b), (c), and (d) show the effect of raising the excitation frequency almost to the cutoff frequency. (Strictly, waves are short enough here to make the long-wave model of questionable validity. From Complex Waves II, Reference 11, Appendix C.)

the correct solution, Eq. 15, it is clear that in this supercritical case there are no eigenmodes, never mind modes that are unstable.

Driven Response of Unbounded System: Consider now the sinusoidal steady-state response to a drive from transverse boundaries in the unbounded configuration, Fig. 11.11.2b. For the quasi-one-dimensional model, solutions are piecewise continuous in the z direction. In regions I and III there is no drive and hence $f = 0$, while in region II there is a drive. With an appropriate assignment of f, the general solution, Eq. 8, can be applied to each region. There are two coefficients, $\hat{A}$ and $\hat{B}$, associated with each region. These represent the amplitudes of the spatial modes and are determined by boundary conditions at infinity and by the conditions prevailing where the regions meet at $z = 0$ and $z = \ell$.

A picture of the sinusoidal steady-state response in the four regimes illustrated in Fig. 11.11.1 is given in Fig. 11.11.6. First, consider the subcritical situations. Here, boundary conditions must exist at $z \to \infty$ and $z \to -\infty$ that have an effect on the asymptotic response. So long as the waves are propagating ($P > 0$ and $P < 0$ but the frequency above cutoff), it is necessary to specify conditions at infinity. One such specification might be a "radiation condition," which requires that boundaries are far enough removed that waves reflecting their presence have not returned to the region of excitation, or that these boundaries absorb the incident wave without there being any reflected wave. In either case, for $|M| < 1$, the response is

$$\xi = \mathrm{Re}\, e^{j\omega_o t}\begin{cases} \hat{A}_I e^{-jk_{-1}z}; & z < 0 \\ \dfrac{\hat{P}\hat{f}e^{-j\beta z}}{D(\omega_o,\beta)} + \hat{A}_{II}e^{-jk_{-1}z} + \hat{B}_{II}e^{-jk_1 z}; & 0 < z < \ell \\ \hat{B}_{III}e^{-jk_1 z}; & \ell < z \end{cases} \qquad (20)$$

where modes representing conditions at infinity have been excluded from regions I and III.

The four coefficients are determined by making the displacement and its spatial derivative piecewise continuous. That is, requiring that ξ and $\partial\xi/\partial z$ be continuous at $z = 0$ and $z = \ell$ gives four conditions allowing the four amplitudes to be determined in terms of $\hat{f}$.

For $P > 0$ and for $P < 0$ with the driving frequency above cutoff, the response outside the excitation region consists of purely propagating waves. Thus, the envelope of the response in the exterior is constant in z. In the magnetic case, where $P < 0$, the response below the cutoff frequency consists of evanescent waves, as sketched in Fig. 11.11.6. As suggested by the general form of the solution, Eq. 20, in the excitation region the response is a sum of the spatial modes representing end effects and a driven response that has the same wavenumber as the drive. For operation below the cutoff frequency, the response in the mid-range of region II at distances removed by several decay lengths from the ends would be just the part having the same spatial periodicity as the drive. This type of behavior is familiar from Sec. 5.17, and also illustrated in detail by Fig. 5.17.8.

The case $P > 0$ and $|M| < 1$ is absolutely unstable. Sooner or later the response to initial conditions would dominate the sinusoidal steady state.

Now, consider the effect of having a supercritical stream, $|M| > 1$. The response in region I is entirely determined by the upstream boundary conditions. If those conditions are homogeneous, or that boundary is too far upstream to have had an effect during times of interest and initial conditions on the stream are zero, then the solution in region I is known to be zero. With this understanding, the response then takes the form

$$\xi = \mathrm{Re}\, e^{j\omega_o t}\begin{cases} 0; & z < 0 \\ \dfrac{\hat{P}\hat{f}e^{-j\beta z}}{D(\omega_o,\beta)} + \hat{A}_{II}e^{-jk_{-1}z} + \hat{B}_{II}e^{-jk_1 z}; & 0 < z < \ell \\ \hat{A}_{III}e^{-jk_1 z} + \hat{B}_{III}e^{-jk_{-1}z}; & \ell < z \end{cases} \qquad (21)$$

The response continues to evolve in the direction of streaming. In region II, the amplitudes are fully determined by the requirement that ξ and $\partial\xi/\partial z$ be zero at $z = 0$. In turn, the downstream response in region III follows by requiring continuity of ξ and $\partial\xi/\partial z$ at $z = \ell$.

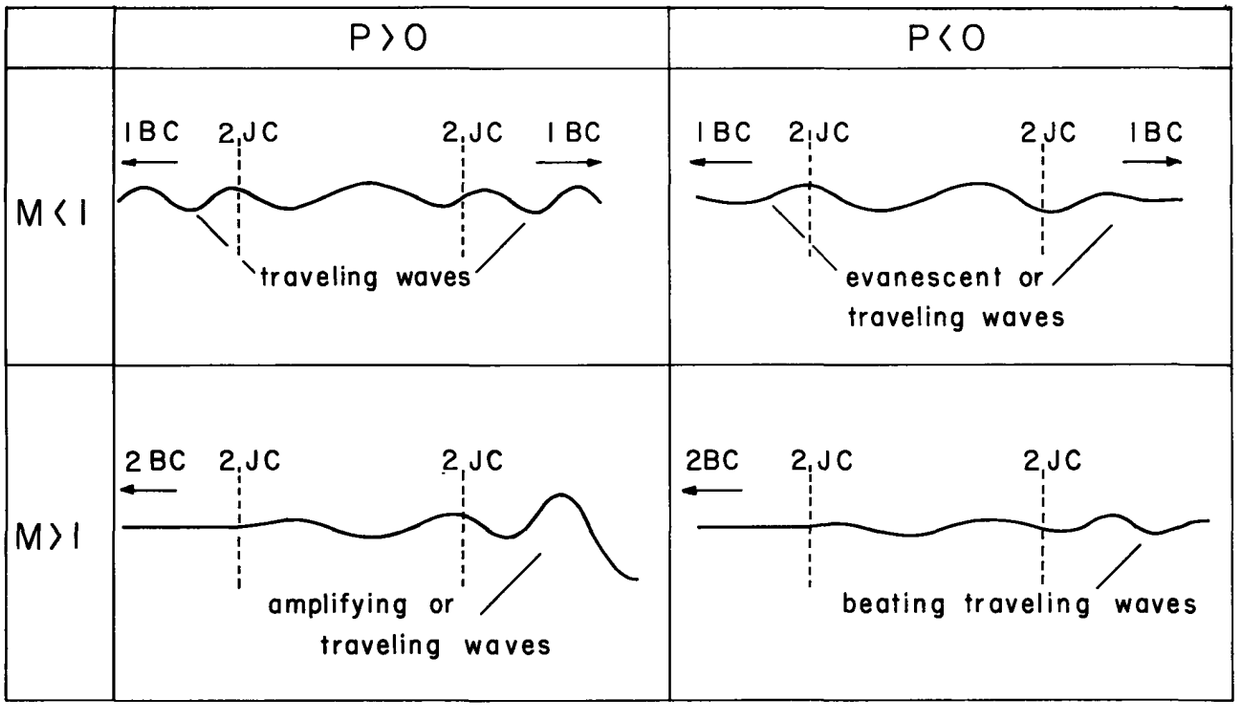

Fig. 11.11.6. Boundary conditions (B.C.) and jump conditions (J.C.) for second order unbounded systems.

In the case P > 0 (the unstable configuration), operation below the cutoff frequency results in an amplifying wave. Thus, it is possible that even within the excitation region the spatially periodic response will not prevail. The spatially amplifying wave certainly dominates in the downstream region, since the only other contribution to the response in that region is a decaying wave.

The downstream responses for the stable and unstable supercritical cases of Fig. 11.11.6 are illustrated experimentally by Figs. 11.11.4 and 11.11.5, respectively.

In retrospect, what is the intellectual basis for the association of the spatial modes with boundary conditions at infinity that made the difference between the supercritical and subcritical solutions? (Certainly it is not an identification of the direction of propagation of the phases.) In fact, left at this point, it is necessary to fall back on the method of characteristics, Sec. 11.10, to justify the association of modes with boundary conditions. In the next section, the objective is to have a method of relating the modes to the conditions of causality. The excitation will be turned on and the appropriate solution found as the asymptotic response. This approach can be used in systems where the method of characteristics is not applicable.

It has been presumed in this discussion of the response for the infinite system that at a given point in space, the response remains bounded as time increases. It will be the purpose of Sec. 11.13 to identify conditions for an absolute instability and to discriminate between it and a convective instability.

11.12 Distinguishing Amplifying from Evanescent Modes

Whether the excitation is from transverse or longitudinal boundaries, the sinusoidal steady-state asymptotic response is a superposition of waves having complex wavenumbers, k, for a real frequency, ω. To understand how these modes are to be combined in this long-time limit, it is necessary to picture the response in relation to the turn-on transient from which it arises.[1,2]

---

1. For a more complete exposition of criteria for identifying the types of complex waves in infinite media, see R. J. Briggs, Electron-Stream Interaction with Plasmas, The M.I.T. Press, Cambridge, Mass., 1964, pp. 8-46. Also, A. Bers, Notes for MIT subject "Electrodynamics of Waves, Media, and Interactions."
2. A. Scott, Active and Nonlinear Wave Propagation in Electronics, Wiley-Interscience, New York, 1970, pp. 27-44.

Laplace and Fourier Transform Representation in Time and Space: In Sec. 5.17, it is assumed from the outset that the temporal dependence can be represented by a complex amplitude, for example $\Phi = \mathrm{Re}\hat{\Phi}(x,y,z,\omega)\exp(j\omega t)$. The spatial transient is in turn represented by a Fourier transform. To permit a representation of the transient which joins the initial conditions to a possible sinusoidal steady state, this temporal complex amplitude is now replaced by the Laplace transform pair

$$\Phi(x,z,t) = \int_{-\infty-j\sigma}^{\infty-j\sigma} \hat{\Phi}(x,z,\omega)e^{j\omega t}\frac{d\omega}{2\pi} \Leftrightarrow \hat{\Phi}(x,z,\omega) = \int_{0}^{\infty} \Phi(x,z,t)e^{-j\omega t}\,dt \tag{1}$$

As in Sec. 5.17, the longitudinal dependence is in turn represented by the Fourier transform

$$\hat{\Phi}(x,z,\omega) = \int_{-\infty}^{+\infty} \hat{\Phi}(x,k,\omega)e^{-jkz}\frac{dk}{2\pi} \Leftrightarrow \hat{\Phi}(x,k,\omega) = \int_{-\infty}^{+\infty} \hat{\Phi}(x,z,\omega)e^{jkz}\,dz \tag{2}$$

The Laplace transform, Eq. 1b, starts when $t = 0$, and so the transform of temporal derivatives brings in initial conditions. For example, the Laplace transform of the first derivative is integrated by parts to give

$$\int_{0}^{\infty} \frac{\partial\Phi}{\partial t}e^{-j\omega t}\,dt = \Phi e^{-j\omega t}\Big|_{0}^{\infty} - \int_{0}^{\infty}(-j\omega)\Phi e^{-j\omega t}\,dt = -\Phi(x,z,0) + j\omega\hat{\Phi} \tag{3}$$

Thus, if a variable is zero when $t = 0$, then the Laplace and Fourier transform of its temporal derivative is simply $j\omega\hat{\Phi}$. Of course, the Laplace and Fourier transform of the derivative with respect to z is $-jk\hat{\Phi}$. That is, relations between complex amplitudes apply also to Laplace-Fourier transforms, provided that rest conditions prevail when $t = 0$ for the transformed variables. If there are finite initial conditions, then care must be taken to include them in transforming all relations.

As an example, consider the second order systems represented by Eq. 11.11.3 in an unbounded configuration. The excitation is from transverse boundaries (Fig. 11.11.2b) where the forcing function is imposed over the interval $0 < z < \ell$ as a traveling wave

$$\begin{aligned} f &= \underline{u}_1(t)[\underline{u}_1(z) - \underline{u}_1(z-\ell)]\mathrm{Re}\hat{f}_o e^{j(\omega_o t-\beta z)} \\ &= \underline{u}_1(t)[\underline{u}_1(z) - \underline{u}_1(z-\ell)]\tfrac{1}{2}[\hat{f}_o e^{j(\omega_o t-\beta z)} + \hat{f}_o^* e^{-j(\omega_o t-\beta z)}] \end{aligned} \tag{4}$$

Substitution, first into Eq. 1b and then into Eq. 2b, gives the transform of the forcing function as

$$\hat{f} = \frac{\hat{f}_o[1 - e^{j(k-\beta)\ell}]}{2(\omega - \omega_o)(k - \beta)} + \frac{\hat{f}_o^*[1 - e^{j(k+\beta)\ell}]}{2(\omega + \omega_o)(k + \beta)} \tag{5}$$

Note that the second term is obtained from the first by substituting $\hat{f}_o \to \hat{f}_o^*$, $\omega_o \to -\omega_o$, and $\beta \to -\beta$. With the understanding that the real response is the sum of the one now found and a response formed by making this substitution, it will be assumed in what follows that the drive is just the first term in Eq. 5. (Note that $\hat{f}_o$ is not a transform, but rather simply a complex number expressing the phase and amplitude of the drive.)

With the understanding that when $t = 0$, ξ and $\partial\xi/\partial t$ are zero, the Laplace-Fourier transform of Eq. 11.11.3 gives an expression for the transform of the sheet deflection:

$$\hat{\xi} = \frac{P\hat{f}}{D(\omega,k)}; \quad D(\omega,k) \equiv (\omega - Mk)^2 - k^2 + P \tag{6}$$

This expression is obtained either by treating variables as though complex amplitudes are being introduced or by starting from scratch by multiplying Eq. 11.11.3 by $\exp[-j(\omega t - kz)]$ and then integrating both sides of the expression from 0 to ∞ on t and from $-\infty$ to ∞ on z. Integrations by parts of the terms involving derivatives and the definitions of the transforms, Eqs. 1b and 2b, then also result in Eq. 6. (Note that consistent with the normalization used in Sec. 11.11 are $\underline{k} \equiv k\tau V$ and $\underline{\omega} = \omega\tau$.) Thus, in view of Eq. 5, the desired Laplace-Fourier transform is written in terms of the specific traveling-wave excitation, turned on when $t = 0$, as

$$\hat{\xi} = \frac{f(\omega)g(k)}{D(\omega,k)} \tag{7}$$

where

$$g(k) = \frac{P\hat{f}_o}{2} \frac{[e^{j(k-\beta)\ell} - 1]}{j(k - \beta)} \tag{8}$$

$$\mathcal{J}(\omega) = \frac{1}{j(\omega - \omega_o)} \tag{9}$$

The model represented by Eqs. 8 and 9 is long-wave. But, the form of the response transform taken by Eq. 7 is representative of a much wider range of physical situations that are uniform in the z direction. The details of a transverse dependence are determined by solving differential equations and boundary conditions over the transverse cross section. This amounts to representing the transformed variables in terms of transfer relations and boundary conditions, as exemplified many times in Chaps. 5, 6, 8, 10 and in Sec. 11.5.

Laplace Transform on Time as the Sum of Spatial Modes; Causality: The evolution in z-t space is determined by using Eq. 7 in evaluating the inverse transforms, Eqs. 1 and 2:

$$\hat{\xi}(z,\omega) = \mathcal{J}(\omega) \int_{C_F}^{+\infty} \frac{g(k)}{D(\omega,k)} e^{-jkz} \frac{dk}{2\pi} \tag{10}$$

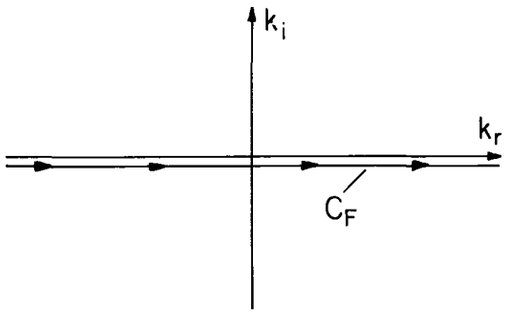

Fig. 11.12.1. Fourier contour.

$$\xi(z,t) = \int_{C_L}^{\infty - j\sigma} \hat{\xi}(z,\omega) e^{j\omega t} \frac{d\omega}{2\pi} \tag{11}$$

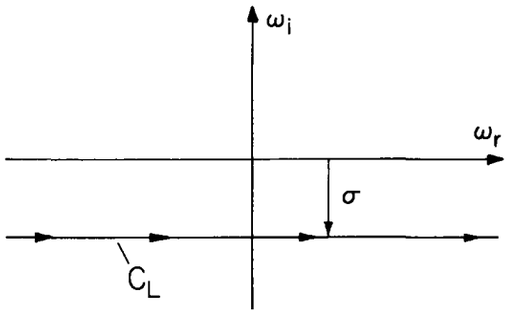

Fig. 11.12.2. Laplace contour.

The ω that appears in Eq. 10 is any one of the frequencies on the Laplace contour, C_L of Fig. 11.12.2. That is, the integral on k is carried out with ω each of the (generally complex) frequencies required to subsequently carry out the integration on ω.

Causality is built into the inversion of the transforms through the choice of the Laplace contour. On this contour, $\omega = \omega_r - j\sigma$, where σ is constant. Thus, in Eq. 11, $\exp(j\omega t) = \exp(j\omega_r t)\exp(\sigma t)$. Thus, for $t < 0$, the integrand goes to zero as $\sigma \to \infty$, and the integrand along the Laplace contour can be replaced by one closed in the lower half plane. That the response for $t < 0$ must be zero is therefore equivalent to requiring that this integral over the closed contour C_{-t} vanish. The closure is illustrated by Fig. 11.12.3. Cauchy's theorem makes it clear that this causality condition will prevail, provided that the Laplace contour is below all singularities of $\hat{\xi}(z,\omega)$ in the ω plane.

For any given frequency on this contour, the situation for inverting the Fourier transform as specified by Eq. 10 is no different than in Sec. 5.17, except that the frequency is in general some complex number. In Sec. 5.17, where it is assumed at the outset that sinusoidal steady-state conditions prevail, the frequency is the real frequency of the drive.

Note that $g(k)$ is not singular at $k = \beta$. Further, for the second order system, and for others having dispersion equations that are polynomial or transcendental in k, the roots of $D(\omega,k_n) = 0$ represent poles in the k plane. Thus, if the integration on the Fourier contour can be converted to one that is closed, then Cauchy's residue theorem

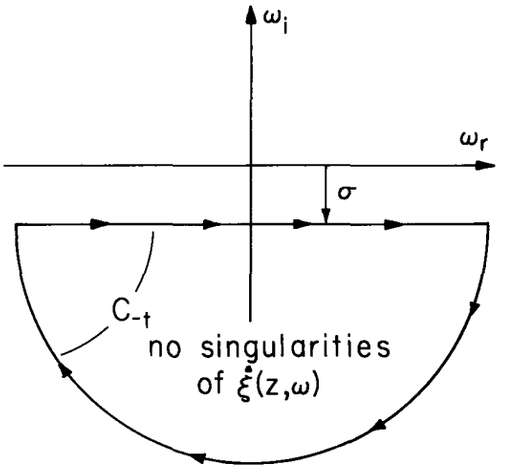

Fig. 11.12.3. Closure of Laplace contour to identify C_L consistent with causality.

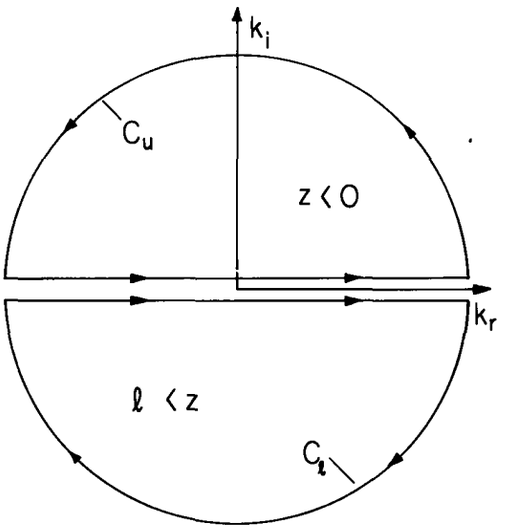

Fig. 11.12.4. Closures to evaluate Fourier integral.

$$\oint_C \frac{N(k)}{D(k)}\,dk = \pm 2\pi j(K_1 + K_2 + \cdots); \quad K_n = \frac{N(k_n)}{D'(k_n)} \tag{12}$$

provides a simple evaluation. The positive and negative signs are for counterclockwise and clockwise directions of integration. For a given frequency on the Laplace contour, the Laplace transform is the sum over the spatial modes.

To see what closed contour can be used to replace the open one that is to be evaluated, observe that in Eq. 10

$$[e^{j(k-\beta)\ell} - 1][e^{-jkz}] = e^{-j\beta\ell}e^{jk_r(z-\ell)}e^{k_i(z-\ell)} - e^{-jk_rz}e^{k_iz} \tag{13}$$

If z is in the range $z < 0$, the entire term goes to zero if $k_i \to +\infty$. Thus, the Fourier integration can be replaced by one on the closed contour C_u in the upper half of the k plane, as shown in Fig. 11.12.4. If z is in the range $\ell < z$, the entire term goes to zero if the contour is closed in the lower half plane, on C_ℓ. In the excitation range, where $0 < z < \ell$, the terms in Eq. 13 must be treated separately. The individual functions are singular at $k = \beta$, so the response in this range includes not only the spatial modes, but a "driven response" having the wavenumber β. This is considered in detail in Sec. 5.17, and will not be highlighted here. With the understanding that the summation is made appropriate to the range of z being considered (to left or right of the excitation range), Eq. 10 is integrated to give the Laplace transform

$$\hat{\xi}(z,\omega) = \pm\mathcal{G}(\omega)\sum_n \frac{jg(k_n)}{D'(\omega,k_n)}e^{-jk_nz} \tag{14}$$

where the upper and lower signs pertain to the upper and lower contours in Fig. 11.12.4. For example, in the case of the second order systems, where Eq. 6 gives the dispersion equation,

$$D(\omega,k) = (M^2 - 1)(k - k_1)(k - k_{-1})$$

$$k_{\substack{1\\-1}} = \frac{\omega M \mp \sqrt{\omega^2 + P(1 - M^2)}}{M^2 - 1} \tag{15}$$

It follows that in Eq. 14

$$D'(k_{\substack{1\\-1}}) = \pm (M^2 - 1)(k_1 - k_{-1}) = \mp 2\sqrt{\omega^2 + P(1 - M^2)} = \mp 2\sqrt{(\omega - \omega_c)(\omega + \omega_c)} \tag{16}$$

Asymptotic Response in the Sinusoidal Steady State: The Laplace contour, C_L, lies below all singularities of $\hat{\xi}(z,\omega)$. In the second order systems, there are singularities of the individual terms in Eq. 14 at $\pm\omega_c$. Whether or not they represent singularities of $\hat{\xi}(z,\omega)$ depends on the yet to be determined appropriate summation in Eq. 14. These branch poles of the individual terms are illustrated for the submagnetic case in Fig. 11.12.5. They are designated as branch poles because the function $D'(\omega)$, where $k_n = k_n(\omega)$, is double-valued if ω is allowed to pass through the branch line joining these poles (see Fig. 11.12.5). Because of $\mathcal{G}(\omega)$, there is clearly a pole of $\hat{\xi}(z,\omega)$ at $\omega = \omega_o$.

Fig. 11.12.5

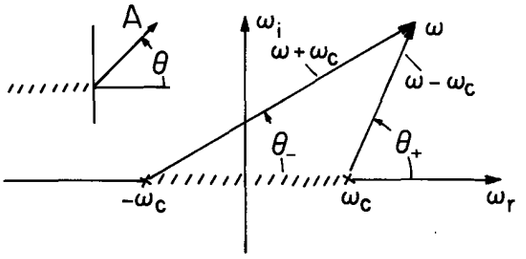

For second order system, singularities of individual terms of Eq. 14 are branch poles at $\omega = \pm\omega_c$, where $\omega_c \equiv \sqrt{-P(1-M^2)}$. Branch lines of $(M^2-1)(k_{+1}-k_{-1}) \equiv \sqrt{(\omega-\omega_c)(\omega+\omega_c)}$ are defined so that the principal value of a complex variable $A\exp(j\theta)$ is $-\pi < \theta < \pi$.

The objective here is not to carry out the second integration called for with Eq. 11, but rather to discern the response when $t \to \infty$. At a given location, z, there are two long-time possibilities. The response can either reach the sinusoidal steady state, or it can become unbounded. To achieve the former, it must be possible to move the Laplace contour, C_L, so that it is as shown in Fig. 11.12.6. This is possible if there are no singularities below the (open) contour. The part, C_L', runs parallel to the real axis with ω_i slightly positive. Thus as $t \to \infty$, the integrand of Eq. 10 on C_L' goes to zero, and this part of the integration gives no asymptotic contribution. The contributions to the integral along the oppositely directed segments, C_L'', cancel. Thus, the integral reduces to a closed integral on C_L'''. The only singularity within this contour is in $\mathcal{G}(\omega)$, at $\omega = \omega_o$. Thus,

$$\xi(z,t) = \sum_{n}^{+} \frac{g(k_n)}{D'(k_n)} e^{j(\omega_o t - k_n z)} \quad ; \quad k_n = k_n(\omega_o) \qquad (17)$$

where upper and lower signs pertain to closures of the contour in the upper and lower plane.

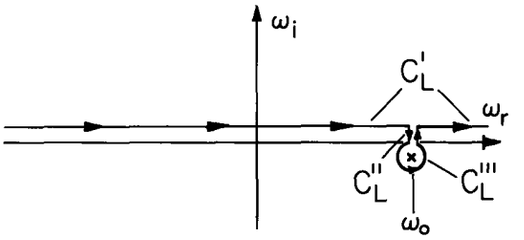

Fig. 11.12.6. Laplace contour in limit $t \to \infty$ with no singularities below contour.

As an example, consider the submagnetic second order system (with $|M| < 1$ and $P < 0$). In this case there are no singularities in the lower half of the ω plane, but there is the embarrassment of branch poles on the ω_r axis, as illustrated in Fig. 11.12.5. However, these occur on the axis because there is no damping in the system. If a force term is added to the equation of motion (Eq. 11.11.3) having the form

$$f = -B\left(\frac{\partial}{\partial t} + U\frac{\partial}{\partial z}\right)\xi \qquad (18)$$

where B is a positive damping coefficient, the branch poles are displaced into the upper half plane.

It is now possible to identify the proper contributions to the Laplace transform, Eq. 14, and hence to the sinusoidal steady-state response given by Eq. 17. For a given Laplace contour, C_L (σ a finite positive constant), the poles, k_n, form a locus of points in the k plane. Again, for the submagnetic case ($P < 0$ and $|M| < 1$), one locus is in the lower half plane and the other in the upper half plane. As the Laplace contour is displaced upward to the ω_r axis, these loci terminate in contours of complex k for real ω shown as dashed lines in Fig. 11.12.7. More prominently shown in this figure are the contours followed by the poles, k_n, as the Laplace contour is displaced upward to the ω_r axis. On these contours, ω_r is constant and σ is decreasing to zero. For example, holding $\omega_r = 0.8$, as σ is reduced to zero gives one pole that moves down and to the right in the second quadrant ($k_n = k_{-1}$) and a second that moves upward and to the left starting in the fourth quadrant ($k_n = k_1$). As σ reaches zero, these poles become complex conjugates. In general, one pole comes from above and one from below, each terminating on the locus of k for real ω. In this example, no pole starting in the lower half plane reaches the upper half plane and vice versa.

It is now clear that the $n = -1$ pole constitutes the only term in the sum in Eq. 17 with closure of the Fourier contour in the upper half plane (for $z < 0$) while $n = 1$ and closure in the lower half plane is appropriate for $z > 0$. Thus, Eq. 17 becomes

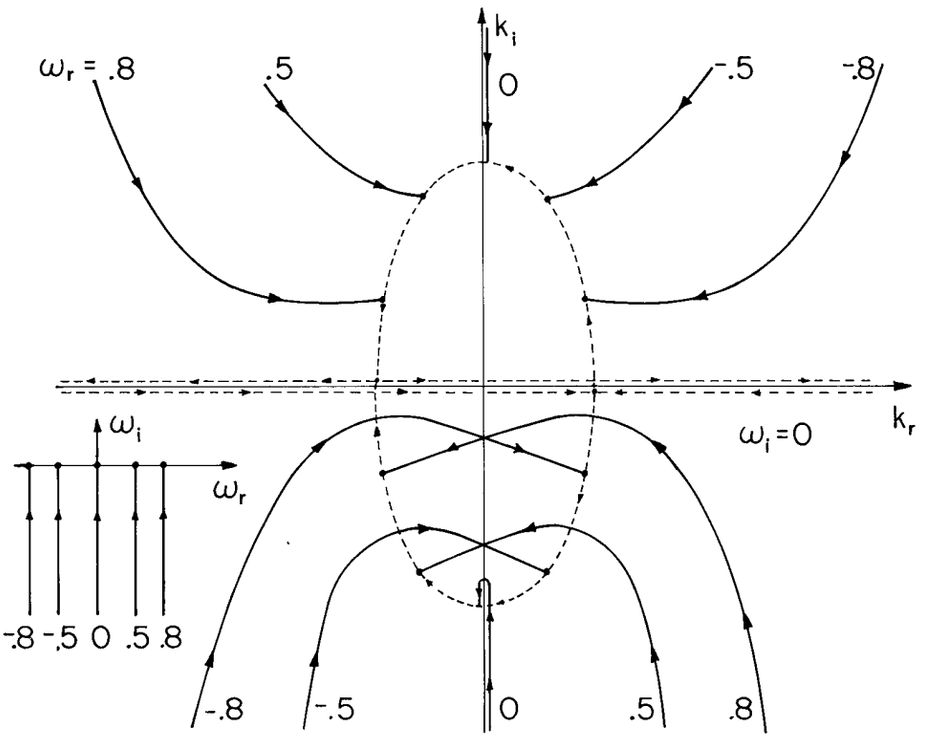

Fig. 11.12.7. Loci of k for loci of ω shown by inset. Broken curves are values of k for real ω. Submagnetic case ($|M| < 1$, $P < 0$) displays evanescent waves (P = 1, M = 0.5).

$$\xi(z,t) = -\frac{P\hat{f}_o}{2}\frac{[1 - e^{j(k_{\mp 1} - \beta)\ell}]e^{j(\omega_o t - k_{\mp 1} z)}}{(k_{\mp 1} - \beta)(k_1 - k_{-1})(M^2 - 1)}; \quad \begin{matrix} z < 0 \\ z > \ell \end{matrix} \qquad (19)$$

That is, if the frequency is in the range $\omega_o < |\omega_c|$ where waves are cut off, these waves are evanescent. They decay away from the excitation. For example, that k_{-1} has a positive imaginary part does not mean that it represents a wave that grows in the +z direction, but rather that it is a wave decaying in the -z direction. Converted to a real function of time in accordance with the discussion following Eq. 5, the result given by Eq. 19 is consistent with the sinusoidal steady-state response deduced in Sec. 11.11 for this case (Eq. 11.11.20).

Consider by contrast the establishment of a sinusoidal steady state in which there is an amplifying wave. As the Laplace contour is pushed upward toward the ω_r axis in the ω plane, one or more roots, k_n, of $D(\omega,k_n) = 0$ move across the k_r axis in the k plane. This is illustrated in Fig. 11.12.8 by the superelectric second order system ($P > 0$ and $|M| > 1$). Here, for σ large both poles, k_n, are in the lower half of the k plane. As σ is decreased keeping ω_r constant, one of the poles terminates in the lower half plane while the other passes through the k_r axis into the upper half plane.

Remember that "pushing" the Laplace contour to the ω_r axis in the ω plane is no more than a way to approximate the inverse Laplace integral in the limit $t \to \infty$. The function represented by the inverse Laplace integral must be the same, regardless of the integration contour. This requires that as the Laplace contour is moved upward, the Fourier integration contour must be distorted so that when it is evaluated by closing the contour, that contour includes the same poles of $D(\omega,k_n)$. That is, it must continue to include those that have passed through the k_r axis into the upper k plane. This "analytic continuation"[3] of the Laplace transformation is therefore obtained by using Fourier contours revised as illustrated in Fig. 11.12.9. By allowing the Fourier contour, Fig. 11.12.9, to be distorted so as to enclose the same singularities, the domain of the ω plane over which $\hat{\xi}(\omega,z)$ is analytic has been extended so that the Laplace contour can be that illustrated in Fig. 11.12.6.

For the second order superelectric system, there are now no poles enclosed by the Fourier contour closed in the upper half plane and hence appropriate to evaluating $\hat{\xi}(z,\omega)$ in the upstream region $z < 0$. Thus, the response $\xi(z,t)$ for $z < 0$ is zero. Note that this is true at any time and not just for the asymptotic response. Moreover, for closure in the lower half plane and hence $z > \ell$ the

3. P. M. Morse and H. Feshbach, Methods of Theoretical Physics, McGraw-Hill Book Company, 1953, p. 392.

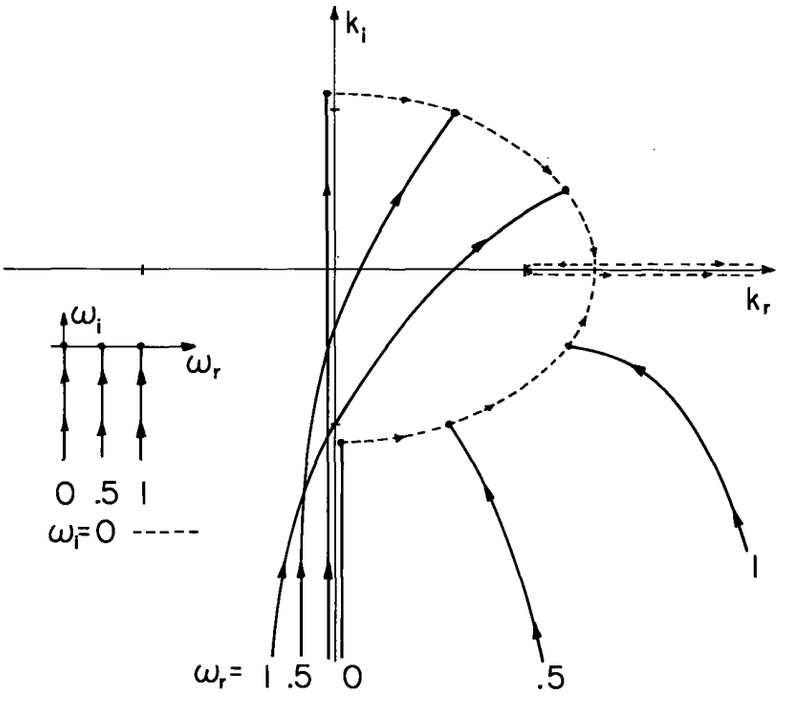

Fig. 11.12.8. Loci of k for loci of ω shown by inset. Broken curves are values of k for real ω. Superelectric case ($|M| > 1$, $P > 0$) displays amplifying waves ($P = 1$, $M = 1.5$).

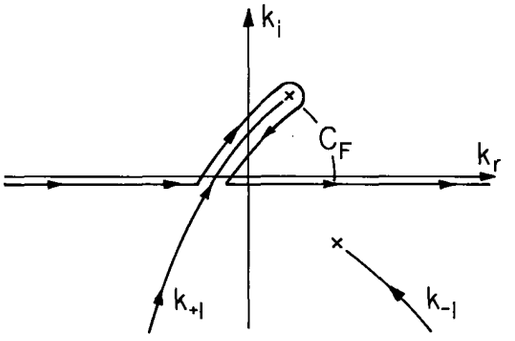

Fig. 11.12.9

As Laplace contour is pushed to ω_r axis, pole k_{+1} crosses k_r axis, indicating wave amplification.

summation for the Laplace transform is over both spatial modes. That is, Eq. 14 becomes

$$\hat{\xi}(z,\omega) = \frac{[g(k_1)e^{-jk_1z} - g(k_{-1})e^{-jk_{-1}z}}{j(\omega - \omega_o)(M^2 - 1)(k_{-1} - k_1)} \qquad (20)$$

Thus, in the long-time limit the Laplace integration along the contour shown in Fig. 11.12.6 results in

$$\xi(z,t) = \frac{j}{(k_{-1} - k_{+1})(M^2 - 1)} [g(k_{+1})e^{j(\omega_o t - k_1 z)} - g(k_{-1})e^{j(\omega_o t - k_{-1} z)}] \qquad (21)$$

Again, remember that the real expression is obtained from this expression as described following Eq. 5.

What has been obtained for the second order example is the same sinusoidal steady-state solution summerized by Eq. 11.11.21c. If the driving frequency is less than ω_c, one of the downstream waves decays away from the source while the other amplifies.

Criterion Based on Mapping Complex k as a Function of Complex ω: Causality requires that the Laplace contour remain below all singularities of $\hat{\xi}(\omega,z)$. In the process of pushing the Laplace contour upward in the ω plane to discover the asymptotic response, singularities of $D'(\omega,k_n)$ must be identified as possible singularities of the Laplace transform, Eq. 14. In the second order system, it is possible to solve explicitly to determine the frequencies, ω_s, at which

$$D'(\omega_s,k_n) \equiv \left[\frac{\partial D}{\partial k}(\omega_s,k)\right]_{k=k_n} = 0 \tag{22}$$

In general, these possible singularities are more difficult to identify. However, they can be determined by examining the dispersion equation.

Remember that Eq. 22 is really an expression for ω_s, because by definition

$$D(\omega_s,k_s) = 0 \tag{23}$$

In the neighborhood of (ω_s,k_s), ω and k are related by

$$D(\omega,k) = 0 = D(\omega_s,k_s) + \left.\frac{\partial D}{\partial \omega}\right|_{\omega_s,k_s}(\omega-\omega_s) + \left.\frac{\partial D}{\partial k}\right|_{\omega_s,k_s}(k-k_s) + \frac{1}{2}\left.\frac{\partial^2 D}{\partial k^2}\right|_{\omega_s,k_s}(k-k_s)^2 + \cdots \tag{24}$$

In view of Eqs. 22 and 23, Eq. 24 approximates the dispersion equation in the neighborhood of (ω_s,k_s) as

$$D(\omega,k) \simeq \left.\frac{\partial D}{\partial \omega}\right|_{\omega_s,k_s}(\omega-\omega_s) + \frac{1}{2}\left.\frac{\partial^2 D}{\partial k^2}\right|_{\omega_s,k_s}(k-k_s)^2 = 0 \tag{25}$$

This expression makes evident what is happening in the k plane as ω approaches ω_s in the ω plane, for Eq. 27 is equivalent to the expression

$$k - k_s = \pm\sqrt{\frac{-2\left.\frac{\partial D}{\partial \omega}\right|_{k_s,\omega_s}(\omega-\omega_s)}{\left.\frac{\partial^2 D}{\partial k^2}\right|_{k_s,\omega_s}}} \tag{26}$$

It is concluded that the coalescence of a pair of poles in the k plane is the result of having the frequency $\omega \to \omega_s$.

Candidates for poles of $\hat{\xi}(\omega,z)$ in the ω plane can be identified by mapping loci of the roots to the dispersion equation in the k plane resulting from varying $\omega = \omega_r - j\sigma$ to cover the lower half ω plane. This is conveniently done by holding ω_r at fixed values and decreasing σ from ∞ to zero.

In retrospect, for the submagnetic and superelectric second order systems, the coalescence of roots k_{+1} and k_{-1} does not occur in the lower half k plane. These mappings were illustrated by Figs. 11.12.7 and 11.12.8, respectively. But, consider the supermagnetic second order system ($|M|>1$, $P<0$). The map, illustrated in this case by Fig. 11.12.10, shows that at $\omega = -j\sqrt{-P(M^2-1)} \equiv -j\sigma_c$ (on the ω_i axis) there is a coalescence of the roots of k, and hence a singularity in the terms of Eq. 14 comprising the Laplace transform. However, because both roots are below the Fourier contour, they both contribute to the Laplace transform for $\ell < z$. In fact, as the roots coalesce, the pair of contributions to the Laplace transform are together not singular. That is, the denominator of the individual terms can be evaluated by taking the derivative of Eq. 25 and then using Eq. 26 to substitute for $k - k_s$,

$$\left.\frac{\partial D}{\partial k}\right|_{k_s,\omega_s}(k-k_s) = \pm\sqrt{-2\left.\frac{\partial^2 D}{\partial k^2}\right|_{k_s,\omega_s}\left.\frac{\partial D}{\partial \omega}\right|_{k_s,\omega_s}(\omega-\omega_s)} \tag{27}$$

where the upper and lower signs refer to the respective roots. Thus, the pair of terms resulting from the residues for the respective roots of k have opposite signs and, in the limit, equal magnitudes. Rather than being singular, the pair tend to the form 0/0, and can be shown to remain finite. It follows that the Laplace contour can be pushed to just above the ω_r axis (Fig. 11.12.6)

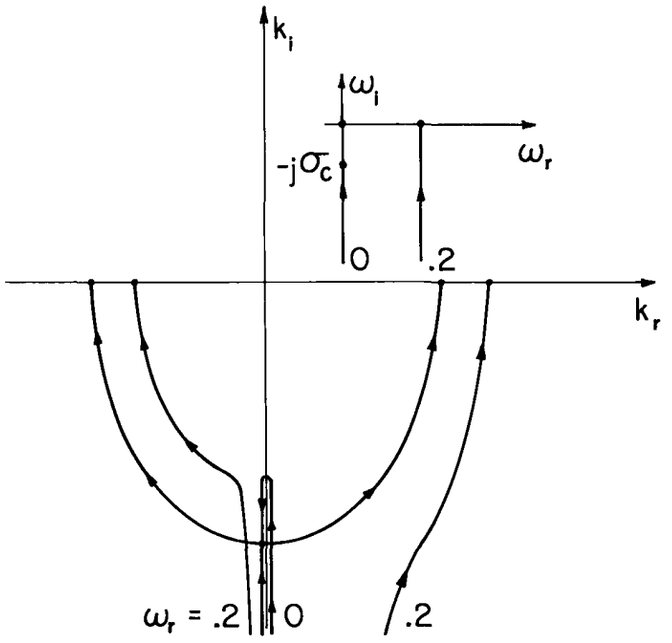

Fig. 11.12.10

Loci of k for loci of ω shown by inset. Supermagnetic case ($|M| > 1$, $P < 0$) displays ordinary waves, both propagating downstream ($M = 1.5$, $P = -1$).

to evaluate the asymptotic response as before. In the upper half k plane, there are no roots of k for ω on the Laplace contour and hence the response is zero for $z < 0$. For $\ell < z$, closure of the Fourier integral in the lower half k plane gives contributions from both k_{+1} and k_{-1}, so the Laplace transform, Eq. 14, has two terms. However, as already pointed out, the only singularity is at $\omega = \omega_o$, and so integration on the Laplace contour leads to Eq. 21. Now, $k_{\pm 1}$ can only be real and the downstream response takes the form of beating traveling waves. This is the same result as given by Eq. 11.11.15 and illustrated by Fig. 11.11.4.

In summary, the key to understanding the physical significance of a wave having complex values of k for real ω is a map of the loci of k that result from varying σ from ∞ to 0 for all values of ω_r. If the loci of a given root terminate in complex k without crossing the k_r axis, then it represents an evanescent wave. That is, in the sinusoidal steady state, the complex k represents a wave that decays away from the source. On the other hand, if loci cross the k_r axis, the mode represents an amplifying wave. At a point where a locus crosses the real k axis, k is obviously real and σ is still positive. Thus, for a crossing of the k_r axis, the dispersion equation must display "unstable" values of ω for real values of k. It is concluded that a necessary condition for existence of an amplifying wave is that wavelengths exist for which a temporal mode is unstable. That is, for k real there must be roots of $D(\omega,k)$ for which $\omega_i < 0$. As a type of instability that grows spatially rather than temporally, the amplifying wave is also termed a convective instability.

11.13 Distinguishing Absolute from Convective Instabilities

In Sec. 11.12, examples were purposely considered which were absolutely stable. Thus, the asymptotic response was in the sinusoidal steady state. A necessary condition for an amplifying wave was found to be "unstable" values of ω given by the dispersion equation for real values of k. How is this response, which is bounded at a given location, z, to be distinguished from one that grows with time at a given location?

Criterion Based on Mapping Complex k as Function of Complex ω: Suppose that a mapping of the dispersion equation, showing loci of k in the complex k plane resulting from varying σ from ∞ to 0 in the complex $\omega = \omega_r - j\sigma$ plane, results in a double pole of the type illustrated in Fig. 11.13.1. Here, as $\omega \to \omega_s$, a pair of roots coalesce, one from the upper half plane and one from the lower half plane. When it is closed, the Fourier contour can no longer be distorted to include the same poles. Before σ reaches zero, C_F is caught between the coalescing poles, one coming from above and the other coming from below.

As for the supermagnetic case from Sec. 11.12, coalescence of the roots, k_n, once again indicates the possibility of a pole of $\xi(\omega,z)$ in the lower half plane. This time the pole in fact exists, because the roots, k_n, are on opposite sides of the Fourier contour. Thus, pushed upward so that most of it is just above the ω_r axis, the Laplace contour is as shown in Fig. 11.13.2. The Fourier contour is caught between the coalescing poles, always including one or the other when closed in the upper or lower half k plane. Integration along the Laplace contour on the segments C_L' just above

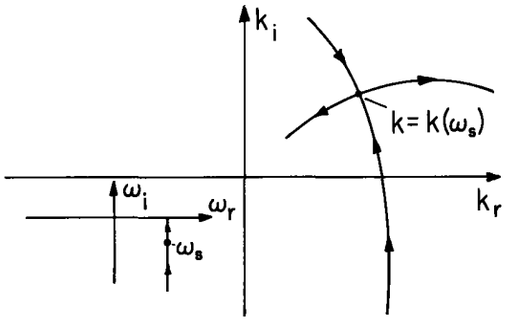

Fig. 11.13.1. Mapping of loci of k in the k plane for trajectory of ω passing through singularity in Laplace transform, showing coalescence of roots from upper and lower half plane indicating absolute instability.

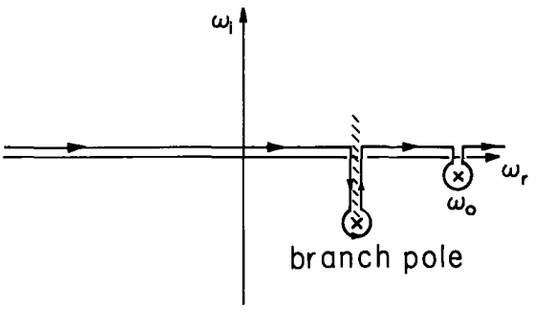

Fig. 11.13.2. Laplace contour for evaluating response as $t \to \infty$ with branch pole in lower half plane.

the ω_r axis gives no contribution as $t \to \infty$. However, integration along the segments, C_L'', adjacent to the branch-cut and around the pole do give contributions. (Note that the segments to either side of the branch-cut do not cancel, because the integrand is of opposite sign on one side from the other.) In the long-time limit, the Laplace integration reduces to

$$\lim_{t\to\infty} \xi(z,t) = \lim_{t\to\infty} \pm \int_{C_L''} \mathcal{J}(\omega) \sum_n \frac{jg(k_n)}{D'(\omega,k_n)} e^{j(\omega t - k_n z)} \frac{d\omega}{2\pi} \tag{1}$$

On the contour segment C_L'', $\omega = \omega_s - j\sigma$ where σ is positive, so the asymptotic response is dominated by a part that grows with time at a fixed location, z.

It is concluded that if the mapping of the dispersion equation from the lower half ω plane into the k plane discloses a pair of coalescing roots, k_n, with one root from the upper half plane and one from the lower half plane, then the pair represent an absolute instability. This is sometimes also called a non-convective instability.

Note that if roots, k_n, of $D(\omega,k_n)$ are to come from the lower and upper half plane and coalesce, one of them must cross the k_r axis. As it does so, σ is positive. Hence, a necessary condition for absolute instability as well as convective instability is that there be "unstable" frequencies for real values of k. That is, for a wave to be a candidate for either spatial or temporal growth, it must have temporal modes that are unstable.

One consequence of this observation relates to numerous situations that can be envisioned as configurations from the sections and problems of Chap. 8 set into a state of uniform motion. For example, consider the jet of liquid described in Sec. 8.15, but now having a stationary equilibrium in which the jet streams in the z direction with velocity U. The dispersion equation is Eq. 8.15.25 with $\omega \to \omega - kU$ and takes the form

$$(\omega - kU)^2 = f(k) \tag{2}$$

Convection or not, there are only two temporal modes and only one of these can be unstable. That is, for real values of k, at most one of the two roots, ω, can have a negative imaginary part.

If the dispersion equation were to be solved for the real frequency spatial modes, there would be an infinite number, about half appearing to "grow" in the z direction. What is clear from the above result is that only one of these is a candidate for being an amplifying wave. The others are evanescent waves.

Second Order Complex Waves: The subelectric second order system ($|M| < 1$ and $P > 0$, Fig. 11.11.1) exemplifies an absolute instability. The $\omega \to k$ mapping is shown in Fig. 11.13.3. In this case, the mapping indicates a branch pole at $\omega = -\omega_c \equiv -j\sqrt{P(1 - M^2)}$, as can also be seen directly from Eq. 11.12.16. The contour to be used for inverting the Laplace transform as $t \to \infty$ is indicated in Fig. 11.13.4.

In more complicated situations, the mapping is carried out numerically by having a routine for determining the roots, k_n, of $D(\omega,k_n)$ given the complex frequency $\omega = \omega_r - j\sigma$. The pattern of the loci in the neighborhood of the coalescing roots, typified by Fig. 11.13.3, can be used to disclose the coalescing roots.

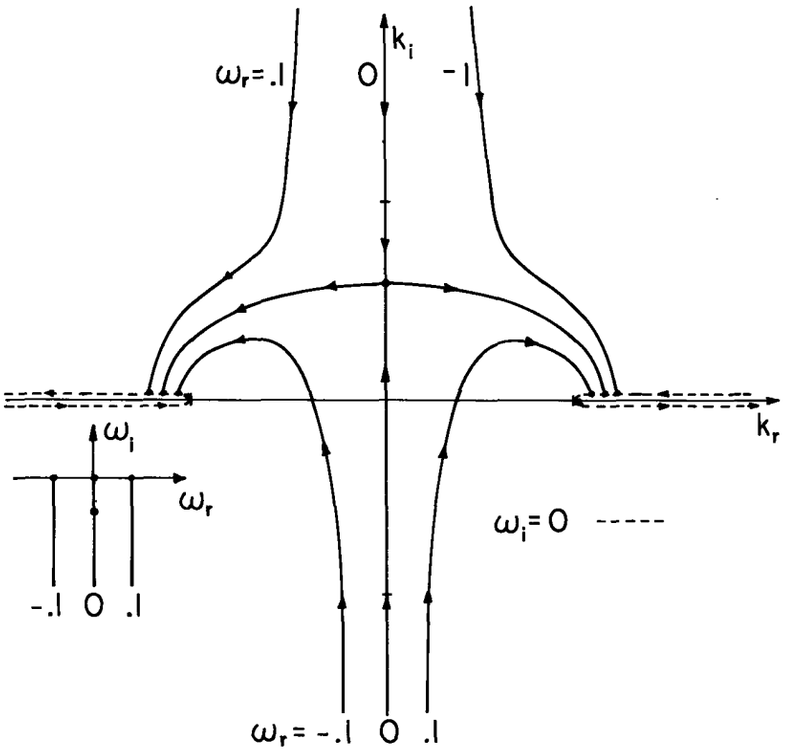

Fig. 11.13.3. Loci of k for loci of ω shown by inset. Subelectric case ($|M| < 1$, $P > 0$) displays absolute instability ($M = 0.5$, $P = 1$).

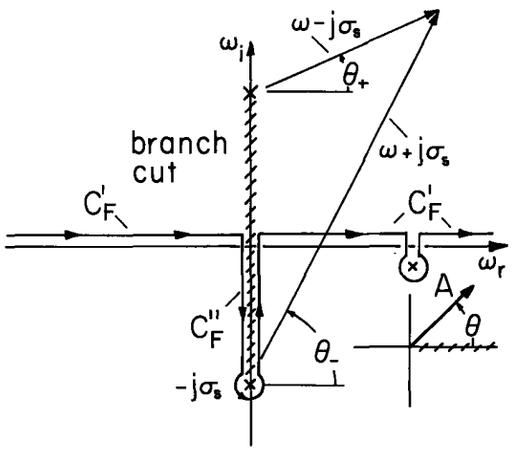

Fig. 11.13.4

Laplace contour, C_F, appropriate for evaluation of asymptotic response of subelectric ($|M| < 1$, $P > 0$) second order system. Branch cut of $\sqrt{(\omega - j\sigma_s)(\omega + j\sigma_s)}$ is defined consistent with branch line for $A \exp(j\theta)$ shown by inset.

11.14 Kelvin-Helmholtz Type Instability

Perhaps the most often discussed instability resulting from the interaction of streams is modeled by contacting layers of inviscid fluid, one having a uniform velocity relative to the other.[1] In Fig. 11.14.1, the lower layer is initially static while the upper one streams in the z direction with a uniform z-directed velocity, U. That the interface is subject to what is sometimes also called Bernoulli instability suggests why there is a critical velocity above which the stationary equilibrium is unstable. An intuitive picture makes clear the mechanism. For interfacial deformations that have a long wavelength compared to a or b, mass conservation requires that

$$v_z(a - \xi) = Ua \qquad (1)$$

1. G. K. Batchelor, Introduction to Fluid Mechanics, Cambridge University Press, London, 1967, pp. 511-517.

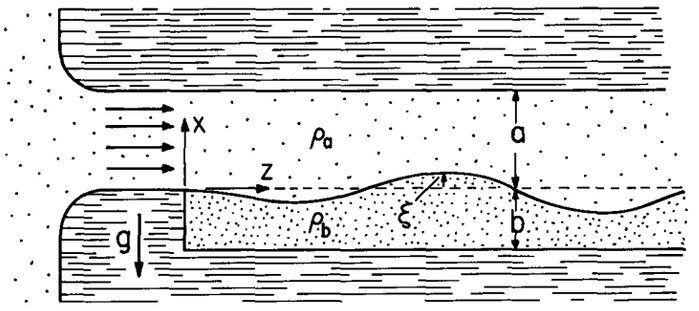

Fig. 11.14.1

In stationary state, lower fluid is static while upper one streams to the right with uniform velocity U. At the interface there is a discontinuity in fluid velocity, and hence a vorticity sheet.

Suppose that an upward directed external surface force density, T, could be applied to a section of the interface. At that point on the interface, normal stress equilibrium for the control volume of Fig. 11.14.2 requires that

$$T = p^d - p^e \tag{2}$$

where, for now, surface tension is ignored. With T applied slowly enough that the effect of the interfacial deformation on the flow can be pictured as a sequence of stationary states, the steady-state form of Bernoulli's equation is applicable to the regions above and below:

$$\begin{aligned} p + \tfrac{1}{2}\rho_a v^2 + \rho_a g x &= \Pi_a; \quad x > 0 \\ p + \rho_b g x &= \Pi_b; \quad x < 0 \end{aligned} \tag{3}$$

Initially, $T = 0$ and the interface is flat, so substitution of Eqs. 3 into Eq. 2 evaluates $\Pi_a - \Pi_b = \rho_a U^2/2$. Thus, the difference of Eqs. 3 becomes

$$p^d - p^e = \tfrac{1}{2}\rho_a(U^2 - v_z^2) + g(\rho_b - \rho_a)\xi \tag{4}$$

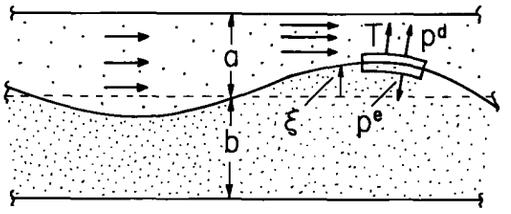

Fig. 11.14.2

Where the interface moves upward the streaming velocity increases. Thus, the pressure above drops and the interface is encouraged to further deform.

The combination of this expression of Bernoulli's equation with mass conservation, Eq. 1, and interfacial stress equilibrium, Eq. 2, gives an expression for the dependence of the surface deflection on the externally applied surface force density:

$$T = \tfrac{1}{2}\rho_a U^2\left[1 - \frac{1}{(1 - \frac{\xi}{a})^2}\right] + g(\rho_b - \rho_a)\xi \tag{5}$$

What is on the right is an equivalent surface force density representing the combined effects of the fluid inertia and gravity. (Rayleigh-Taylor instability is not of interest here, so it is assumed that the heavier fluid is on the bottom, $\rho_b - \rho_a > 0$.) If positive, it acts downward. The equilibrium is stable if a positive upward deformation results in a positive (restoring) surface force density. Thus, for instability,

$$\frac{dT}{d\xi}(\xi = 0) > 0 \Rightarrow \frac{g(\rho_b - \rho_a)a}{\rho_a} < U^2 \tag{6}$$

The effects of surface tension, finite wavelength and unsteady flow left out of this intuitive picture are brought in by a small-amplitude model that is little different from that developed in Sec. 8.9. What has changed is the transfer relation for the streaming layer, which in view of Eq. (c) from Table 7.9.1, is

$$\begin{bmatrix} \hat{p}^c \\ \\ \hat{p}^d \end{bmatrix} = \frac{j(\omega - k_z U)\rho_a}{k} \begin{bmatrix} -\coth ka & \frac{1}{\sinh ka} \\ \\ \frac{-1}{\sinh ka} & \coth ka \end{bmatrix} \begin{bmatrix} \hat{v}_x^c \\ \\ \hat{v}_x^d \end{bmatrix} \tag{7}$$

and the linearized relation between the vertical fluid velocity at the interface and the surface deformation (Eq. 7.5.5):

$$\hat{v}_x^d = \hat{v}_x^e = j(\omega - k_z U)\hat{\xi} \tag{8}$$

These expressions replace Eqs. 8.9.4a and 8.9.6 in an otherwise unchanged derivation resulting in the dispersion equation

$$\frac{(\omega - k_z U)^2 \rho_a \coth ka}{k} + \frac{\omega^2 \rho_b \coth kb}{k} = \gamma k^2 + g(\rho_b - \rho_a) \tag{9}$$

This expression is quadratic in ω but transcendental in k. Thus, there are only two temporal modes, but an infinite number of spatial modes. In the limit $U \to 0$, these are discussed in Sec. 8.9.

Consider first the temporal modes, having frequencies that follow from Eq. 9:

$$\omega = \frac{k_z U \rho_a \coth ka \pm \sqrt{(\rho_a \coth ka + \rho_b \coth kb)[\gamma k^3 + g(\rho_b - \rho_a)k] - \rho_b \rho_a k_z^2 U^2 \coth ka \coth kb}}{\rho_a \coth ka + \rho_b \coth kb} \tag{10}$$

It follows that the temporal mode exhibits an oscillatory instability if the U is large enough to make the radicand negative. For instability,

$$U^2 > \left[\frac{\tanh kb}{\rho_b} + \frac{\tanh ka}{\rho_a}\right]\left[\frac{\gamma k^3}{k_z^2} + g(\rho_b - \rho_a)\frac{k}{k_z^2}\right] \tag{11}$$

Deformations with wavenumbers in the direction of streaming are most unstable, so in the following, $k = k_z$. The first wavelength to become unstable as U is raised can be found analytically in two limits. First, in the short-wave limit, where ka and kb >> 1, Eq. 11 reduces to

$$U^2 > \left[\frac{1}{\rho_b} + \frac{1}{\rho_a}\right]\left[\gamma k + \frac{g(\rho_b - \rho_a)}{k}\right] \tag{12}$$

This expression exhibits a minimum at the Taylor wavenumber

$$k^* = \sqrt{\frac{g(\rho_b - \rho_a)}{\gamma}} \tag{13}$$

which is familiar from Secs. 8.9 and 8.10. Again, this is the wavenumber of incipient instability and Eq. 12 gives the critical velocity as

$$U^* = \left\{\left[4g(\rho_b - \rho_a)\gamma\right]\left[\frac{1}{\rho_a} + \frac{1}{\rho_b}\right]^2\right\}^{1/4} \tag{14}$$

In the opposite extreme of long waves (ka and kb << 1) Eq. 11 becomes

$$U^2 > \left[\frac{b}{\rho_b} + \frac{a}{\rho_a}\right]\left[\gamma k^2 + g(\rho_b - \rho_a)\right] \tag{15}$$

In this limit, the first wavenumber to become unstable as U is raised is zero and the critical velocity is

$$U^* = \sqrt{\left(\frac{b}{\rho_b} + \frac{a}{\rho_a}\right) g(\rho_b - \rho_a)} \qquad (16)$$

Note that, in the limit $b/\rho_b << a/\rho_a$, this condition is the same as obtained by the intuitive arguments leading to Eq. 6.

With the understanding that the temporal modes so far considered here represent the response to initial conditions that are spatially periodic, or the response of a system that is reentrant in the z direction, note that the salient difference between the Kelvin-Helmholtz instability and the Rayleigh-Taylor instability of Sec. 8.9 is that the former appears oscillatory under the critical condition and as a growing oscillation for conditions beyond incipience. This is by contrast with the Rayleigh-Taylor instability which is static at incipience and grows exponentially. Note that the dynamic state at incipience is not included in the arguments leading to Eq. 6.

In connection with instabilities of the Rayleigh-Taylor type, it can be argued that because incipience occurs with a vanishing time rate of change, effects of fluid viscosity are ignorable. Here, the dynamic nature of the incipience points to inadequacies of the inviscid model.

To demonstrate the instability without there being more dominant mechanisms of instability coming into play, the configuration shown in Fig. 11.14.1 is arranged so that the upper fluid enters from a plenum to the left through a section that is perhaps of a length several times the channel height, a, to establish the essentially uniform velocity profile. This distance cannot be too large, or viscous effects from the wall and interface will have expanded into the mainstream. What is not desired is anything approaching a fully developed flow for $z > 0$. In fact, the viscous boundary layer will continue to expand over the interface, and what has been described is deformations of the interface that have effective lengths large compared to the dimensions of the boundary layer.

Complications that are not accounted for by the model include the following. First, if the interface is clean, the lower fluid will be set into motion by the viscous shear stress from the streaming fluid. Thus, the postulated static fluid equilibrium for the fluid below is not strictly valid. One way to avoid this complication would be to "turn on" the flow abruptly and establish the instability before there is time for much effect of the viscous shear stress. Another is to have an interface supporting a monomolecular film.[1] This would compress in the z direction, until the interface would be brought to a static state by the gradient in tension of the film. For certain types of films the incremental dynamics from this static equilibrium would then be as described here, with a surface tension consistent with incremental deformations about this static equilibrium.

What is actually observed at the interface could also be unrelated to the Kelvin-Helmholtz instability as modeled here because the developing boundary layer has become unstable over the interfacial region being observed. Boundary layer instability results in growing perturbations having a scale on the order of the boundary layer thickness.

Certainly, if the fluid entering from the left has a fluctuating component to begin with, interfacial motions would result that had little to do with the model. These are the types of difficulties that often make ambiguous association of the Kelvin-Helmholtz model with effects of wind and water.

In using the Kelvin-Helmholtz model to explain and predict phenomena, it is important to know whether it predicts absolute or convective instability. Does the interfacial deflection at a given position in Fig. 11.14.1 tend to grow in amplitude until it reaches a state of saturation, or is it capable of responding to an upstream sinusoidal excitation as a spatially growing wave?

Of the infinite set of spatial modes, only one exhibits a crossing of the k_r axis, and then only if Eq. 11 is satisfied. Thus, there is only one candidate for an amplifying wave. The other spatial modes must be evanescent, and are present to satisfy longitudinal boundary conditions.

Consider the (first four) lowest order spatial modes in the long-wave limit (ka and kb << 1). The dispersion equation, Eq. 9, is then quartic in k and quadratic in ω:

$$k^4 + k^2[G - U^2] + rU\omega k - \omega^2 = 0 \qquad (\underline{17})$$

where the wavenumber is normalized to an arbitrary length, ℓ, so that

$$k = \underline{k}/\ell; \quad \omega = \underline{\omega}\sqrt{\frac{\gamma}{\left(\frac{\rho_a}{a} + \frac{\rho_b}{b}\right)\ell^4}} \qquad (18)$$

---

1. J. T. Davis and E. K. Rideal, Interfacial Phenomena, Academic Press, 1963, Chap. 5.

$$G \equiv \frac{\ell^2 g(\rho_b - \rho_a)}{\gamma}; \quad r \equiv 2/\sqrt{1 + \frac{a\rho_b}{b\rho_a}}$$

$$\underline{U} \equiv U\ell\sqrt{\frac{\rho_a}{a\gamma}} \qquad \text{(18 cont.)}$$

The loci of the four roots to this expression in the complex k plane obtained by letting ω_i increase from $-\infty$ to 0 at fixed values of ω_r is shown in Fig. 11.14.3. It is clear that for the parameters summarized in the caption, there is a coalescence of roots coming from the lower and upper half planes. Thus, it is concluded that the instability is absolute and grows with time at a fixed location. This same conclusion is reached by Scott[2] in the short-wave limit ($|ka|$ and $|kb| \gg 1$).

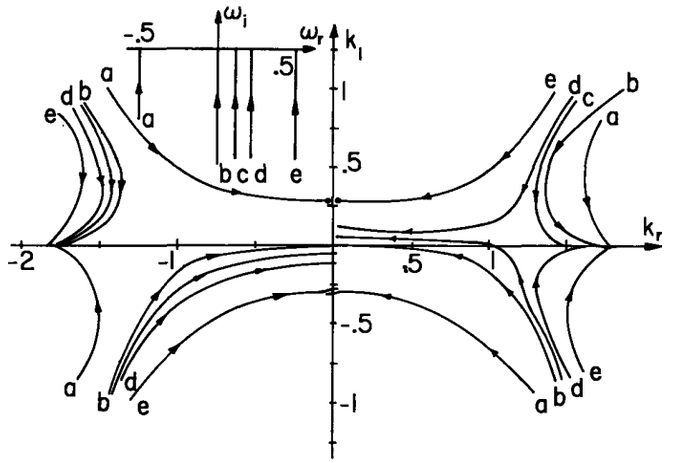

Fig. 11.14.3

For Kelvin-Helmholtz instability, loci of complex k resulting from varying ω as shown by inset. Coalescence of poles from upper and lower planes indicates that for parameters chosen, instability is absolute (G = 1, U = 2, γ = 0.1).

Spatially growing waves associated with wind blowing over water appear to require a model with more physical content than the simple one considered here.

11.15 Two-Stream Field-Coupled Interactions

Electric or magnetic coupling between streams having different velocities can occur without the necessity for physical contact between the streams. Thus, the long-wave models developed in Sec. 11.10 (Fig. 11.10.4) make a more satisfying representation of streaming interactions than does the traditional Kelvin-Helmholtz model of Sec. 11.14.[1] Transverse deflections of the respective streams are described by Eqs. 11.10.19-11.10.22, where e and v are as defined by Eq. 11.10.4. With f_1 and f_2 linearized, these expressions become

$$\left(\frac{\partial}{\partial t} + M_1 \frac{\partial}{\partial z}\right)^2 \xi_1 = \frac{\partial^2 \xi_1}{\partial z^2} + P\xi_1 - \frac{1}{2} P\xi_2 \qquad (1)$$

$$\left(\frac{\partial}{\partial t} + M_2 \frac{\partial}{\partial z}\right)^2 \xi_2 = \frac{\partial^2 \xi_2}{\partial z^2} + P\xi_2 - \frac{1}{2} P\xi_1 \qquad (2)$$

Normalization is as given by Eqs. 11.10.3 and 11.10.6. Remember, what is described is a pair of "strings" respectively convecting in the z direction with Mach numbers M_1 and M_2. With an electric field coupling the streams, P is positive, whereas with a magnetic field, P is negative. The "super" and "sub" responses to initial conditions and boundary conditions consistent with causality are discussed in detail in Sec. 11.10. There, the method of characteristics is used to describe the dynamics in real space and time.

The discussion is now limited to a description of the interaction of a stream with a fixed "string." That is, $M_2 = 0$ and $M_1 \equiv M$. The model is typical of interactions between electron beams

---

2. A. Scott, Active and Nonlinear Wave Propagation in Electronics, Wiley-Interscience, New York, 1970, pp. 83-87.

1. For a detailed discussion of the many possibilities for the model considered in this section, see F. D. Ketterer and J. R. Melcher, "Electromechanical Costreaming and Counterstreaming Instabilities," Phys. Fluids 11, 2179-2191 (1968) and "Electromechanical Stream-Structure Instabilities," Phys. Fluids 12, 109-117 (1969).

and transmission lines and plasmas. Counterstreaming and costreaming cases are considered in he problems.

What are the conditions for instability of the temporal modes, and is a given mode absolut ly or convectively unstable?

Substitution of complex amplitudes in Eqs. 1 and 2 results in the dispersion equation

$$[(\omega - Mk)^2 - k^2 + P][\omega^2 - k^2 + P] - \frac{1}{4}P^2 = 0 \qquad (3)$$

This expression is quartic in either ω or k. Subroutines for numerically finding the roots of polynomials are readily available.

Consider first the superelectric case, where $M > 1$ and $P > 0$. The temporal modes are summerize by the plots of complex ω for real k illustrated in Fig. 11.15.1. For $M > 2$ and $M < 2$, respectively, Parts (a) and (c) illustrate the dynamics of the stream if the structure were held fixed, and of the structure if the stream were fixed. These are the superimposed dispersion relations for an absolute and a convective instability.

The self-consistent solutions to Eq. 3 are illustrated by Parts (b) and (d). For $M > 2$, Pt. (b), very small k results in four roots having the same real part and forming two complex conjugate pairs. At a midrange of k, two complex conjugate pairs result with the pairs having different real parts but imaginary parts of the same magnitude. At high k, waves are formed that are typical of those on the convecting string and fixed string respectively.

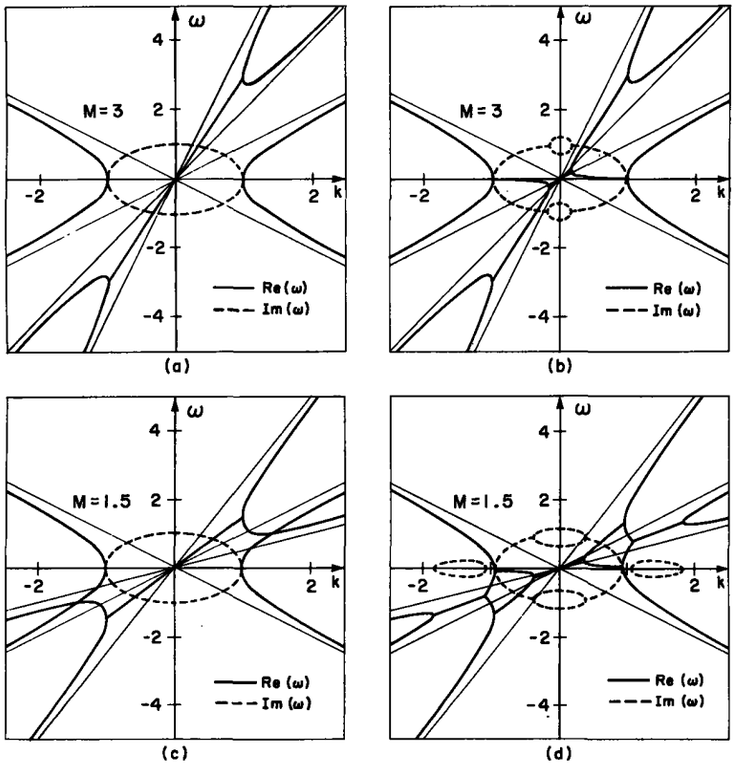

Fig. 11.15.1

Complex ω as a function of real k for electric stream structure ($P > 0$) interaction. Parts (a) and (c), which are drawn with mutual coupling terms ignored, are shown for respective comparison to Parts (b) and (d) ($P = 1$).

For $1 < M < 2$, an overstability results over a range of k where the uncoupled systems show no instability. This has a character that would not be expected from either the stream or the structure alone.

The plots of complex k for fixed ω_r as ω_i is increased from $-\infty$ to 0, shown in Fig. 11.15.2, disclose the character of these instabilities. One pair of roots move from above and below the k_r axis to coalesce in the upper half plane. Thus, this pair represent an absolute instability. The other pair migrate upward from the lower half plane, one extending into the upper half plane. This represents an amplifying wave.

It might be expected that the absolute instability eventually dominates the response. In the next section, a physical demonstration illustrates how this same system, confined to a finite length, can exhibit an oscillatory overstability that can be traced to the wave amplification.

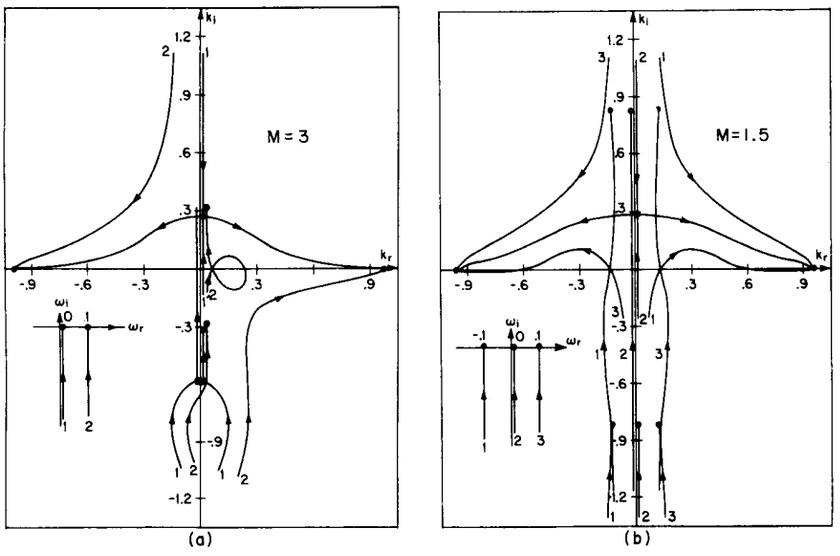

Fig. 11.15.2

For superelectric stream interacting with fixed "string" ($P > 0$) mapping of complex k plotted for fixed ω_r as ω_i is increased from $-\infty$ to 0.

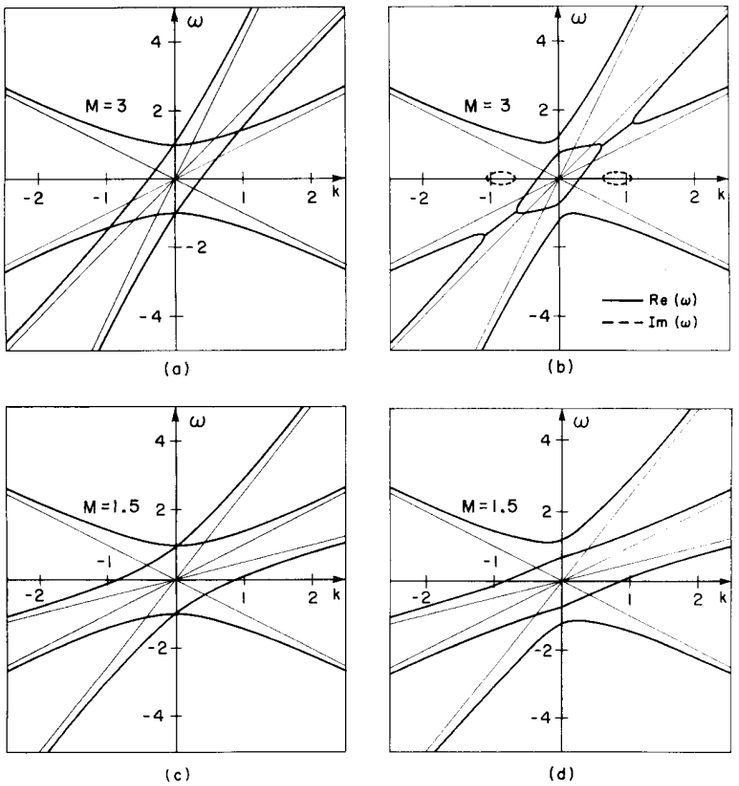

Fig. 11.15.3

Complex ω as a function of real k for magnetic stream-structure ($P < 0$) interaction. Parts (a) and (c), which are drawn with mutual coupling terms ignored, are shown for respective comparison to Parts (b) and (d) ($P = -1$).

Consider next the supermagnetic case, where $M > 1$ and $P < 0$. Now, the temporal modes are as shown by the dispersion plots of Fig. 11.15.3. Purely propagating waves result if $1 < M < 2$. However, if M is in the range $2 < M$, there is a range of k over which overstability is exhibited. Because the uncoupled stream and structure are completely stable, this temporal mode instability has some of the character of the Kelvin-Helmholtz instability. Note that it is similar to the high wavenumber overstability exhibited for the superelectric case by Fig. 11.15.1d. Whether the force on one stream due to a deflection of the other pushes or pulls, the result is a growing oscillation.

By contrast with the Kelvin-Helmholtz instability, this one is convective. This follows from the mapping of complex k for complex ω in the lower half plane illustrated (for this $2 < M$ case) by Fig. 11.15.4. The instability is indeed convective. The example is also worthy of remembrance because it illustrates how longitudinal boundary conditions, which have not yet come into play here, can have a dramatic effect. In Sec. 11.16, it is found that with boundary conditions (consistent with causality) this convective instability can become absolute.

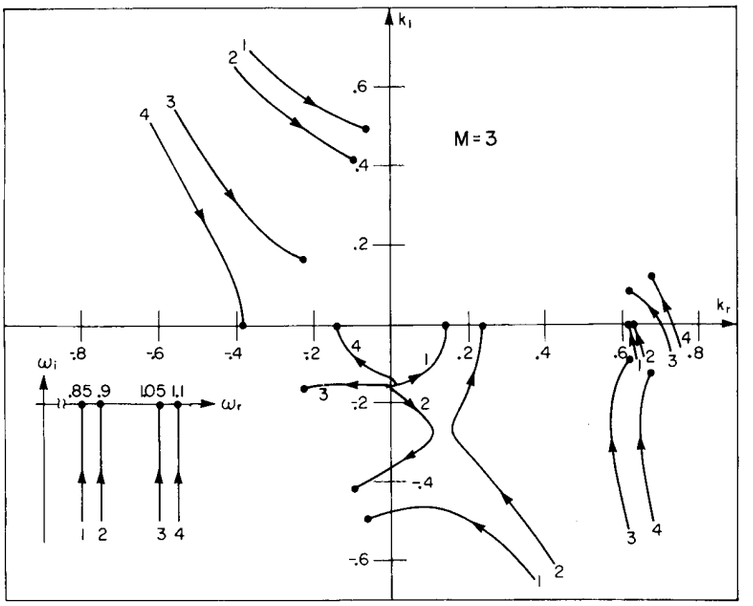

Fig. 11.15.4

For supermagnetic stream interacting with fixed "string" ($P < 0$), mapping of complex k plotted for fixed ω_r as ω_i is increased from $-\infty$ to 0.

11.16 Longitudinal Boundary Conditions and Absolute Instability

Quasi-one-dimensional linearized models, which retain the fundamental modes of a two-dimensional system having an infinite set of modes, can be obtained from the exact model by taking the long-wave limit. The coupled second order system used as a prototype model in Sec. 11.15 is one example. The following steps are generally applicable to determining the eigenfrequencies of such systems subject to homogeneous longitudinal boundary conditions. From a point of view somewhat different from that taken in Sec. 11.10, this section also emphasizes the importance of being sure that the boundary conditions are consistent with causality.

Suppose that there are N spatial modes. That is, with the frequency specified, there are N roots, k_n, to the dispersion equation $D(\omega,k_n) = 0$:

$$k_n = k_n(\omega) \tag{1}$$

Then, the response can be written as

$$\xi_2 = \mathrm{Re}\left(\sum_{n=1}^{N} A_n e^{-jk_n z} \right) e^{j\omega t} \tag{2}$$

where A_n are arbitrary coefficients. Although it remains to be found, the frequency of each term in Eq. 2 is the same. Thus, for initial conditions having the z dependence of the function in brackets in Eq. 2, the response would have the one (generally complex) frequency, ω. All other dependent variables can be written in terms of these solutions, and hence in terms of the N coefficients, A_n.

There are N homogeneous boundary conditions imposed either at $z = 0$ or at $z = \ell$. Evaluated using Eq. 2 and the other dependent variables written in terms of these same coefficients, these boundary conditions comprise N equations that are linear in the coefficients, A_n. The condition that the coefficient determinant vanish,

$$\mathrm{Det}(\omega,k_1,k_2,\cdots k_N) = 0 \tag{3}$$

together with the dispersion equation, Eq. 1, is the desired eigenfrequency equation.

To be specific, consider the stream coupled (either by the electric field or by a magnetic field) to a stationary continuum. The configuration is as shown physically by Fig. 11.10.4 and described by Eqs. 11.15.1 and 11.15.2 with $M_2 = 0$. Longitudinal boundary conditions, illustrated schematically by Fig. 11.16.1, are

$$\xi_1(0,t) = 0; \quad \frac{\partial \xi_1}{\partial z}(0,t) = 0; \quad \xi_2(0,t) = 0; \quad \xi_2(\ell,t) = 0 \tag{4}$$

That these are consistent with causality is demonstrated in Sec. 11.10 by appealing to the method of

characteristics. Here, the same conclusions might be reached by identifying three of the four spatial modes with the upstream boundary where z = 0 and the other with the downstream boundary where z = ℓ. Whether the coupling is electric (Fig. 11.15.2) or magnetic (Fig. 11.15.4), the mapping of the dispersion equation with ω_i increased from $-\infty$ to 0 at constant ω_r into the k plane gives rise to three loci originating in the lower half plane and one in the upper half plane.

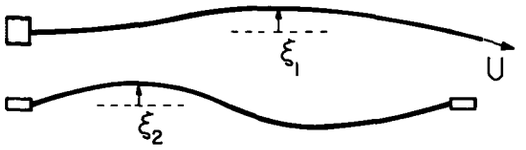

Fig. 11.16.1. Schematic of stream-structure interaction, showing three upstream boundary conditions and one downstream condition for $M_1>1$ and $M_2=0$.

The stream deflection is given by Eq. 2 with N = 4. It follows from Eq. 11.15.1 that the stationary continuum has a deflection that can be written in terms of these same coefficients as

$$\xi_1 = \mathrm{Re}\left(\sum_{N=1}^{4} Q_n A_n e^{-jk_n z}\right)e^{j\omega t}; \quad Q_n \equiv \frac{2}{P}(\omega^2 - k^2 + P) \qquad (5)$$

The four linear equations obtained by using Eqs. 2 and 5 to express the homogeneous boundary conditions, Eqs. 4, give

$$\begin{bmatrix} 1 & 1 & 1 & 1 \\ e^{-jk_1\ell} & e^{-jk_2\ell} & e^{-jk_3\ell} & e^{-jk_4\ell} \\ Q_1 & Q_2 & Q_3 & Q_4 \\ k_1Q_1 & k_2Q_2 & k_3Q_3 & k_4Q_4 \end{bmatrix}\begin{bmatrix} A_1 \\ A_2 \\ A_3 \\ A_4 \end{bmatrix} = 0 \qquad (6)$$

The determinant of the coefficients in this expression set equal to zero takes the form of Eq. 3 and is a complex equation for the complex variable, ω. Remember that the k_n's are determined in terms of the frequency from the dispersion equation found from Eqs. 11.15.1 and 11.15.2.

In general, finding the roots of the complex transcendental combination of Eqs. 3 and 1 is difficult.[1] Carrying out a numerical search for the roots is as straightforward as using the root-finding techniques illustrated by Fig. 5.17.5. However, unless the computer is guided, it can easily fail to converge on certain roots. One way to obtain solutions in a relatively automated way is to start by finding the roots in a limit in which one of the parameters is small enough to make an analytical approximation possible. Then, these roots can be followed as that parameter is raised to the desired value.

Numerically determined normalized eigenfrequencies are shown as a function of the normalized length in Fig. 11.16.2. Illustrated here is the electrically coupled system (P > 0). The first mode reflects the destabilizing effect of the electric field. At low fields, the effect of the coupling is to produce damping, but as the field is raised, there is a threshold for static instability in this mode, much as if the stationary continuum were coupled to rigid walls. The real part of the frequency below this threshold and the condition for incipience are little different from what would be obtained if the stream were rigid.

The effect of the coupling on the second mode is something new. According to the model (which ignores viscous drag), this mode is overstable with the application of even the slightest electric field.

In the magnetic case, with eigenfrequencies shown in Fig. 11.16.3, the static instability of the lowest mode is replaced by a damping that only becomes larger as the field is raised. But, reflecting a regenerative feedback mechanism, the higher order modes exhibit overstabilities similar to those for the electric case. The eigenfunctions for the first three modes, illustrated by Fig. 11.16.4, give some idea as to the origins of this spontaneous oscillation of growing amplitude.

The theoretical second eigenfunction for the electric case, having eigenfrequencies given by Fig. 11.16.2, has an appearance little different from that of the demonstration experiment shown by Figs. 11.16.5 and 11.16.6. In the first of these, a time exposure is shown of the water jet coupled electrically to a stretched spring. A sequence of instantaneous exposures of the same system following the dynamics through one oscillation is shown in the second figure. Deflections that amplify spatially on the jet are fed back upstream by the spring with a phase that makes the feedback loop regenerative.

---

1. F. D. Ketterer, Electromechanical Streaming Interactions, Ph.D. Thesis, Department of Electrical Engineering, Massachusetts Institute of Technology, 1965.

That the system with magnetic field coupling displayed the same instability makes it clear that this mechanism of instability has little to do with the nature of the coupling between stream and structure. It is the reflection of a wave on the spring by the downstream boundary condition that turns the magnetic field configuration from an infinite system exhibiting an amplifying wave into one that is finite and absolutely unstable.

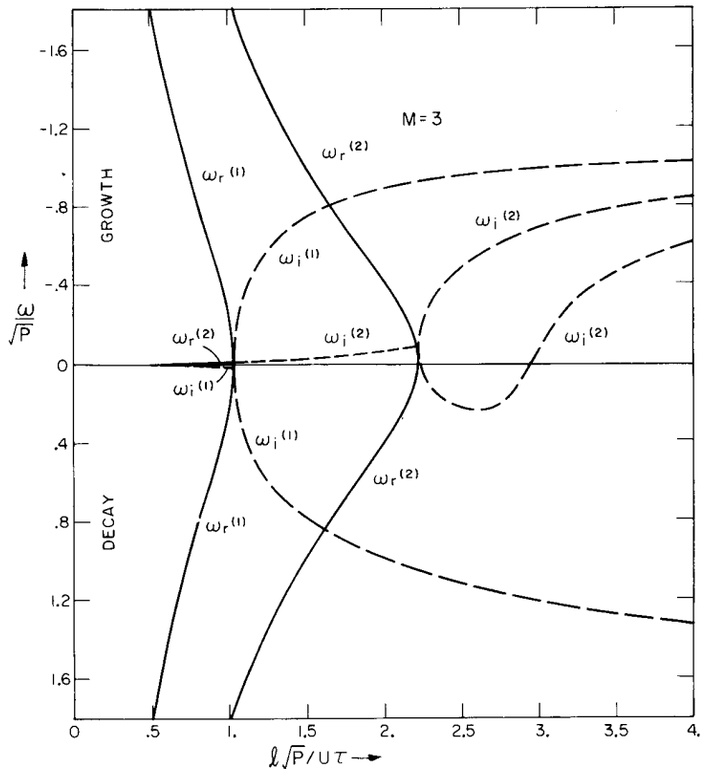

Fig. 11.16.2

Complex eigenfrequency as a function of normalized length for superelectric stream-structure interaction.

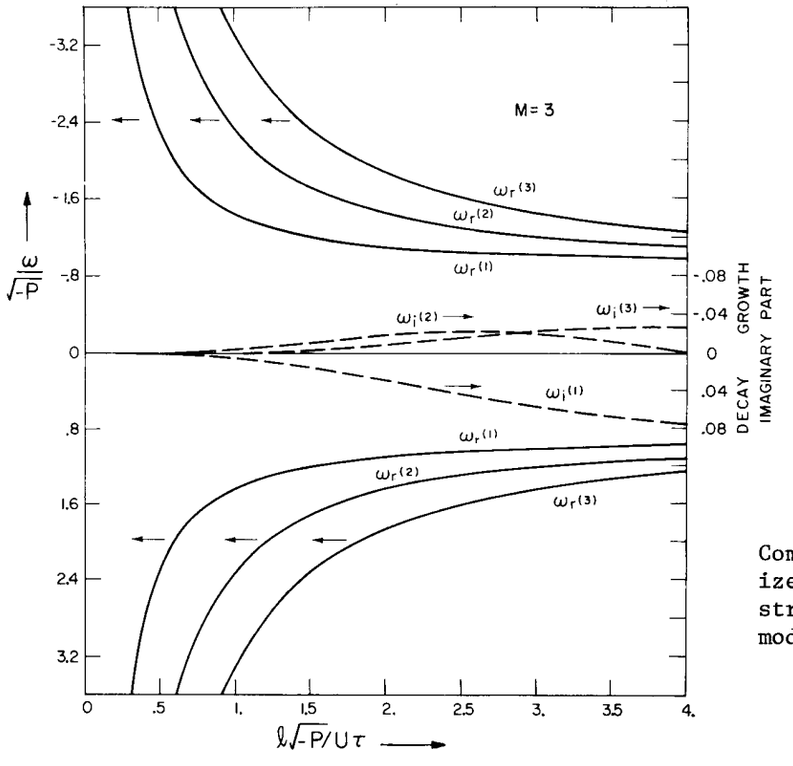

Fig. 11.16.3

Complex eigenfrequency versus normalized length for a magnetic stream-structure system for the lowest three modes.

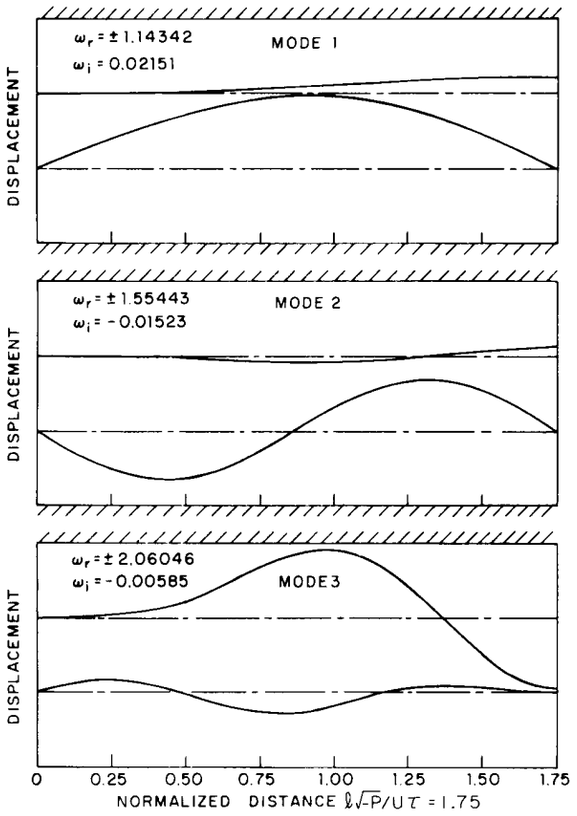

Fig. 11.16.4. Eigenfunctions for the three lowest modes for the magnetic system of Fig. 11.16.3.

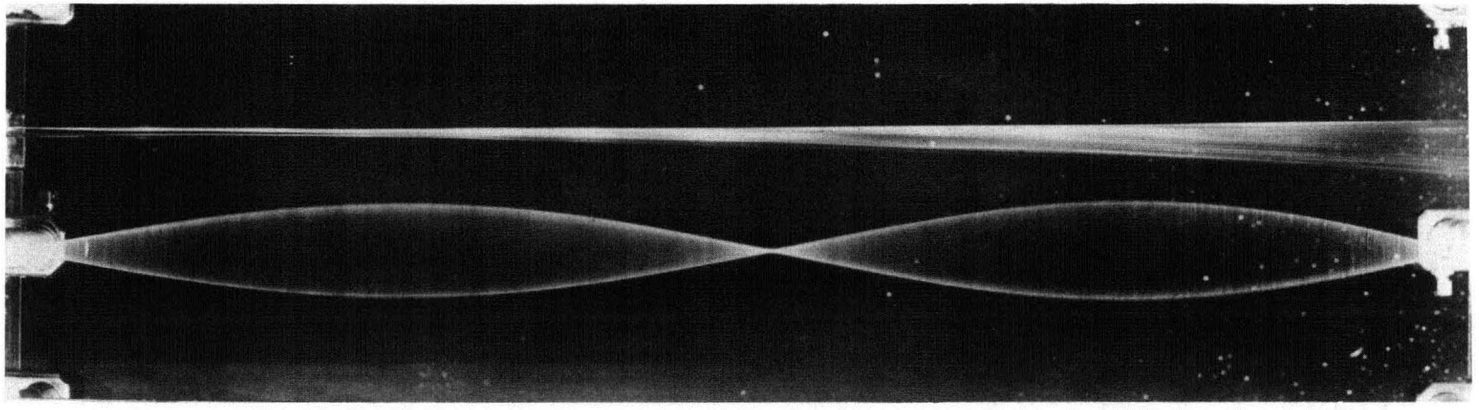

Fig. 11.16.5

Time exposure over several periods of oscillation during build-up of electric-field-coupled streaming overstability ($P>0$, $|M|>1$). Spring (bottom) and jet (top) are essentially in second mode (from film Reference 11, Appendix C).

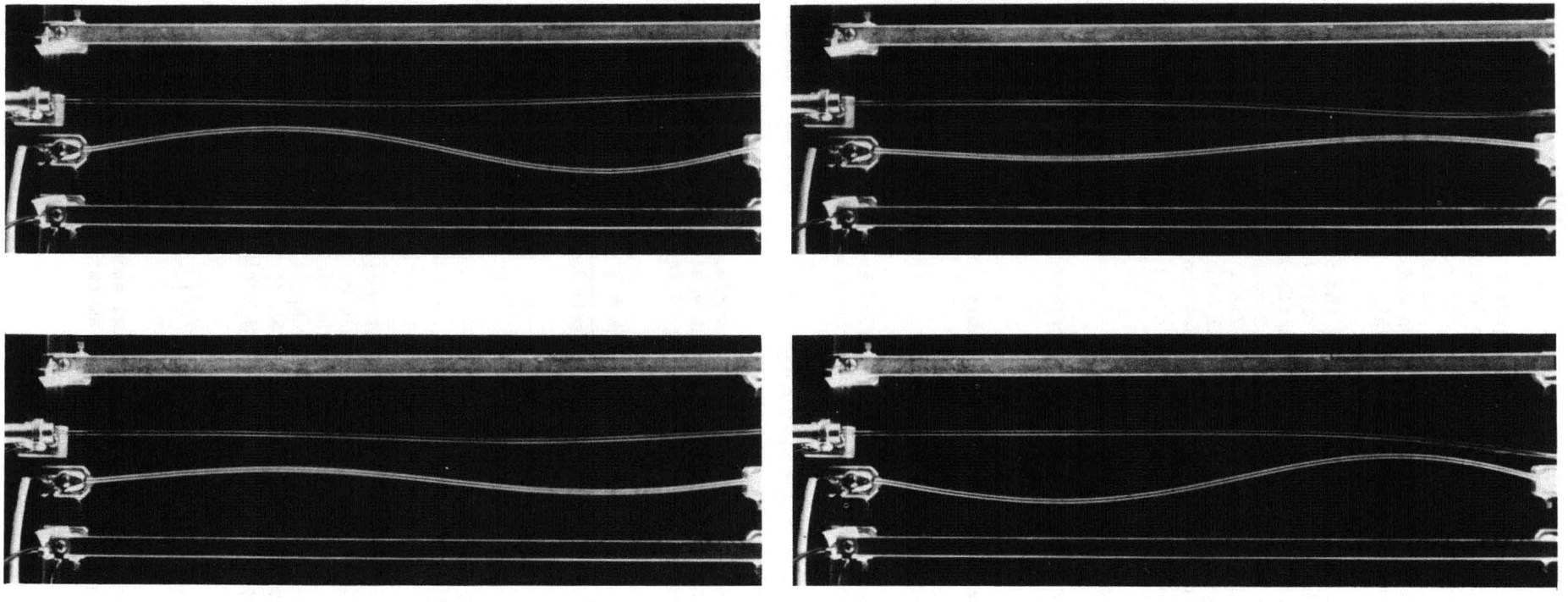

Fig. 11.16.6. Instantaneous photographs of the streaming overstability in Fig. 11.16.5. The time interval between exposures is equivalent to about 60° in phase. The frequency of oscillation is about 7 Hz (from film Reference 11, Appendix C).

11.17 Resistive-Wall Electron Beam Amplification

Either as a limitation in a linear accelerator or as the basis for making an amplifier,[1] the convective instability induced by the interaction of an electron beam with charges induced on a neighboring wall provides an interesting example of how lossy and propagating systems can interact to produce a spatially growing wave. The planar version shown in Fig. 11.17.1 incorporates the beam described in Sec. 11.5. What has been added is walls if finite conductivity, σ, themselves backed by much more highly conducting material.

With the objective of obtaining the dispersion equation for the beam coupled to the resistive layer, observe that fields in the layer (described in Sec. 5.10) are represented by the flux-potential transfer relations [Eq. (a) of Table 2.16.1]. In view of the highly conducting material bounding the resistive layer, $\hat{\Phi}^a = 0$, and it follows that on the lower surface of the layer,

$$\hat{D}_x^b = \varepsilon k \coth kd\, \hat{\Phi}^b \tag{1}$$

At this surface, the potential is continuous

$$\hat{\Phi}^b = \hat{\Phi}^c \tag{2}$$

and conservation of charge requires that

$$(j\omega + \frac{\sigma}{\varepsilon})\hat{D}_x^b - j\omega\hat{D}_x^c = 0 \tag{3}$$

In view of Eqs. 1 and 2, this expression becomes one representing the layer as "seen" by the electron beam:

$$\hat{D}_x^c = \frac{1}{j\omega}(j\omega + \frac{\sigma}{\varepsilon})(\varepsilon k \coth kd)\hat{\Phi}^c \tag{4}$$

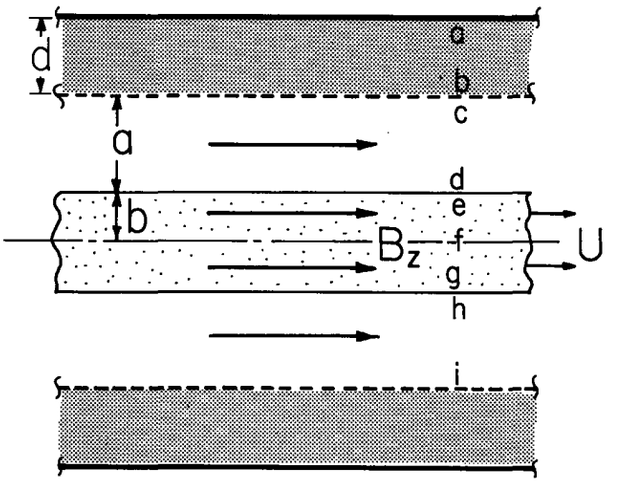

Fig. 11.17.1. Cross section of planar electron beam coupled to resistive wall.

The beam is represented at this same surface by Eq. 11.5.11 (with $\varepsilon = \varepsilon_o$). (Remember that it has already been assumed in Sec. 11.5 that electron motions are even.) Thus, the dispersion equation is obtained by setting D_x^c as given by Eq. 4 equal to D_x^c as given by Eq. 11.5.11:

$$\frac{1}{j\omega}(j\omega + \frac{\sigma}{\varepsilon})(\varepsilon k \coth kd) = \frac{-\varepsilon_o k(k + \gamma \coth ka \tanh \gamma b)}{k \coth ka + \gamma \tanh \gamma b} \tag{5}$$

where

$$\gamma^2 = k^2\left(1 - \frac{\omega_p^2}{(\omega - kU)^2}\right) \tag{6}$$

The discussion of temporal and spatial modes for the beam coupled to an equipotential wall given in Sec. 11.5 makes it clear that there are an infinite number of either temporal or spatial modes. Because of the Laplacian character of the field that couples the wall to the beam, the interaction between wall and beam tends to be strongest for the longest wavelengths. Thus, the long-wave limit of Eq. 5 is now taken by considering $ka \ll 1$, $kb \ll 1$, and $kd \ll 1$. Thus, Eqs. 5 and 6 become a polynomial dispersion equation that is cubic in ω and quartic in k,

$$(j\omega R_e + 1)\{(\omega - k)^2[\frac{b}{a} + k^2] - \omega_p^2 k^2\} = -j\omega R_e r k^2[(\omega - k)^2(1 + \frac{b}{a}) - \frac{b}{a}\omega_p^2] \tag{7}$$

and the higher order transverse spatial modes are neglected. Here the frequency and wavenumber have been normalized and dimensionless parameters introduced:

$$\underline{\omega} = \frac{b}{U}\omega; \quad R_e \equiv \frac{U\varepsilon}{b\sigma}; \quad r \equiv \frac{d\varepsilon_o}{b\varepsilon}$$

$$\underline{k} = kb; \quad \underline{\omega}_p \equiv \frac{b\omega_p}{U} \tag{8}$$

---

1. C. K. Birdsall, G. R. Brewer and A. V. Halff, "The Resistive-Wall Amplifier," Proc. IRE 41, 865-875 (1953).

The modes that have been retained by this long-wave model can be identified by considering two limits of Eq. 7. In the first, $\sigma \to \infty$ ($R_e \to 0$) and the expression reduces to one for space-charge oscillations superimposed on the convection:

$$\omega = kU \pm \frac{\omega_p k}{\sqrt{\frac{1}{ab} + k^2}} \tag{9}$$

These are the lowest modes from Sec. 11.5. In the second, the beam is removed by setting $\omega_p \to 0$. Then, Eq. 7 requires that

$$j\omega = -\frac{\sigma}{\varepsilon}\left[1 + \frac{d\varepsilon_o}{b\varepsilon}\frac{(1+\frac{b}{a})k^2}{(\frac{1}{ba} + k^2)}\right] \tag{10}$$

This is the damped charge relaxation mode resulting from the ohmic loss in the layer and energy storage both within the layer and in the region of the gap and beam.

What can be expected for the coupled modes? First, to consider the temporal modes, Eq. 7 is written as a cubic in ω:

$$\omega^3\left\{jR_e[(\frac{b}{a} + k^2) + rk^2(1+\frac{b}{a})]\right\} + \omega^2\left\{\frac{b}{a} + k^2 - 2jR_e k[(\frac{b}{a} + k^2) + rk^2(1+\frac{b}{a})]\right\}$$

$$+\omega\left\{jR_e k^2[\frac{b}{a} + k^2(1 + r + \frac{br}{a}) - \omega_p^2(1+\frac{rb}{a})] - 2k(\frac{b}{a} + k^2)\right\} + k^2(\frac{b}{a} + k^2 - \omega_p^2) = 0 \tag{11}$$

Numerical solution of this expression is illustrated by Fig. 11.17.2, where complex $\underline{\omega}$ is shown as a function of real $\underline{k}$. For the given parameters, the growth rate, $\underline{\omega}_{2i}$, is small compared to the other frequencies, and so it is shown on a separate plot.

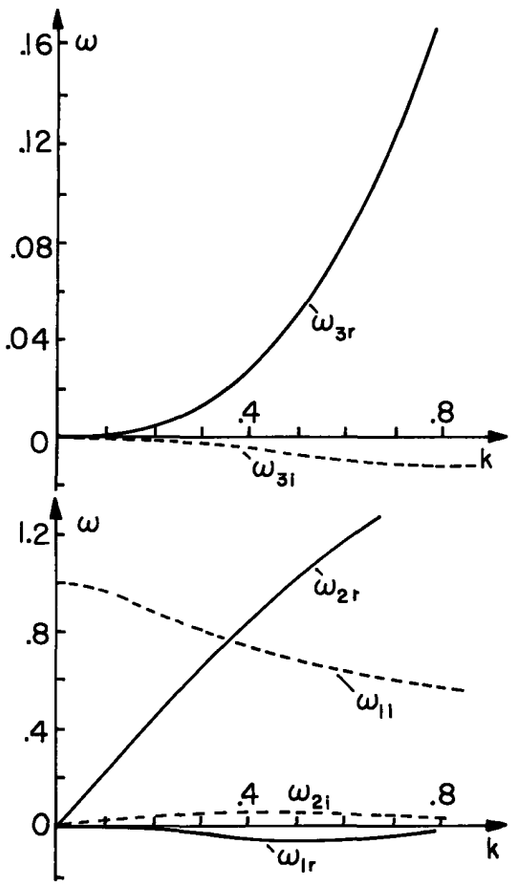

Fig. 11.17.2

Plot of dispersion equation for long-wave coupling of electron beam to resistive wall, showing normalized complex ω for normalized real k ($b/a = 1$, $r = 1$, $R_e = 1$, $\underline{\omega}_p = 1$).

That the system is unstable raises the second question. Would this instability result in a beam oscillation that grew in time at a fixed location, or would it result in a spatial amplification of any disturbance? The limitation on a particle accelerator, or the possibility of using the interaction to make an amplifier, hinge on whether the instability is convective or absolute.

In order to plot loci of complex k as ω is varied at constant ω_r from $\omega_i = -\infty$ to 0, Eq. 7 is expressed as a polynomial in $\underline{k}$:

$$k^4\left\{j\omega R_e[1 + r(1 + \frac{b}{a})] + 1\right\} + k^3\left\{-2j\omega^2 R_e[1 + r(1 + \frac{b}{a})] - 2\omega\right\}$$

$$+ k^2\left\{j\omega R_e[\omega^2 + \frac{b}{a} - \omega_p^2 + r\left(\omega^2(1 + \frac{b}{a}) - \frac{b}{a}\omega_p^2\right)] + (\omega^2 + \frac{b}{a} - \omega_p^2)\right\} \qquad (12)$$

$$+ k\left\{-2\omega\frac{b}{a}(j\omega R_e + 1)\right\} + \frac{\omega^2 b}{a}(j\omega R_e + 1) = 0$$

The loci of the four roots to Eq. 12 obtained by varying ω_i from $-\infty$ to 0 with ω_r fixed are shown in Fig. 11.17.3. Of course, all values of ω_r must be considered. The ones shown are typical. Apparently the instability is convective. Thus, fluctuations on the beam as it enters the interaction region would amplify in space. To contend with an undesired instability on a beam having a given entrance fluctuation level, the length of the interaction region would have to be limited.

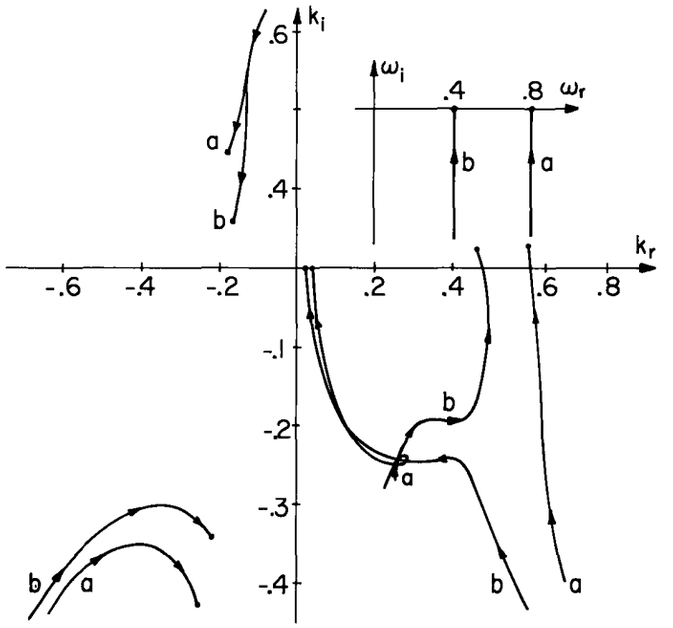

Fig. 11.17.3

For resistive wall interacting with electron beam, the loci of the four long-wave modes in the $\underline{k}$ plane are shown as $\underline{\omega}_i$ is varied from $-\infty$ to 0 holding $\underline{\omega}_r$ fixed. The inset shows the associated trajectories of $\underline{\omega}$ in the complex $\underline{\omega}$ plane. The instability is apparently convective.

The problems give some hint of the wide variety of physical situations in which amplifying waves result from coupling between charged particle streams and various types of structures and media. Electron beam interactions and plasma dynamics are rich with examples of the various forms of complex waves. So also is fluid mechanics, where boundary layer instabilities and other precursors of turbulence are often amplifying waves.